VARIATIONS IN ATMOSPHERIC ANGULAR MOMENTUM AND THE LENGTH OF DAY

by

Richard D. Rosen[†]
David A. Salstein[†]

Environmental Research & Technology, Inc.
696 Virginia Road
Concord, MA 01742

ERT Technical Report A345-T2

prepared with support provided by the
Lageos Project
National Aeronautics and Space Administration
under contract NAS5-25870

October 1982

[†]Present address: Atmospheric and Environmental Research, Inc.
840 Memorial Drive, Cambridge, MA 02139

Variations in Atmospheric Angular Momentum and the Length of Day

Richard D. Rosen and David A. Salstein

Twice-daily global analyses of the zonal winds prepared by the U.S. National Meteorological Center for the period from 1 January 1976 through 31 December 1981 have been used to construct a time series of the atmosphere's angular momentum (M). Three-day means of this quantity for the first five years of the data set are spectrally analyzed and compared with independent observations of changes in the solid earth's rate of rotation. The most prominent feature in the M time series is an annual signal, and this is mirrored by similar behavior in changes in the length of the day (l.o.d.). Other noteworthy fluctuations in M and l.o.d. on time scales of less than a year also occur, however, and these too agree well with each other. In this regard, a near 50 day fluctuation in both time series, also noted in other studies, is especially visible. We conclude on the basis of these comparisons that indeed most of the variability in our time series for M is real and that, as others have suggested, the atmosphere plays a dominant role in forcing changes in l.o.d. on time scales of about a year and less.

We divide the mean meridional plane into a number of regions to investigate the contributions made by different parts of the atmosphere to the changes found in the global statistic M. Our approach is to calculate empirical orthogonal functions that define the major spatial modes of variation among the regional time series of angular momentum. As expected, we find the annual cycle in M is associated with seasonal

changes in the major jet streams of the two hemispheres, with the larger of these changes occurring in the Northern Hemisphere. We also find that all the statistically significant spatial modes of non-seasonal variation depict behavior organized over large horizontal scales with a high degree of vertical stratification. Non-seasonal changes in M emerge from the imbalances among these regional variations in momentum, with the largest contributions on time scales less than a year coming from the subtropical portions of each hemisphere.

1. Introduction

A fundamental measure of the dynamic state of the atmosphere is its angular momentum about the polar axis relative to the earth. Indeed, study of the maintenance of the atmosphere's angular momentum against dissipation has long been at the forefront of meteorological research (see Lorenz, 1967, for a review of this history). In an early, and now classic, paper on the topic, Starr (1948) also noted that "there is no reason to expect that the partition of angular momentum [between the earth and the atmosphere] should remain constant when seasonal and other short time-intervals are considered". Since then, numerous studies have been undertaken to quantify more precisely the relationship between changes in atmospheric momentum and the rotation rate of the solid earth on a variety of time scales.

Actually, the rotation of the solid earth is affected by a wide range of geophysical phenomena besides those related to the atmosphere. These include the effects of tides, earthquakes, core-mantle coupling (Yoder et al., 1981; Lambeck and Cazenave, 1977; Hide, 1977) and perhaps the melting of polar ice (Etkins and Epstein, 1982). On periods of less than about a year, however, the atmospheric excitation of changes in the earth's rotation rate appears to dominate (except at the fortnightly and monthly solid body tidal periods). Indeed, the atmosphere seems to play a considerable role in this regard out to periods of about four years (Lambeck and Hopgood, 1981, 1982), which has made more precise determinations of the atmospheric contribution of great interest to geodesists and geophysicists.

Most of our previous knowledge concerning temporal changes in the atmosphere's angular momentum has been derived from monthly mean zonal

wind data at the network of upper-air sounding stations. These stations, though, are irregularly spaced and for the most part are located over the land north of 20° S, so that their representativeness has been a concern. Within the last decade, however, several large meteorological centers have introduced global analyses of the wind field that routinely assimilate data not only from the rawinsonde stations, but also from commercial aircraft and satellites which provide important new information in the station-sparse regions. In addition, these global analyses are convenient to use, since they provide wind values directly on a latitude-longitude grid. In particular, the computation of atmospheric angular momentum on a daily basis is straightforward. Recently, Hide et al. (1980) demonstrated the potential that now exists for studying high frequency changes in atmospheric angular momentum by using the global grid point analyses produced by the British Meteorological Office and by the U.S. National Meteorological Center (NMC) for the same four-month period. We extend the work of Hide et al. here by using six years (1976-81) of NMC twice-daily global analyses to create and study a lengthy time series of high temporal resolution angular momentum values. We also compare changes in these atmospheric values to independently determined changes in the rotation rate of the solid earth. Finally, we examine the atmospheric data in more detail to determine the time and space scales on which variations in momentum occur within the atmosphere and which regions are contributing most to the changes we find in the global integral. We begin in the next section, though, with a description of the data and techniques used to derive our time series of momentum values.

2. Derivation of Atmospheric Angular Momentum Values

NMC introduced its first operational global analysis scheme in September 1974. Since then, numerous modifications to the scheme have been introduced (a detailed description of a recent version is provided by McPherson et al., 1979), but from the start the output has included twice-daily (0000 and 1200 GMT) values of the zonal wind analyzed over a grid with points spaced every 2.5° in both latitude and longitude, at each of 12 pressure levels in the vertical (1000,850,700,500,400,300, 250,200,150,100,70 and 50 mb). NMC has archived certain general circulation statistics derived from these grid point analyses beginning 1 January 1976 (Miller et al., 1975). Included in this archive are zonally averaged values of the eastward component of the wind at each latitude and level, [u]. To derive estimates of the angular momentum (M) of the atmosphere about the polar axis, relative to an earth-fixed frame, these [u] values have been integrated, with the appropriate weighting, over latitude (ϕ) and pressure (p):

$$M = \frac{2\pi a^3}{g} \int_{1000\ mb}^{100\ mb} \int_{\pi/2}^{-\pi/2} [u] \cos^2\phi \, d\phi \, dp \qquad (1)$$

where a is the mean radius of the earth (6.37×10^6 m) and g is the acceleration due to gravity (9.81 ms^{-2}). Equation (1) is based on the assumption that the atmosphere is in hydrostatic equilibrium and ignores the variation with altitude and latitude of the distance of a parcel of air from the center of the earth. We have not used any of the wind data at the two levels above 100 mb where the reliability of the NMC analysis

is questionable. The trapezoidal rule was used in evaluating (1) numerically.

Occasional brief gaps exist in the NMC archive and no attempt has been made to fill these in. However, there are also two relatively lengthy gaps, one from 1 April through 15 August 1977 and one from 1 February through 8 April 1981. For these periods, we obtained copies of the original NMC grid point analyses (for 0000 GMT only) from the National Center for Atmospheric Research, and we used these to fill in the missing values for [u] and M.

Errors in our estimates of global momentum values arise through the approximations involved in deriving (1) as well as through inaccuracies in the NMC wind analyses. With regard to the former source of error, the most serious aspect is undoubtedly the neglect of the upper atmosphere at pressures less than 100 mb. We have examined some calculations made with and without data from the 70 and 50 mb levels, and based on these we conclude that neglecting the upper 10% of the atmosphere incurs a systematic underestimate in the mean level of M of about 10% or less, but it has a much smaller impact on our determination of most short-term changes in M. (On the other hand, some variations in M such as a semi-annual or a quasi-biennial cycle may well be affected by the lack of data from much of the stratosphere and above.)

An error also results from our treatment of the lower boundary in (1). In the NMC analysis, the lower boundary is taken to be smooth and fixed at a constant pressure of 1000 mb, regardless of where this level lies relative to the earth's surface at a particular grid point on a given day. When the surface of the earth is actually at pressures less than 1000 mb, the NMC analysis will nevertheless place non-zero winds

beneath the topography. These spurious winds have been included in our [u] data, but a test in which we removed them from a short period of data revealed that their presence alters M by no more than about 1%. On the other hand, when the 1000 mb level happens to lie above the earth's surface, our approach neglects the contribution to M made by the part of the atmosphere at pressures greater than 1000 mb. Because, however, the average surface pressure over the globe is around 985 mb (Trenberth, 1981a), this error is small.

As we noted above, another source of error in our values of M results from inaccuracies in the basic NMC grid point wind analyses themselves. Although NMC incorporates measurements from an extensive observing network, large data gaps still exist, particularly over the oceans. Therefore, the analyses over such areas are bound to be imperfect. Nonetheless, our examination of an early version of the NMC global analysis over the Northern Hemisphere did not reveal any obvious defects in the zonal wind field (Rosen and Salstein, 1980). Some aspects of the analysis error in a more recent version of the NMC analysis are presented by McPherson et al. (1979), but it is difficult to estimate from their discussion what the magnitude of the error in M is likely to be. Oort (1978) examined the adequacy of the rawinsonde network for determining circulation statistics and found that the most significant error in M was on the order of 5% and caused by the presence of spatial gaps in this network. Although Oort's study was not based on the NMC analysis and did not account for the effect of satellite observations, his result does provide some basis for estimating the size of the random errors in our M values. The comparisons between the NMC analysis and that of the British Meteorological Office made by Hide et al. (1980)

are also revealing in this respect. Differences as large as 10% between the two analyses did occasionally occur, but much of this appeared to be systematic in nature.

Occasional procedural changes at NMC during the six-year period introduce an unknown degree of heterogeneity to our data. Major changes occurred in September 1978 and May 1980 when new analysis methods were introduced (again see McPherson et al., 1979; also Sela, 1980), but other important modifications have also been made that were not always well documented. In addition, there have been continuing changes in the satellite observing systems used by the NMC analysis. For the most part, though, we feel that these sorts of changes have little impact on day-to-day variations in our M values.

In summary, we believe that we may be systematically underestimating the mean value of M by about 10%. Random errors that affect our estimates of most short-term changes in M are probably less than 10%.

3. Results for Atmospheric Angular Momentum

All available values of M for each of the calendar years 1976-1981 are plotted in Figs. 1(a)-(f). In addition to the global atmospheric momentum values, time series are also plotted for the angular momentum of the atmosphere above the Northern Hemisphere (NH) and the Southern Hemisphere (SH). (The scale on the right in the figure gives the equivalent measure of M in terms of inferred changes in the length of day; more on this in section 4.)

Perhaps the most striking feature displayed in Fig. 1 is the annual signal in the global M values. Largest values occur in December or January, and the smallest in July or August. This pattern occurs

because the momentum time series of the two hemispheres are far from being mirror images. Although the annual wave in each hemisphere peaks in its respective winter season, its amplitude is clearly much larger in the NH. In the SH, the peak in the time series is generally quite broad and values in the SH winter are typically only 25% larger than in the summer. Presumably, this contrast between the two hemispheres is related to their very different distributions of land and ocean. Our results for the SH appear to be supported by those derived by Swanson and Trenberth (1981a) from the SH geopotential height analyses of the Australian Weather Bureau. They find that the SH winter westerly geostrophic jet is only 25% stronger than the summer jet at upper levels, whereas at 500 mb and below the maximum winds actually occur during the SH summer (albeit at more northerly latitudes than in the winter, thereby diminishing their effect on M). A final note regarding the hemispheric differences in Fig. 1 is that instances occur during which the relative momentum of the atmosphere above the NH is actually negative; this never happens over the SH.

The dominance of the annual signal in the time series for global M is clearly evident when we compress our data into a single plot. This is done in Fig. 2, wherein we present all our M values for the five-year period 1 January 1976 through 31 December 1980.[1] One feature of the annual signal made especially visible in Fig. 2 is its departure from a pure sinusoidal form, with its peaks tending to be broader than its valleys. It is clear, too, that interannual variations in M exist. An obvious example is afforded by the anomalously low M values during the first part of 1976. Inspection of Fig. 1 reveals this is due mainly to

---

[1] Because we acquired the data for 1981 just recently, they have not been included in Fig. 2 nor in any of the subsequent analyses presented here. The data for 1976-80 are tabulated in Rosen and Salstein (1981).

behavior in the SH, although NH momentum values are also somewhat depressed at this time. Since observations are particularly sparse over much of the SH, one may well question the reality of this anomaly. On the other hand, Krueger (1982) has analyzed monthly mean values of global M back to early 1975 and finds that the behavior of M during the period from late 1975 through 1976 resembles that of some other atmospheric indices including a measure of the Southern Oscillation.[2] Also, using analyses by the Australian Weather Bureau, Swanson and Trenberth (1981b) find that the geostrophic westerly zonal wind component was anomalously weak during early 1976 throughout the depth of the SH subtropics. Although there is some indication (Anderson, 1982) that the NMC wind analysis in higher SH latitudes may have been faulty during this period, we have chosen in the face of inconclusive evidence simply to accept the M data for 1976 as they stand here.

Higher frequency variations are, of course, also present in the M time series. Returning to Fig. 1, for example, a small diurnal component is visible when most of the curve is contrasted with a period when only once-daily data were available such as April through mid-August 1977. A fairly large fluctuation of about 50 days may also be seen at times, for example during 1981 when it is particularly strong. We will have more to say about this 50-day fluctuation in later sections, but first let us consider more generally a time series of M from which the large annual signal has been removed. To construct such a series, we began by forming the average of all available 0000 GMT values of M in each successive 3-day period for 1976-80. Aside from filtering out contributions

---

[2]Utilizing monthly mean winds for May 1963-April 1973, Stefanick (1982) also finds a relationship between M and the Southern Oscillation.

by very high frequencies (according to Table 1, fluctuations with periods of less than 3 days contain only about 2% of the total variance in the full M time series), this procedure also provides a convenient means for bridging gaps in the original time series. Thus, although 10% of the once-daily data were missing during the 5-year (1827 day) period, only five of the 609 3-day periods had no data (M values for these were assigned by interpolating surrounding 3-day means).

To define the annual signal, we averaged the corresponding 3-day means from each of the five years. This signal was then subtracted from the original 3-day mean values to yield the result in Fig. 3. The variance remaining in this residual data set is about 15% of that contained in the original time series of M displayed in Fig. 2. Much of the variability in Fig. 3 appears to be associated with the near 50-day fluctuation noted earlier. Clearly, its phase and amplitude change considerably throughout the record.

A quantitative assessment of the frequencies present in Fig. 3 may be obtained, of course, through use of spectral analysis techniques. Because we wished to place confidence limits on our estimate of the spectra and because our data are limited to a five year period, we decided to adopt an analysis technique that would focus on fluctuations with periods shorter than about 100 days, roughly 1/18 of the length of our record. Our approach follows that outlined by Welch (1967). We first organized our time series of 3-day mean values of M for 1976-80 into eight overlapping blocks spanning most of these five years. Each block consists of 128 consecutive values of the 3-day means multiplied by a weighting function suggested by Welch which sets the endpoints of each block to zero. A fast Fourier transform method was then applied to determine the

Table 1

Mean, standard deviation and variance of global M during 1976-80 (00 GMT only)

Sampling Period	Number of Available Observations	Mean 10^{26} kg m^2 s^{-1}	Standard Deviation 10^{26} kg m^2 s^{-1}	Variance 10^{50} kg^2 m^4 s^{-2}
Once-daily	1643	1.400	0.249	6.214
3-day means	609	1.398	0.247	6.085
3-day means, annual signal removed	609	0.000	0.097	0.940

power spectrum in each block. Lastly, the resulting eight spectra were averaged to produce a final result.

By organizing our data into smaller blocks, the possibility is lessened that shifts in the phase of a particular frequency during the course of the entire record will act to reduce the power perceived at that frequency. Another advantage of the approach followed here is that it permits the statistical significance of peaks in the spectrum to be readily assessed. We do so by first making a power-law best fit to the spectrum (except for its highest frequencies), in concert with the known (Ward and Shapiro, 1961) red-noise nature of most meteorological time series. We then obtain confidence limits about this best-fit curve by applying Welch's model of the spectrum expected from random noise.

We present the final results of our spectral decomposition of M for oscillations with periods of from 6 to 128 days in Fig. 4. Spectra of atmospheric momentum fluctuations on periods of two months and longer were presented by Lambeck and Hopgood (1981) based on monthly mean values of M. Our data, of course, can reveal higher frequency components, and as the figure demonstrates several peaks in the 6-128 day range, such as the prominent one near 30 days, do approach or exceed our 95% level of statistical significance. Of particular note is the rather broad peak centered at about 50 days, confirming our earlier qualitative remarks about the presence of this signal. (The strength of the 50-day peak would likely have been even larger had we included the 1981 data in our analysis, given the obviously strong presence of this signal in Fig. 1f.) We should remark, of course, that passing a test of statistical significance does not guarantee that a particular fluctuation results from an underlying physical mechanism. Additional support for the reality of

the 50-day fluctuation, however, is provided by studying independent measures of the rotation rate of the solid earth. More about this matter is discussed in the next section.

4. Relationship Between Changes in the Momenta of the Atmosphere and Solid Earth

As we discussed at the outset, there have been a number of studies relating changes in the atmosphere's momentum to changes in the rotation rate of the solid earth. The simplest model relating these two is to treat the (rigid) earth and atmosphere as a closed dynamical system and assume that a change ΔM in the angular momentum of the atmosphere is accompanied by an equal, but opposite, change in the angular momentum of the earth. The consequent change in the angular velocity ω of the surface of the earth is given by:

$$\Delta\omega = \frac{-\Delta M}{I} \qquad (2)$$

where I is the principal (axial) moment of inertia of that portion of the earth that responds to the change in M on the time scale being considered. Here we are mostly interested in time scales on the order of one year or less, and fluctuations on these periods are thought to affect only the earth's crust and mantle (i.e., its shell) and not its core (Hide et al., 1980). Following Langley et al. (1981b), therefore, we have set $I = I_{shell} = 7.04 \times 10^{37}$ kg m^2.

It has become customary to speak of changes in the solid earth's rotation rate not in terms of $\Delta\omega$ but rather in terms of changes in the length of day (Δl.o.d.). The two are simply related by:

$$\frac{\Delta 1.o.d.}{1.o.d.} = \frac{-\Delta\omega}{\omega + \Delta\omega} \simeq \frac{-\Delta\omega}{\omega} \quad . \tag{3}$$

Combining (2) and (3) and setting 1.o.d. = 86400 s, $\omega = 7.29 \times 10^{-5}$ s^{-1} and I as above, we find the following linear relation between ΔM and the Δ1.o.d. associated with it:

$$\Delta 1.o.d. \simeq \frac{1.o.d.}{\omega I} \Delta M = 1.68 \times 10^{-29} \Delta M \tag{4}$$

where Δ1.o.d. is in units of seconds and ΔM is in kg m^2 s^{-1}. Noting from Table 1 that the mean value of M during 1976-80 was $\sim 1.4 \times 10^{26}$ kg m^2 s^{-1}, we may infer from (4) that were this amount to be transferred entirely to the earth's shell the 1.o.d. would change by 2.3 ms.

For convenience, we have chosen to reckon ΔM as changes in M from a hypothetical base state in which M = 0. Using this definition in (4) allows us to equate the time series of M values directly in terms of their implied changes in 1.o.d. from this base state, and we have done so in the scale drawn along the right-hand ordinate of Figs. 1-3. The question naturally arises then as to how closely these inferred values of Δ1.o.d. compare with those determined directly through astronomical measurements.

The classical technique for measuring changes in the earth's rotation is based on observing the transit times of stars at a network of astronomical observatories. This approach and the results derived from it have been reviewed by Lambeck (1980). Recently, two other space-based techniques have begun to provide values of Δ1.o.d. One of these is very long baseline interferometry (VLBI), in which different

antennas receive radio emissions from the same distant quasar (Robertson and Carter, 1982). The other technique involves measuring the time required by a laser beam to travel from the earth to a satellite and reflect back. The satellite can either be a specially designed artificial one, as in the case of the Lageos satellite (Smith et al., 1979; Schutz et al., 1981), or the Moon, which was equipped with mirrors placed by the astronauts (Mulholland, 1980; Langley et al., 1981a). Values of Δl.o.d. at 5-day intervals for the 1976-80 period determined by lunar laser ranging (LLR) have been kindly provided to us by R.B. Langley and colleagues at M.I.T. and, therefore, serve as a convenient data set for us to use. The fortnightly and monthly tidal terms have been removed from these data, and the resulting values are plotted in Fig. 5 along with our own time series of Δl.o.d. inferred from M through (4).

We should first point out that the zero level on the scale for each curve in Fig. 5 is arbitrary. The curve using the M data is, as we noted above, reckoned from the hypothetical base state in which $M = 0$; the curve using the LLR data measures the length of day in excess of that of the mean solar day during the nineteenth century, which by convention is 86400 s (Hide et al., 1980). The mean levels of the two curves in the figure do happen to be close, but of course we should not conclude from this that M was zero on the average during the nineteenth century. Rather, it is clear that torques other than those imparted by the atmosphere must be important in affecting the rotation rate of the shell on these decade and century-long time scales. Even for the five year period shown in Fig. 5, the LLR curve shows evidence of a trend that is not apparent in the M curve, again implying that (4) oversimplifies the situation that exists on time scales beyond about a year.

On time scales shorter than a year or so, however, the two curves in Fig. 5 agree quite well. Certainly they both contain similar annual signals. The resemblance between the two curves at higher frequencies may be more strikingly displayed if the mean levels and annual and semi-annual variations are removed from each and the residuals smoothed, as Langley et al. (1981b) do for each of the years 1976-79[3]. We reproduce their result here as our Fig. 6. The most prominent feature in this figure is the close correspondence in the amplitude and phase of the two curves on periods of about 50 days. The agreement is particularly good during 1979, the year of the Global Weather Experiment in which more extensive observations may have resulted in improved NMC wind analyses. Interestingly, the other astronomical measures of Δl.o.d. mentioned before also exhibited the nearly same ∿50-day fluctuation during 1979 (Feissel and Gambis, 1980). We gain confidence, therefore, in the reality of this fluctuation in our M time series. In fact, we can more generally conclude on the basis of the comparisons here (and in Feissel et al., 1982, between our M data and the classical technique for measuring Δl.o.d.) that most of the variability in our M data is realistic, at least on time scales from about a week to a year where support is offered by the independent data sets. We may also conclude from Fig. 6, as do Langley et al. (1981b), that the differences between the two curves lie within their combined uncertainties and that contributions from non-atmospheric torques on the time scales displayed can probably be discounted.[4]

---

[3] A guassian-shaped low-pass filter with a window width of about 8 days was used in the smoothing.

[4] Recall, though, that the large effects associated with tidal induced changes in the earth's moment of inertia on fortnightly and monthly periods have been removed from the observed (LLR) changes in l.o.d.

Finally, we should note that the approach followed here does not shed any new light on the manner in which momentum is exchanged between the atmosphere and solid earth. We have simply demonstrated that such an exchange must be taking place. Swinbank (1981), however, has recently examined the roles played by the two major torques (surface friction and mountain) that must be responsible for the momentum exchange. Using daily data for the two special observing periods of the Global Weather Experiment (a total of about four months during 1979) and a suitable model for the frictional torque, he shows that most of the variability in the rate of change in M is due to the mountin torque. Friction, although of comparable magnitude to the mountain torque, is however much steadier, and it does not correlate at all well with the time derivative of M. Naturally, it would be desirable to extend Swinbank's study to other periods and to other models of these torques.

5. Variations of Angular Momentum within the Atmosphere

a. Variations in latitude-height cross sectional boxes

Thus far we have dealt with the atmosphere's momentum on either global or hemispheric spatial scales. To understand more about the reasons for the fluctuations observed in these large-scale statistics, however, it is necessary to examine the atmosphere on smaller scales. For example, the origin of the ∿50-day variation in M cannot be explained on the basis of these global values alone. On the other hand, Madden and Julian (1971, 1972) have reported that such a periodicity existed in several tropical station upper-air wind reports during 1957-67,[5] thereby

[5] It was on the basis of this work by Madden and Julian, in fact, that Lambeck and Cazenave (1974) first suggested there might be atmospheric forcing of a ∿50-day fluctuation in l.o.d.

providing a regional focus for further study of this particular phenomenon. We are, of course, interested in studying initially the entire broad range of fluctuations present in our atmospheric data, and so we have not specially isolated any one periodicity for detailed scrutiny here.

Our first step in studying the structure and behavior of the field of momentum within the atmosphere was to compress our zonal mean wind data set. With values of [u] available at 73 latitudes and 10 pressure levels, we could conceivably deal with 730 different time series. This amount of data, however, would have proven too cumbersome for the analysis approach we planned to use, and so we took advantage of the known spatial cohesiveness of large-scale atmospheric motions to congregate the 730 grid points into 27 equal mass "boxes." These boxes were formed by dividing the atmosphere into three equal mass layers in the vertical (1000-700 mb, 700-400 mb, 400-100 mb representing the low, middle and upper troposphere, respectively) and nine equal area belts in the horizontal with boundaries at 6.4°, 19.5°, 33.7°, 51.1° and 90° in each hemisphere. For simplicity, we will refer to the zones delimited by these latitude circles in the following way: 6.4°S - 6.4°N, equatorial; 6.4° - 19.5°, tropical; 19.5° -33.7°, subtropical; 33.7° - 51.1°, mid-latitude; and 51.1° - 90°, high latitude. We recognize the possibility that this scheme may stratify our data too severely to investigate properly the structure of the momentum field. Preliminary calculations with the full 730 grid point data set by us and work by Anderson (1982) with these same data suggest, however, this is generally not the case. Finally, we note that the zones and layers we are using do correspond roughly to the broad climatological regions of the general circulation.

We next computed the angular momentum of the atmosphere within each box, B, viz:

$$m_B = \frac{2\pi a^3}{g} \int_B [u] \cos^2 \phi \, dA \qquad (5)$$

where dA is an elemental area of the box in the pressure-latitude plane. We will refer to m_B as the momentum density. To evaluate (5) numerically, we applied the trapezoidal rule in the pressure and latitude coordinates piecewise between the 730 data points, being careful to ensure that $\sum_{27 \text{ boxes}} m_B = M$ each day.

We have chosen here to work entirely with 3-day means of the once-daily (00 GMT) m_B values, which we formed in the same manner described in section 3 to construct 3-day means of M. A plot of the 5-year mean momentum density field based on these data for 1976-80 is given in Fig. 7. The figure reflects the well-known main features of the general circulation: low-level easterlies in the equatorial and tropical regions, and zonal mean westerly jets farther poleward in the upper troposphere of each hemisphere. The variance of the m_B time series in each box for 1976-80 is displayed in Fig. 8. The maxima in this field are clearly associated with the zonal mean jets. Moreover, it is evident that although m_B is larger in connection with the SH jet, it is more variable in the region of the NH jet.

We wish to examine the spatial and temporal relationships that link the behavior of the m_B time series in the different boxes and give rise to the variance values in Fig. 8. To this end, we have adopted an analysis approach, known as empirical orthogonal function (EOF) or principal component analysis, that yields modes which can identify patterns of

large-scale variability. A major advantage this approach has over the more conventional one of expanding data in terms of a pre-chosen set of analytic functions is that the EOFs explain the variance in the data in the most efficient manner possible. We will not detail the basis of the approach here (Lorenz, 1956 and Kutzbach, 1967 are excellent references for this), but we will briefly outline the manner in which we have applied it. First we formed a 27 x 27 covariance matrix by removing the mean value from each m_B time series and then multiplying the resulting m_B anomaly series in each box by itself and by that in every other box. This matrix is then diagonalized and its eigenvalues and eigenvectors (the EOFs) found. The anomaly data are then projected onto each eigenvector to determine the time series associated with it. The amount of the variance in the original data explained by each eigenvector is equal to the variance in the vector's associated time series, but it is more usual to compute the percent of the total variance explained by each vector by simply taking the ratio of its eigenvalue to the sum of all the eigenvalues.

Fig. 9 presents the first mode of the variability in the momentum density field for 1976-80 and its associated time series. It is clear from the time series that this mode is mostly depicting the annual signal in the field. The vector, which explains 81.5% of the total variance in the data, displays two main centers of action, one in the subtropical upper troposphere of each hemisphere.[6] This result and the fact that the NH center is the larger may, of course, have been anticipated on the basis of the picture in Fig. 8 of the m_B variance. Note

[6]Each EOF mode has been normalized so that the sum of the squares of the 27 non-dimensional box values is unity.

finally with regard to Fig. 9 that the two centers have opposite signs, so that when the momentum is larger than average in the NH (as in the NH winter when the positive value in the NH center is multiplied by a positive value in the time series), it is smaller than average in the SH (since the positive value in the time series now multiplies a negative value in the SH center) and vice versa.

The second EOF is presented in Fig. 10 along with its time series and a spectrum of the time series determined in the same manner used to derive the global M spectrum. This mode explains 5.7% of the variance in the m_B data, or nearly 1/3 of the variability left unexplained by the first mode. Unlike the first mode, the major contribution to mode 2 is made by the SH tropical and subtropical upper-troposphere regions, with these acting in phase with their counterparts in the NH. Many of the statistically significant periodicities evident in the global M spectrum (Fig. 4), including the one near 50 days, reappear here in connection with this EOF.

Rather than presenting the EOFs remaining beyond mode 2 at this stage, it seems prudent instead to first remove the large annual signal from the m_B data before examining them much further. We defined an annual signal in each of the 27 m_B time series in the same manner described in section 3 in connection with our M data (i.e., each 3-day mean value in the first year was averaged with the corresponding 3-day mean values in succeeding years). These annual signals were then subtracted from the original time series. The variance remaining in these residuals is plotted in Fig. 11. Removing the annual signal has clearly reduced the variance in the field a great deal, although the patterns in Figs. 11 and 8 remain similar. To study the basis for the structure in Fig. 11

further, we have subjected the m_b residual data to the same sort of EOF analysis we applied above to the total (i.e., including annual signal) m_B data.

Although 26 independent EOFs can be derived in our analysis, many of these can be expected to depict mostly noise in the data that happens by chance to be correlated among some of the 27 boxes during the (finite) study period. We, of course, are interested in studying only those EOFs that are likely to owe their existence to the presence of some underlying physical mechanism. Recently, we (Salstein et al., 1982) and Overland and Preisendorfer (1982) have stressed the importance of determining the statistical significance of individual EOFs to separate those that might be meaningful from those that are not. Our approach here is to construct for each box a time series of normally distributed random numbers whose mean and variance are equal to those of the real m_B residual data. These 27 independently derived series of random numbers are then submitted to an EOF analysis yielding an eigenvalue corresponding to each mode. After repeating this experiment a number of times with different sets of random numbers, we noticed that the collection of eigenvalues corresponding to each mode number tended to cluster about the same value. We decided, therefore, simply to select the largest eigenvalue obtained for a mode from 10 experiments as the level of statistical significance required for that mode number. As Fig. 12 illustrates, the first six modes of the m_B data with the annual signal removed passed this test for significance. Beyond mode 6, however, the eigenvectors explain no more of the variance in the data than would vectors obtained from a random set of numbers. We, therefore, discuss only modes 1 through 6 here.

These pictures of the modes of non-seasonal variability in the momentum density field are contained in Fig. 13. The time series associated with each of the modes is presented in Fig. 14, and a spectrum of each time series in Fig. 15. Not surprisingly, mode 1 in Fig. 13 resembles the picture in Fig. 10 of the second EOF for m_B before the annual signal was removed. The resemblance is not perfect, however (especially when their respective time series are compared). The spectra are quite similar, though, indicating the expected result that the annual signal as we define it contains little power at higher frequencies. We prefer to view the vector in Fig. 13 as the better for depicting the major mode of non-seasonal variations in m_B. The maxima in this mode are located in the same regions as the maxima in the variance field of the filtered data (Fig. 11), although in the EOF the magnitudes of the SH centers are larger than the one in the NH. The large values of mode 1 (and the variance) in the SH mid-latitudes appear to be related, at least in part, to the anomalous behavior in M during 1976. In light of our earlier discussion about the uncertainty in the reality of this anomaly, we suggest caution in relying too strongly on our results for the SH mid-latitude boxes. Finally, with regard to the spectrum for mode 1, we should note especially the presence of the significant peak near 50 days. Unfortunately, the analysis approach we have chosen here is inadequate for isolating further which subset of the boxes is most responsible for this particular periodicity. The work by Madden and Julian referenced earlier and the recent study by Anderson and Rosen (1982), however, strongly suggest the large values in the tropical boxes in Fig. 13a are related to this phenomenon.

The somewhat muted role in mode 1 played by the NH sub-tropics, despite the maximum there in the m_B variance, appears to be largely compensated for by this region's role in mode 2 (Fig. 13b). The value reached by the NH subtropical, upper-troposphere box in this mode is, in fact, the largest to be found in any of the fields in Fig. 13. The striking feature about the spectrum of the mode 2 time series is its large peak around 30 days. Given the major role of the NH subtropics in this mode (the three boxes in this belt account for 64% of the variance in the mode), we can infer this region is responsible in large measure for this periodicity.[7] Interestingly, the next most important region in the mode 2 vector is the SH mid-latitudes, which has the same sign as the NH subtropics. Trenberth (1981b) has demonstrated that this area does contain a considerable amount of variance on time scales of 8-64 days in such fields as 500 mb geopotential height and kinetic energy. Our results for this region here for mode 2 and earlier for mode 1 are not inconsistent with this.

Although modes 3 through 6 explain successively smaller amounts of the variance in m_B, they nonetheless depict large-scale cohesive patterns of behavior. In mode 3, the NH mid-latitudes are highlighted for the first time. The very significant peak in the mode 3 time series spectrum near 13-14 days is due mostly to behavior in this region. This periodicity corresponds closely to that found by Miller (1974) in time series of various measures of the troposphere's energy cycle north of 20° N, and attributed by Miller to lunar tidal forcing mechanisms and/or amplitude vacillation of tropospheric wave patterns.

---

[7] An independent check of the m_B time series spectrum for the NH subtropical, upper-level box confirms the presence of a significant peak near 30 days.

The mode 4 vector is noteworthy for its remarkable degree of symmetry about the equator and striking banded structure. In mode 5, the maximum in the SH high latitudes is out of phase with the rest of the hemisphere. Interestingly, the spectrum of this mode is distinguished by its lack of strong peaks. In mode 6, the SH high latitudes are again at a maximum, but this time they are in phase with the rest of the hemisphere. The strong influence of the SH high latitudes in both modes 5 and 6 calls for some caution in light of the sparsity of observations there.

A striking aspect of the mode 6 vector is its largely uniform sign over the globe. In fact the sum of the 27 box values in mode 6 is larger than that in any other vector. This raises an important point regarding the relative importance of these vectors in explaining the variance in the global M time series. Our analysis approach, of course, has selected those eigenvectors that explain most efficiently the variance in the field of m_B values, not in M, which is the global sum of this field. Therefore, a vector that explains a large portion of the variance in the density field need not be important with regard to the behavior of M if that vector consists of elements that mostly balance each other, i.e., if the variability depicted by the vector in one part of the atmosphere is of opposite sign to equally strong variability in another part of the atmosphere. As we show in the Appendix, the amount of the variance in M explained by each of our density field eigenvectors is proportional to $\lambda_i \mu_i^2$, where λ_i is the eigenvalue of the $i^{\underline{th}}$ vector and μ_i is the sum of the 27 box values in the vector (which we may think of as the globally integrated momentum associated with that vector). The relative role played by each of our six modes in terms of explaining the variance

in M can, therefore, be readily evaluated; the result of "reordering" the vectors in this way is shown in Table 2. Note in this context the increased importance of mode 6, now just below that of mode 2. We will have more to say about this result in the following subsection.

b. Variations in zonal belts

Earlier, we mentioned our desire to compress the zonal mean wind data set to make our analysis more tractable. We chose to do so in the form of boxes because we were uncertain of the structure, both horizontal and vertical, of the EOFs that might emerge. Viewing the significant box modes 1-6 in Fig. 13, however, it is now clear that their vertical structure is quite regular. This allows us to suppress the vertical component of variability in the data, by dealing with vertically integrated fields, without much loss of information. At the same time, we gain the freedom to use a finer horizontal resolution than in our box analysis while still retaining a manageable data set. Thus, we divided the atmosphere into as many belts as our data would allow, and we computed the angular momentum of the atmosphere between 1000 and 100 mb in each belt for every day from 1976-80.

Because we wished our belts to intersect equal surface areas on the earth[8] and because our zonal mean wind data are at 2.5° latitude intervals, we constrained all our belts to have the same area as the one between the equator and 2.5° N. Forty-six zonal belts over the globe emerge in this manner. Their latitudinal boundaries are listed

[8]The use of data that are distributed evenly over an area avoids the problem of "weighted double-counting" mentioned by Johnston (1981).

Table 2

Relative importance of modes 1-6 of box analysis (annual signal removed) in explaining variance in M

Mode #	Eigenvalue (λ) 10^{48} kg^2 m^4 s^{-2}	μ	% of total M variance explained
2	8.83	1.847	32.0
6	3.60	2.852	31.2
4	4.96	1.724	15.7
1	11.04	0.957	10.8
5	4.20	0.408	0.7
3	7.48	-0.151	0.2
Sum			90.6

in Table 3. Within each belt, we computed the angular momentum of the atmosphere, m_b via

$$m_b = \frac{2\pi a^3}{g} \int_b \int_{1000\ mb}^{100\ mb} [u] \cos^2 \phi \, dp \, d\phi \qquad (6)$$

where ϕ runs between the southern and northern boundaries of belt b. As for m_B, we evaluated (6) by applying a trapezoidal rule (in latitude) in such a way that $\sum_{46\ belts} m_b = M$ each day. Also as for m_B, we deal only with 3-day means of once-daily m_b values here.

The 5-year mean distribution of m_b and its standard deviation are given in Fig. 16. As in the field of m_B, the maximum m_b values can be identified with the zonal mean jets of each hemisphere, although we can now resolve the position of these maxima more precisely as lying in the vicinity of 40° S and 37° N. Again, the SH maximum is larger, but the NH one is more variable. Most of this variance is associated with the annual signal, as the comparison in Fig. 17 shows.

We performed an EOF analysis on the full m_b time series in the same manner used with the box data. The first two modes (each normalized so that the sum of the squares of their 46 belt values is unity) and their associated time series are contained in Fig. 18. The first mode identifies the spatial structure of the annual signal, and both it and mode 2 closely parallel their analogs for m_B in Figs. 9 and 10.

Upon removing the annual signal, we find that the first eight modes pass our test of statistical significance (Fig. 19). These modes are depicted in Fig. 20, their time series in Fig. 21, and spectra of the time series in Fig. 22. Modes 1 and 2 closely resemble their counterparts in the box analysis and little more need be said of them. Modes 3

Table 3

Latitudinal boundaries used to define
46 equal area belts on the globe

Belt	Latitude limits (either °N or °S)
1	73.0 - 90.0
2	65.9 - 73.0
3	60.4 - 65.9
4	55.7 - 60.4
5	51.5 - 55.7
6	47.7 - 51.5
7	44.1 - 47.7
8	40.7 - 44.1
9	37.5 - 40.7
10	34.4 - 37.5
11	31.4 - 34.4
12	28.6 - 31.4
13	25.8 - 28.6
14	23.0 - 25.8
15	20.4 - 23.0
16	17.7 - 20.4
17	15.1 - 17.7
18	12.6 - 15.1
19	10.0 - 12.6
20	7.5 - 10.0
21	5.0 - 7.5
22	2.5 - 5.0
23	0.0 - 2.5

in the belt and box analyses are also similar, although the NH mid-latitude maximum in the latter is not so pronounced in the former, where in fact the largest value now occurs in the 55.7-60.4° S belt. By mode 4, significant differences between the belt and box analyses begin to appear. In particular, the maximum at the equator in box mode 4 does not exist in the belt mode. The fact that such differences between the two analyses exist should not be surprising though, in light of the additional degrees of freedom (and number of significant modes) in the belt data.

Interestingly, the major features in mode 6 of the belt analysis are similar to those in the box analysis mode 6. Some differences in detail do exist (for example in SH mid and high latitudes), and there are some notable differences between the spectra of their time series. One important similarity belt mode 6 shares with its counterpart, though, is its importance in explaining non-seasonal changes in global M. In fact, as Table 4 shows, belt mode 6 alone explains almost half of these changes, more than twice the amount explained by the next largest "reordered" mode. This result is all the more remarkable when it is realized that (a) our analysis approach has not been specifically designed to evaluate modes of global M change and (b) mode 6 explains but 6.9% of the variability in m_b. The implication of the latter is that non-seasonal changes in M on the time scales viewed here result to a considerable extent from relatively small imbalances among regional variations in momentum. Much of the more important changes in momentum density, in the sense of large-scale cohesive changes that are depicted by modes 1-5, actually cancel each other in the context of a global integral. Only after these five modes, which in total explain 73% of the m_b variance,

Table 4

Relative importance of modes 1-8 of belt analysis (annual signal removed) in explaining variance in M

Mode #	Eigenvalue (λ) 10^{48} kg^2 m^4 s^{-2}	μ	% of total M variance explained
6	2.47	4.186	46.0
2	6.46	1.748	21.0
3	5.04	1.704	15.6
8	1.57	-2.241	8.4
1	7.29	0.519	2.1
7	1.69	0.556	0.6
5	2.80	-0.369	0.4
4	4.33	0.025	0.0
Sum			94.1

are accounted for does the pattern emerge that explains the bulk (i.e., 46%) of the variability in global M (annual signal removed; Fig. 3).

The contribution made by each belt to the non-seasonal changes in M can, of course, be determined directly by computing the covariance between the time series of m_b and M, after removing their annual signals. Note that the sum of these 46 covariances will yield the variance in M with its annual signal removed (0.94×10^{50} kg^2 m^4 s^{-2} from Table 1). These covariances are plotted in Fig. 23, along with a plot of the covariance between m_b and M when besides the annual signal, interannual fluctuations are also removed (by averaging the covariances determined separately for each of the years 1976-80). Comparing the two curves reveals generally small differences, indicating that most of the behavior shown is associated with non-seasonal fluctuations on time scales of less than a year. An exception occurs in the vicinity of 50° S where much, but not all, of the difference can be attributed to the 1976 anomaly discussed in section 3. Finally, we note that the pattern of the covariance curve (annual signal removed) in Fig. 23 can be mathematically related to the EOF patterns in Fig. 20. Treating the covariance curve as a 46-component vector, we show in (A11) in the Appendix that the dot product between it and the $i^{\underline{th}}$ eigenvector is given by $\lambda_i \mu_i$. Referring to Table 4, it is apparent, therefore, that the covariance curve is shaped largely by modes 2, 6 and 3 (in that order). In any case, Fig. 23 clearly illustrates that the largest contributions to non-seasonal variations in M on time scales of less than a year come from the subtropics of each hemisphere. The strong influence of the SH in forcing both interannual and higher frequency non-seasonal changes in so funda-

mental a parameter as M argues, of course, for increasing efforts to observe the atmosphere in that half of the world.

6. Concluding Remarks

We have diagnosed the behavior of the atmosphere's angular momentum during the past several years on time scales as short as a day. Our ability to focus on the higher frequency changes in M is a novel aspect of this study and was made feasible only by the development at NMC of routine global analyses which include the basic wind fields. Fortuitously, this development has coincided with major improvements in techniques by geodesists for measuring earth rotation. The variations we detected in M could therefore be checked against independent values of changes in the length of the day. By and large, the data sets do compare favorably on time scales of less than a year or so, thereby providing not only a confirmation of the theory relating ΔM and $\Delta l.o.d.$ but also a measure of confidence in the quality of these data sets. Naturally, it would also be desirable to test the NMC-based momentum values against those obtained from analyses by other meteorological services, such as Hide et al. (1980) did for a brief period. Not only would this enable more definitive error bars to be placed on the calculation of M, but also it would provide a focus for examining differences between the meteorological analyses.

We have also gone beyond the study of atmospheric momentum integrated over the whole globe to consider the manner in which fluctuations in momentum on regional scales are interrelated. The most obvious such fluctuation involves the seasonal change in the major jets of both hemispheres, with the asymmetry in these signals giving rise to the dominant

signature in M. To identify regional fluctuations in momentum beyond those connected with the annual cycle, we adopted an empirical orthogonal function technique to compute the major modes of variability in the momentum density field. We have not attempted here to focus in depth on the structure of any one particular periodicity. To do so, we might have considered analyzing directly the time series of the density field in each box or belt or, better still, have pre-filtered our zonal wind data so as to pass only the period of interest. The latter approach has, in fact, been taken by Anderson and Rosen (1982) in connection with the ∿50-day periodicity. They applied a band-pass filter centered at about 45 days to our zonal wind data and found that this periodicity appears to originate in the tropics and then propagates (in phase) to NH mid-latitudes. (A large component of the 50-day periodicity also exists in the SH mid-latitude band-pass data, but unlike its NH counterpart it does not appear to be linked coherently with the tropical fluctuation.) The EOF analysis used by us here, of course, has not been designed to reveal such propagating phenomenon, since it utilizes only contemporary covariances among the momentum density field variations.

We are inclined to look to processes within the atmosphere for an explanation of the various fluctuations present in the M and Δl.o.d. time series. On the other hand, we cannot but help notice that significant signals exist near 30 and 14 days in M and some of the EOFs of the density field variations, and that these periods correspond closely to those associated with tides. Perhaps some element of these signals in the atmosphere are forced by tides in the solid earth, but such speculation can be confirmed only by further detailing the atmospheric structure of these fluctuations. This is beyond our present scope.

Our last figure indicates that much of the SH accounts for a considerable portion of the non-seasonal variability in global atmospheric angular momentum. There has been a new appreciation among meteorologists for the importance of the SH in global climate, and Trenberth (1979) has noted the large interannual variability there. Our results for the SH, if generally correct, indicate that indeed a broad range of fluctuations in its zonal wind field exists and is important.

Heretofore, the globally integrated value of atmospheric angular momentum has been more of theoretical interest to meteorologists than of practical consequence. It should be clear by now, however, that M is a fundamental measure of the interaction between the earth and the atmosphere. Importantly, this interaction provides an independent means of checking fluctuations analyzed in M. Moreover, considering the work by Krueger (1982) referenced earlier, it is not unlikely that M may prove itself worthwhile as an index of climate variability. More work needs to be done along these lines, of course, but we feel our efforts here have helped place such inquiry on a firmer foundation.

Acknowledgements. It is a pleasure to acknowledge the generosity and effort of A. J. Miller of NMC in providing us with most of the atmospheric data used here. Our understanding of earth rotation issues has benefitted considerably from exchanges with numerous colleagues including R. Hide, R. Langley and R. King, to whom we are grateful. J. Anderson brought to our attention the existence of the variance relationship derived in the Appendix. Programming support was ably provided by J. Ho. This study was performed under contract NAS5-25870 as part of the Lageos Project of the National Aeronautics and Space Administrat. n. The

support given our interdisciplinary research by the staff of NASA's Geodynamics Program and especially by D. E. Smith, Project Scientist, has been most gratifying.

APPENDIX

1. Variance in M explained by eigenvectors.

Let $\underset{\sim}{B}$ be the PxQ matrix of m_B (or m_b) values, each of whose Q columns is the P-component vector for a 3-day period. Thus, P = 27 for the box analysis and P = 46 for the belt analysis, and Q = 609 for either. Also, let $\underset{\sim}{u}$ be the P-dimensional column vector all of whose elements are equal to 1 and let $\underset{\sim}{M}$ represent the Q-dimensional row vector of the values of global angular momentum M. Since M is the sum of all m_B values,

$$\underset{\sim}{M} = \underset{\sim}{u}^T \underset{\sim}{B} \tag{A1}$$

where the superscript T indicates the transpose of a matrix (vector). The variance, V, in $\underset{\sim}{M}$ can be expressed as:

$$V = Q^{-1} \underset{\sim}{M}\underset{\sim}{M}^T = Q^{-1} \underset{\sim}{u}^T \underset{\sim}{B}\underset{\sim}{B}^T \underset{\sim}{u} = \underset{\sim}{u}^T \underset{\sim}{R}\underset{\sim}{u} \tag{A2}$$

where $\underset{\sim}{R}$ is the PxP covariance matrix formed from the m_B data (i.e., $\underset{\sim}{R} = Q^{-1}\underset{\sim}{B}\underset{\sim}{B}^T$).

Now, let $\underset{\sim}{E}$ be the PxP matrix whose columns are the eigenvectors $\underset{\sim}{e}_i$ of $\underset{\sim}{R}$, which are the EOFs derived in Section 5. Because $\underset{\sim}{E}$ is an orthonormal basis of the box vector space, then $\underset{\sim}{E}\underset{\sim}{E}^T = \underset{\sim}{I}$, the identity matrix, and we can multiply the matrix $\underset{\sim}{R}$ in (A2) by $\underset{\sim}{E}\underset{\sim}{E}^T$, so that

$$V = \underset{\sim}{u}^T \underset{\sim}{R}\underset{\sim}{E}\underset{\sim}{E}^T \underset{\sim}{u} \tag{A3}$$

Furthermore,

$$\underset{\sim}{R}\underset{\sim}{E} = \underset{\sim}{E}\underset{\sim}{L} \tag{A4}$$

where $\underset{\sim}{L}$ is a PxP diagonal matrix whose elements are λ_i, the P eigenvalues of $\underset{\sim}{R}$, and so

$$V = \underset{\sim}{u}^T \underset{\sim}{E}\underset{\sim}{L}\underset{\sim}{E}^T \underset{\sim}{u} \tag{A5}$$

The vector $\underset{\sim}{\mu}$, whose i^{th} element is the sum of the components of $\underset{\sim}{e}_i$ can be written as

$$\underset{\sim}{\mu} = \underset{\sim}{E}^T \underset{\sim}{u} \qquad \text{(A6)}$$

Using (A6) in (A5) we get

$$v = \underset{\sim}{\mu}^T \underset{\sim}{L} \underset{\sim}{\mu} \qquad \text{(A7)}$$

which, when written in terms of components of $\underset{\sim}{L}$ and $\underset{\sim}{\mu}$, yields the relationship we seek:

$$v = \sum_{i=1}^{P} \lambda_i \mu_i^2 \qquad \text{(A8)}$$

2. Relationship of eigenvectors $\underset{\sim}{e}$ to the covariance between m_b and M.

The vector $\underset{\sim}{c}$, consisting of the 46 values of the covariance between m_b and M and displayed in Figure 23 is given by

$$\underset{\sim}{c} = Q^{-1} \underset{\sim}{B} \underset{\sim}{M}^T = Q^{-1} \underset{\sim}{B} \underset{\sim}{B}^T \underset{\sim}{u} = \underset{\sim}{R} \underset{\sim}{u} = \underset{\sim}{E} \underset{\sim}{L} \underset{\sim}{\mu} \qquad \text{(A9)}$$

Multiplying both sides of (A9) by $\underset{\sim}{E}^T$, we get the following relation between two column vectors:

$$\underset{\sim}{E}^T \underset{\sim}{c} = \underset{\sim}{L} \underset{\sim}{\mu} \qquad \text{(A10)}$$

Finally, because the i^{th} element on the left of (A10) is simply the dot product of $\underset{\sim}{e}_i$ with $\underset{\sim}{c}$, we may write

$$\underset{\sim}{e}_i \cdot \underset{\sim}{c} = \lambda_i \mu_i \qquad \text{(A11)}$$

References

Anderson, J.R., Space-Time Structure of Changes in Atmospheric Angular Momentum, S.M. thesis, Dept. of Meteorology and Physical Oceanography, M.I.T., Cambridge, 1982.

Anderson, J.R., and R.D. Rosen, The latitude-height structure of 40-50 day variations in atmospheric angular momentum, submitted to J. Atmos. Sci., 1982.

Etkins, R., and E.S. Epstein, The rise of global mean sea level as an indication of climate change, Science, 215, 287-289, 1982.

Feissel, M., R.D. Rosen, and D.A. Salstein, Changes in the duration of the day as inferred from atmospheric momentum and astronomical evidence, in Annual Report for 1981, Bureau International de l'Heure, pp. D79-D82, Paris, 1982.

Feissel, M., and D. Gambis, La mise en évidence de variations rapides de la durée du jour, Comptes Rendus Hebdomadaires des Seéances de l'Académie des Sciences, Série B, 291, 271-273, 1980.

Hide, R., Towards a theory of irregular variations in the length of day and core-mantle coupling, Phil. Trans. R. Soc. Lond., A284, 547-554, 1977.

Hide, R., N.T. Birch, L.V. Morrison, D.J. Shea and A.A. White, Atmospheric angular momentum fluctuations and changes in the length of the day, Nature, 286, 114-117, 1980.

Johnston, R.J., Regarding the delimitation of regions according to climatic fluctuations, Arch. Met. Geoph. Biokl., Ser. B, 29, 215-228, 1981.

Krueger, A.F., The circulation over the tropics during 1980-81, in Proceedings of the Sixth Annual Climatic Diagnostics Workshop, pp. 32-44, NOAA, Washington, DC, 1982. [NTIS PB82-219486]

Kutzbach, J., Empirical eigenvectors of sea level pressure, surface temperature and precipitation complexes over North America, J. Appl. Meteor., 6, 791-802, 1967.

Lambeck, K., The Earth's Variable Rotation, Cambridge University Press, Cambridge, 1980.

Lambeck, K., and A. Cazenave, The earth's rotation and atmospheric circulation II. The continuum, Geophys. J. R. astr. Soc., 38, 49-61, 1974.

Lambeck, K., and A. Cazenave, The earth's variable rate of rotation: a discussion of some meteorological and oceanic causes and consequences, Phil. Trans. R. Soc. Lond., A284, 495-506, 1977.

Lambeck, K., and P. Hopgood, The earth's rotation and atmospheric circulation from 1963 to 1973, Geophys. J. R. astr. Soc., 64, 67-89, 1981.

Lambeck, K., and P. Hopgood, The earth's rotation and atmospheric circulation: 1958-1980, submitted to Geophys. J. R. astr. Soc., 1982.

Langley, R.B., R.W. King and I.I. Shapiro, Earth rotation from lunar laser ranging, J. Geophys. Res., 86, 11913-11918, 1981a.

Langley, R.B., R.W. King, I.I. Shapiro, R.D. Rosen, and D.A. Salstein, Atmospheric angular momentum and the length of day: a common fluctuation with a period near 50 days, Nature, 294, 730-732, 1981b.

Lorenz, E.N., Empirical orthogonal functions and statistical weather prediction, Sci. Rep. 1, Statistical Forecasting Project, Dept. of Meteorology and Physical Oceanography, M.I.T., Cambridge, 1956. [NTIS AD110268]

Lorenz, E.N., The Nature and Theory of the General Circulation of the Atmosphere, World Meteorological Organization, Geneva, 1967.

Madden, R.A., and P.R. Julian, Detection of a 40-50 day oscillation in the zonal wind in the tropical Pacific, J. Atmos. Sci., 28, 702-708, 1971.

Madden, R.A., and P.R. Julian, Description of global-scale circulation cells in the tropics with a 40-50 day period, J. Atmos. Sci., 29, 1109-1123, 1972.

McPherson, R.D., K.H. Bergman, R.E. Kistler, G.E. Rasch, and D.S. Gordon, The NMC operational global data assimilation system, Mon. Wea. Rev., 107, 1445-1461, 1979.

Miller, A.J., Periodic variation of atmospheric circulation at 14-16 days, J. Atmos. Sci., 31, 720-726, 1974.

Miller, A.J., W. Collins, and D. Dubofsky, The NMC operational global energy program, Office Note 109, National Meteorological Center, Washington, DC, 1975.

Mulholland, J.D., Scientific achievements from ten years of lunar laser ranging, Rev. Geophys. Space Phys., 18, 549-564, 1980.

Oort, A.H., Adequacy of the rawinsonde network for global circulation studies tested through numerical model output, Mon. Wea. Rev., 106, 174-195, 1978.

Overland, J.E., and R.W. Preisendorfer, A significance test for principal components applied to a cyclone climatology, Mon. Wea. Rev., 110, 1-4, 1982.

Robertson, D.S., and W.E. Carter, Earth rotation information derived from MERIT and POLARIS VLBI observations, in High-Precision Earth Rotation and Earth-Moon Dynamics (O. Calame, ed.), pp. 97-122, D. Reidel Publishing Co., Hingham, Mass., 1982.

Rosen, R.D., and D.A. Salstein, A comparison between circulation statistics computed from conventional data and NMC Hough analyses, Mon. Wea. Rev., 108, 1226-1247, 1980.

Rosen, R.D., and D.A. Salstein, Variations in atmospheric angular momentum, 1 January 1976 - 31 December 1980, Technical Report A345-T1, Environmental Research & Technology, Inc., Concord, Mass., 1981. [NTIS N82-11690]

Salstein, D.A., R.D. Rosen, and J.P. Peixoto, Modes of variability in annual hemispheric water vapor and transport fields, to appear in J. Atmos. Sci., 1982.

Schutz, B.E., B.D. Tapley, and R.J. Eanes, Earth rotation from Lageos laser ranging, in Annual Report for 1980, Bureau International de l'Heure, pp. D27-D36, Paris, 1981.

Sela, J.G., Spectral modeling at the National Meteorological Center, Mon. Wea. Rev., 108, 1279-1292, 1980.

Smith, D.E., R. Kolenkiewicz, P.J. Dunn, and M. Torrence, Determination of polar motion and earth rotation from laser tracking of satellites, in Time and the Earth's Rotation (D.D. McCarthy and J.D. Pilkington, eds.), pp. 231-238, D. Reidel Publishing Co., Hingham, Mass., 1979.

Starr, V.P., An essay on the general circulation of the earth's atmosphere, J. Meteor., 5, 39-43, 1948.

Stefanick, M., Interannual atmospheric angular momentum variability 1963-1973 and the southern oscillation, J. Geophys. Res., 87, 428-432, 1982.

Swanson, G.S., and K.E. Trenberth, Trends in the southern hemisphere tropospheric circulation, Mon. Wea. Rev., 109, 1879-1889, 1981a.

Swanson, G.S., and K.E. Trenberth, Interannual variability in the southern hemisphere troposphere, Mon. Wea. Rev., 109, 1890-1897, 1981b.

Swinbank, R., The global atmospheric angular momentum balance inferred from analyses made during the FGGE and general circulation model experiments, Technical Note II/173, British Meteorological Office, Bracknell, 1981.

Trenberth, K.E., Interannual variability of the 500 mb zonal mean flow in the southern hemisphere, Mon. Wea. Rev., 107, 1515-1524, 1979.

Trenberth, K.E., Seasonal variations in global sea level pressure and the total mass of the atmosphere, J. Geophys. Res., 86, 5238-5246, 1981a.

Trenberth, K.E., Observed southern hemisphere eddy statistics at 500 mb: frequency and spatial dependence, J. Atmos. Sci., 38, 2585-2605, 1981b.

Ward, F., and R. Shapiro, Meteorological periodicities, J. Meteor., 18, 635-656, 1961.

Welch, P.D., The use of fast Fourier transform for the estimation of power spectra: a method based on time averaging over short modified periodograms, IEEE Trans. Audio and Electroacoustics, AU-15, 70-73, 1967.

Yoder, C.F., J.G. Williams, and M.E. Parke, Tidal variations of earth rotation, J. Geophys. Res., 86, 881-891, 1981.

Legends for Figures

Figure 1 Values of the angular momentum of the atmosphere above the globe, the Northern Hemisphere (NH) and the Southern Hemisphere (SH) during calendar years (a) 1976; (b) 1977; (c) 1978; (d) 1979; (e) 1980; and (f) 1981. The scale for M is given along the left-hand ordinate. Inferred values of Δl.o.d., derived from M through equation (4), are given along the right-hand ordinate. Time is marked along the abscissa in terms of days from 1 January 1976.

Figure 2 Values of the angular momentum of the atmosphere above the globe, as in Fig. 1 but compressed for the five-year period from 1 January 1976 to 31 December 1980. (Note also that the ordinate scale has been expanded from that in Fig. 1.)

Figure 3 Three-day mean values of the angular momentum of the atmosphere above the globe during 1976-80 after removing an annual signal.

Figure 4 Power spectrum of the angular momentum of the atmosphere above the globe during 1976-80 on periods of from 6 to 128 days (heavy curve). The ordinate is in units of $(\text{kg m}^2 \text{ s}^{-1})^2 \cdot \text{day}$. The abscissa is linear with respect to frequency. The thin curve is an estimate of the 95% level of significance.

Figure 5 Variations in the length of day during 1976-80 determined from lunar laser ranging observations (solid line) and inferred from M through equation (4) (dashed line). The fortnightly and monthly tidal terms in the lunar laser ranging values have been removed. The two curves are displaced relative to each other by an arbitrary constant amount (see text).

Figure 6 Variations in the length of day during 1976-79 determined from LLR observations (solid line) and inferred from M (dashed line), as in Fig. 5 but now with the mean levels and annual and semiannual variations also removed each year from both sets of data. Time is marked in terms of days from 1 January 1976. (Taken from Langley et al., 1981b.)

Figure 7 Mean distribution of the momentum density field m_B based on 3-day averages of once-daily data for 1976-80. Values are plotted (in units of 10^{24} kg m^2 s^{-1}) at the midpoint of each (equal mass) latitude-height cross sectional box. Isolines have been drawn only for ease of viewing the figure; negative values are shaded.

Figure 8 The variance of m_B in each box determined from 3-day mean values of once-daily data for 1976-80. Units are 10^{48} $(\text{kg } m^2 \text{ } s^{-1})^2$.

Figure 9 The (a) first EOF of variability in m_B during 1976-80 and (b) its associated time series. The percent of the total variance in m_B explained by this mode is given at the top. Values of the EOF are non-dimensional and have been multiplied by 10 here; negative values are shaded.

Figure 10 The (a) second EOF of variability in m_B during 1976-80, (b) its associated time series and (c) power spectrum of the time series. The non-dimensional values of the EOF have been multiplied by 10. As in Fig. 4, the thin curve in the power spectrum plot is an estimate of the 95% level of significance.

Figure 11 The variance of m_B after removing an annual signal from each box's time series of 3-day means of once-daily data for 1976-80. Units are 10^{48} $(kg\ m^2\ s^{-1})^2$.

Figure 12 Percent of the variance in m_B, with its annual signal removed, explained by the first 7 EOFs (solid line) and the same for EOFs calculated from random data (dashed line) for 1976-80.

Figure 13 EOF modes 1 through 6 [(a) through (f)] of non-seasonal variability in η_B for 1976-80. The non-dimensional values of all the EOFs have been multiplied by 10; negative values are shaded.

Figure 14 Time series associated with each of the EOFs displayed in Fig. 13.

Figure 15 Power spectrum of each of the time series in Fig. 14. The format and units are as in Fig. 4, with the thin curve representing an estimate of the 95% level of significance.

Figure 16 Mean distribution and standard deviation of the momentum density field m_b derived from 3-day averages of once-daily data for 1976-80. The means are plotted as dots at the midpoint of each zonal belt. Values of ±1 standard deviation of m_b in each belt are connected by the solid line.

Figure 17 The variance in m_b during 1976-80 derived from the full set of 3-day means of once-daily data (crosses) and from these same data but with their annual signal removed (dots).

Figure 18 The (a) first two EOFs of variability in m_b during 1976-80, (b) time series associated with mode 1, and (c) time series associated with mode 2. The percent of the total variance in m_b explained by each mode is included in its label. The non-dimensional values of the EOF have been multiplied by 10.

Figure 19 Percent of the variance in m_b, with its annual signal removed, explained by the first 10 EOFs (solid line) and the same for EOFs calculated from random data (dashed line) for 1976-80.

Figure 20 EOF modes 1 through 8 of non-seasonal variability in m_b for 1976-80. The non-dimensional values of all the EOFs have been multiplied by 10.

F [illegible] time series associated with each of the EOFs displayed in [illegible].

Figure 22 Power spectrum of each of the time series in Fig. 21. The format and units are as in Fig. 4, with the thin curve representing an estimate of the 95% level of significance.

Figure 23 The covariance between the time series of m_b in each zonal belt and global M after removing their annual signals (dots) and after removing both their annual and interannual signals (crosses) for 1976-80. Units are 10^{48} $(kg\ m^2\ s^{-1})^2$.

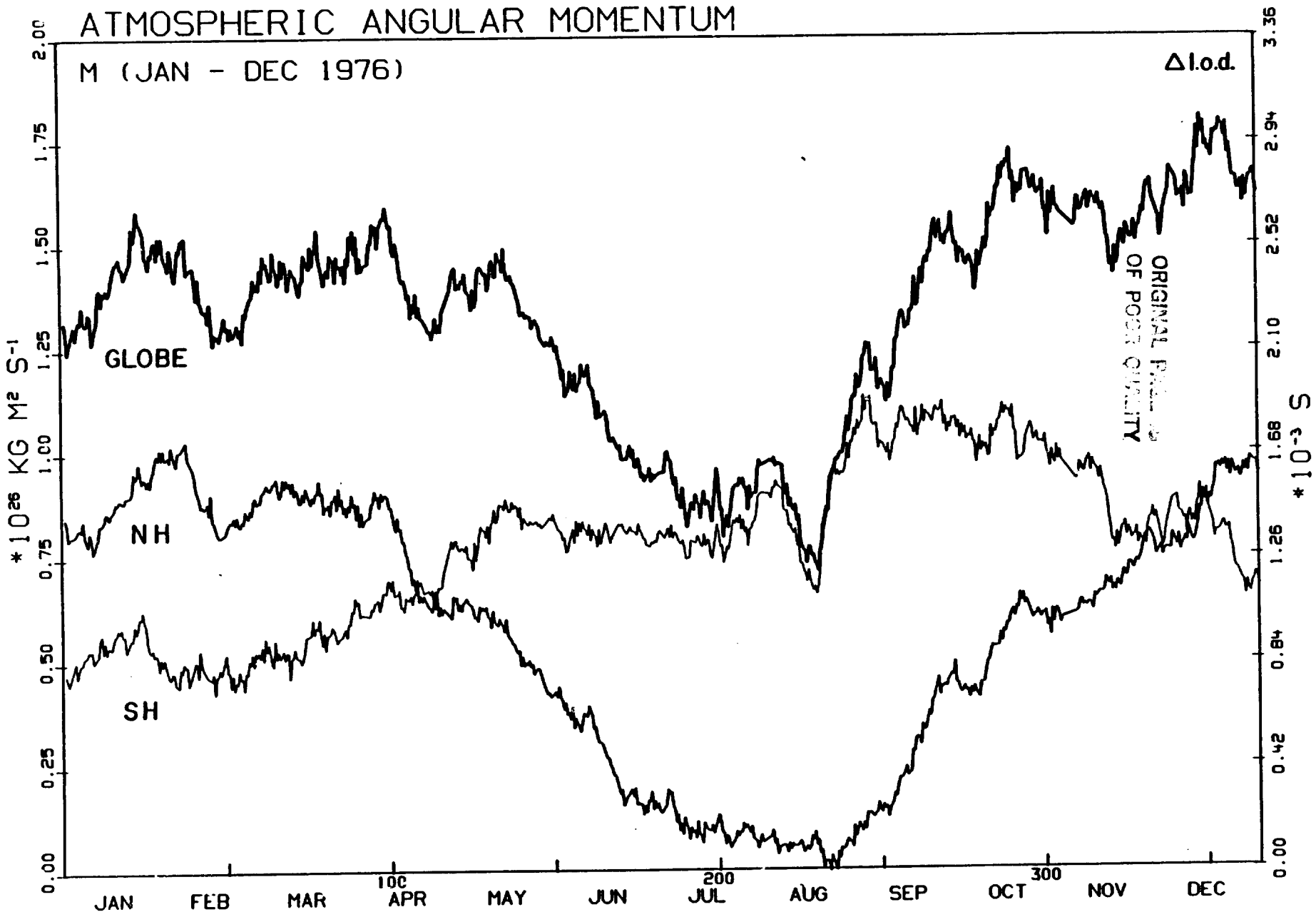
ATMOSPHERIC ANGULAR MOMENTUM
M (JAN - DEC 1976)
Δl.o.d.
GLOBE
NH
SH
*10^26 KG M^2 S^-1
*10^-3 S
2.00
1.75
1.50
1.25
1.00
0.75
0.50
0.25
0.00
3.36
2.94
2.52
2.10
1.68
1.26
0.84
0.42
0.00
JAN
FEB
MAR
APR
MAY
JUN
JUL
AUG
SEP
OCT
NOV
DEC
100
200
300
ORIGINAL PAGE IS
OF POOR QUALITY

Figure 1a

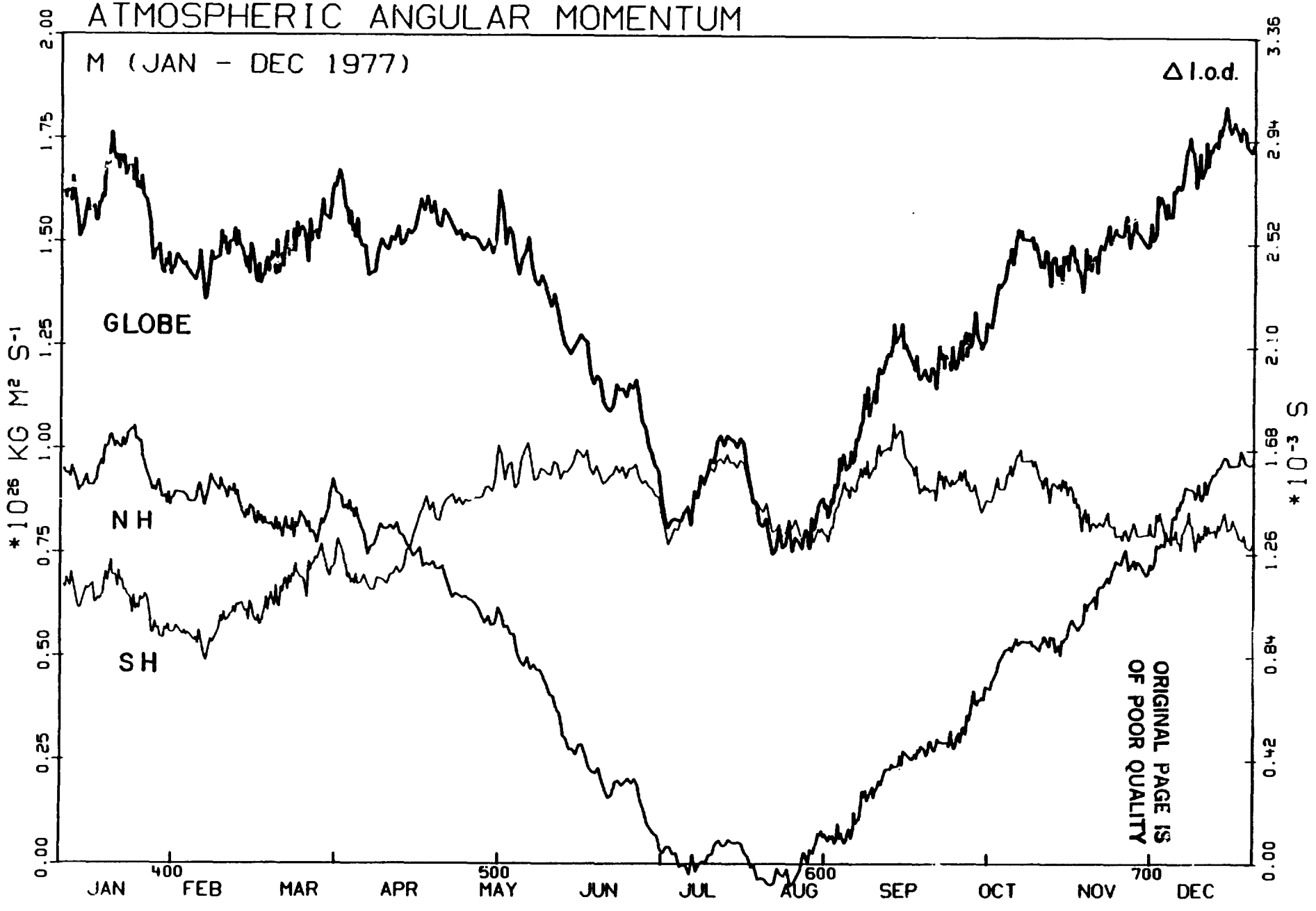
ATMOSPHERIC ANGULAR MOMENTUM
M (JAN - DEC 1977)
Δ l.o.d.
GLOBE
NH
SH
*10^26 KG M^2 S^-1
*10^-3 S
2.00
1.75
1.50
1.25
1.00
0.75
0.50
0.25
0.00
3.36
2.94
2.52
2.10
1.68
1.26
0.84
0.42
0.00
400
500
600
700
JAN
FEB
MAR
APR
MAY
JUN
JUL
AUG
SEP
OCT
NOV
DEC
ORIGINAL PAGE IS
OF POOR QUALITY

Figure 1b

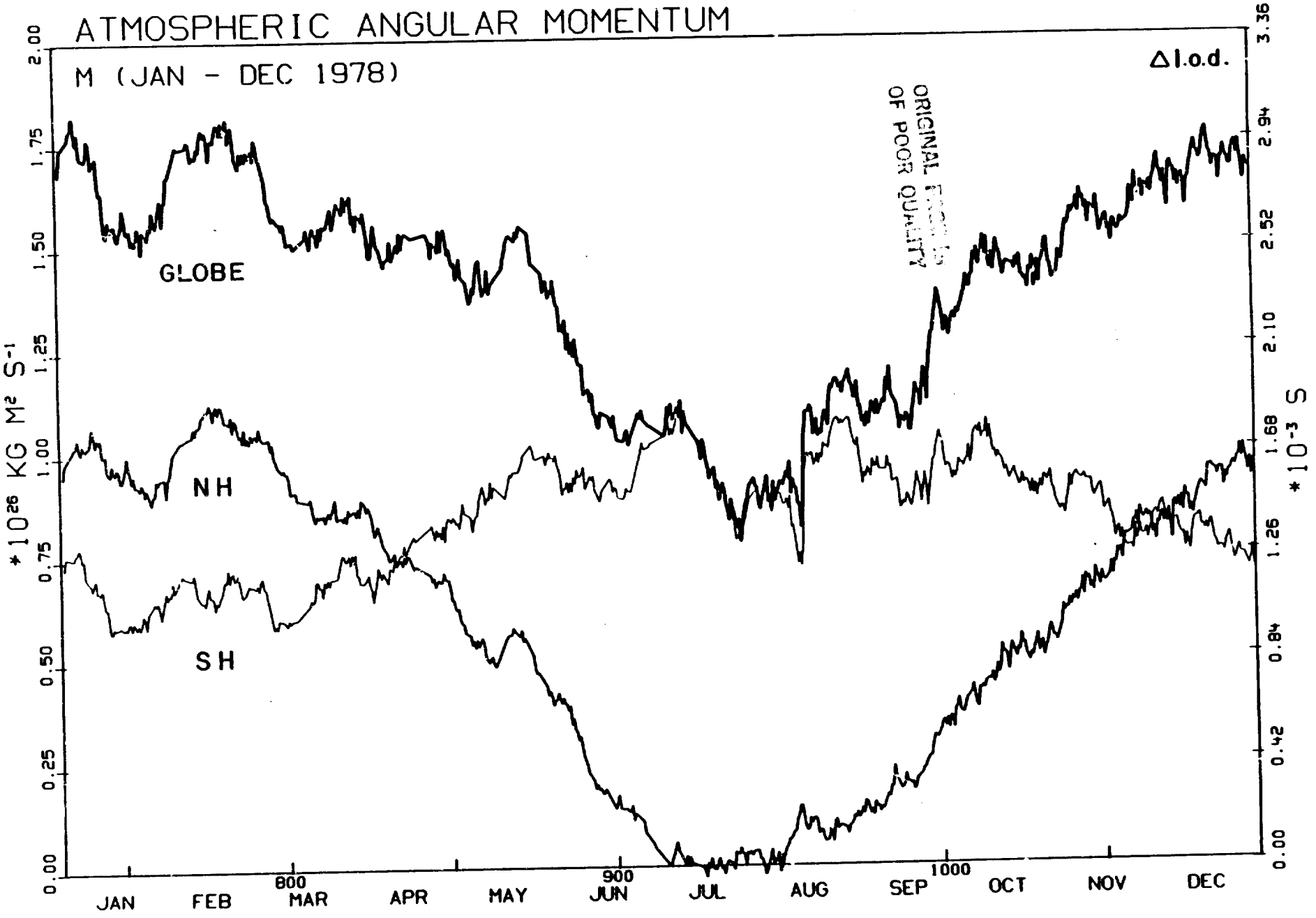

Figure 1c

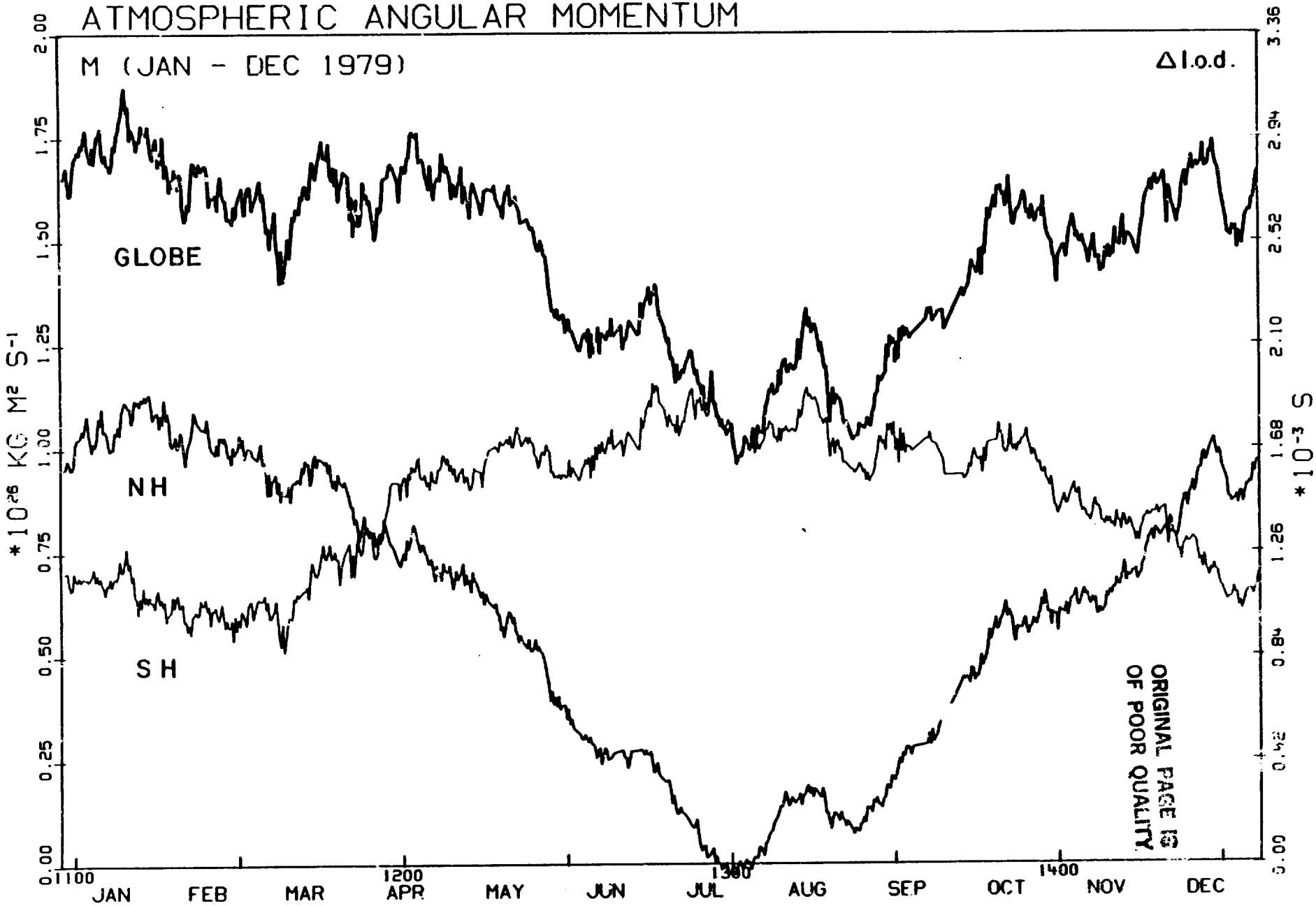
ATMOSPHERIC ANGULAR MOMENTUM
M (JAN - DEC 1979)
Δl.o.d.
GLOBE
NH
SH
*10^26 KG M^2 S^-1
*10^-3 S
2.00
1.75
1.50
1.25
1.00
0.75
0.50
0.25
0.00
3.36
2.94
2.52
2.10
1.68
1.26
0.84
0.42
0.00
1100
1200
1300
1400
JAN
FEB
MAR
APR
MAY
JUN
JUL
AUG
SEP
OCT
NOV
DEC
ORIGINAL PAGE IS
OF POOR QUALITY

Figure 1d

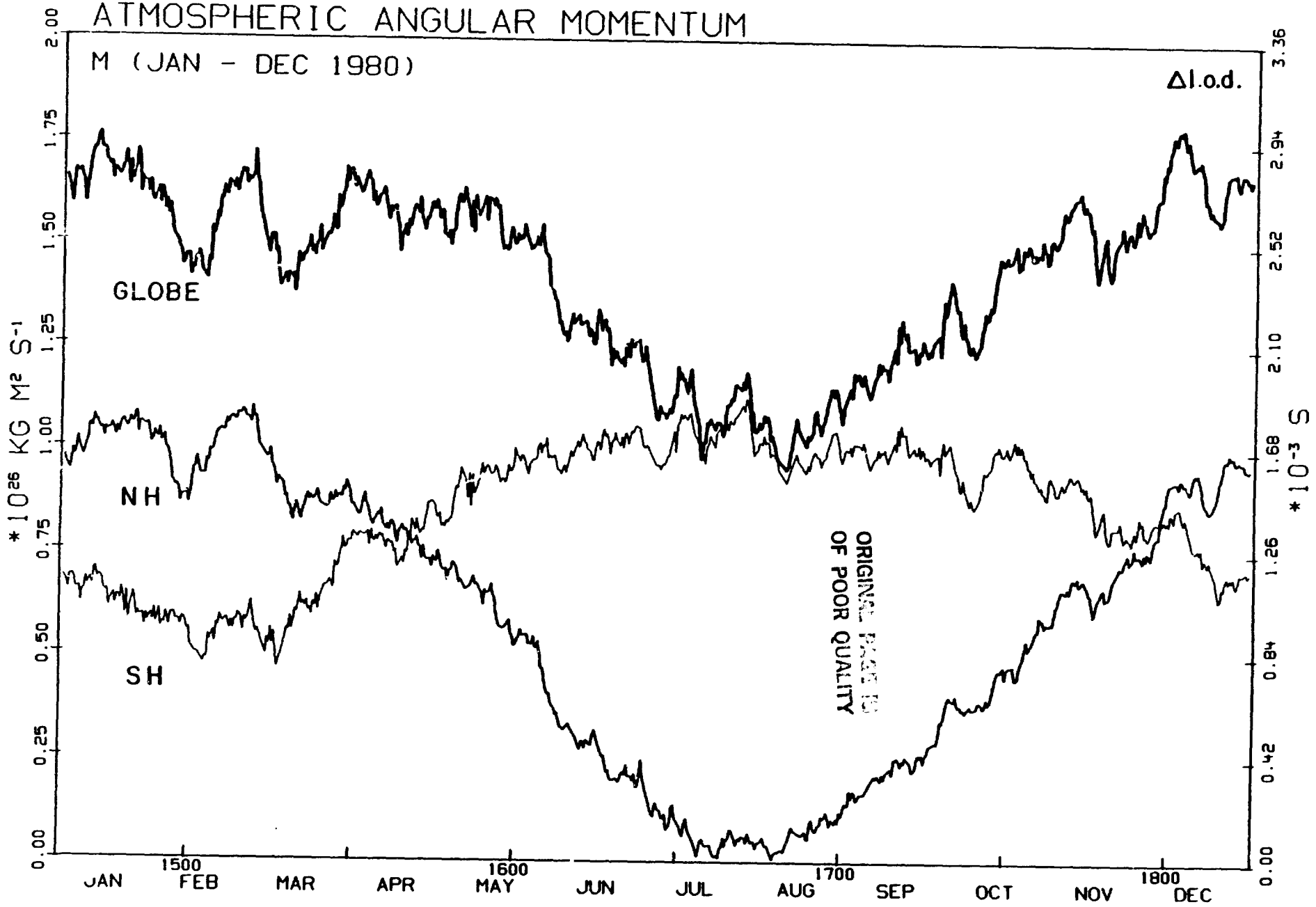
ATMOSPHERIC ANGULAR MOMENTUM
M (JAN - DEC 1980)
Δl.o.d.
GLOBE
NH
SH
*10^26 KG M^2 S^-1
*10^-3 S
2.00
1.75
1.50
1.25
1.00
0.75
0.50
0.25
0.00
3.36
2.94
2.52
2.10
1.68
1.26
0.84
0.42
0.00
1500
1600
1700
1800
JAN
FEB
MAR
APR
MAY
JUN
JUL
AUG
SEP
OCT
NOV
DEC
ORIGINAL PAGE IS
OF POOR QUALITY

Figure 1c

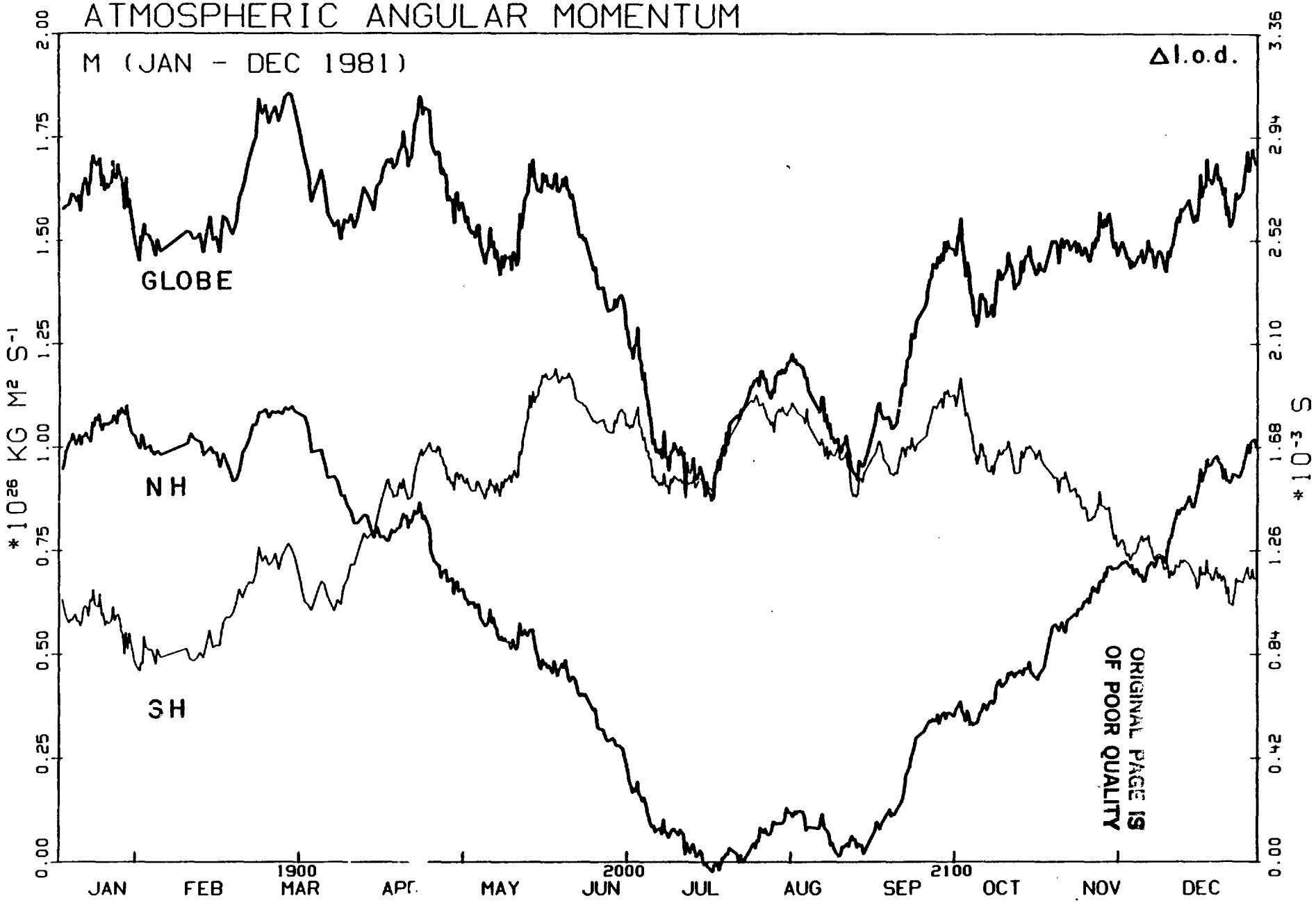
ATMOSPHERIC ANGULAR MOMENTUM
M (JAN - DEC 1981)
Δl.o.d.
GLOBE
NH
SH
*10^26 KG M^2 S^-1
*10^-3 S
2.00
1.75
1.50
1.25
1.00
0.75
0.50
0.25
0.00
3.36
2.94
2.52
2.10
1.68
1.26
0.84
0.42
0.00
1900
2000
2100
JAN
FEB
MAR
APR
MAY
JUN
JUL
AUG
SEP
OCT
NOV
DEC
ORIGINAL PAGE IS
OF POOR QUALITY

Figure 1f

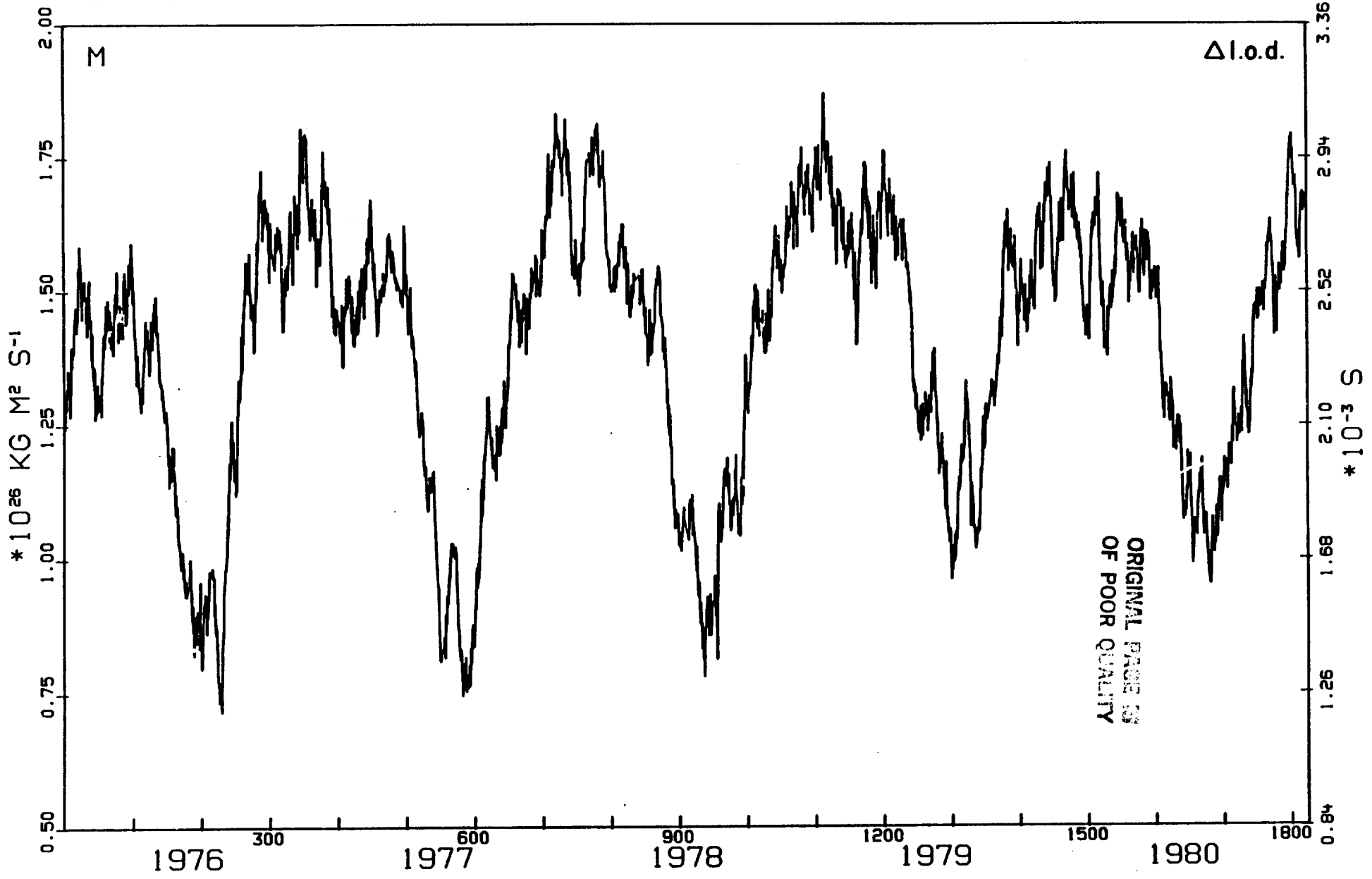
GLOBAL ATMOSPHERIC ANGULAR MOMENTUM
JAN 1976 - DEC 1980
M
Δl.o.d.
*10^26 KG M^2 S^-1
*10^-3 S
2.00
1.75
1.50
1.25
1.00
0.75
0.50
3.36
2.94
2.52
2.10
1.68
1.26
0.84
300
600
900
1200
1500
1800
1976
1977
1978
1979
1980
ORIGINAL PAGE IS
OF POOR QUALITY

Figure 2

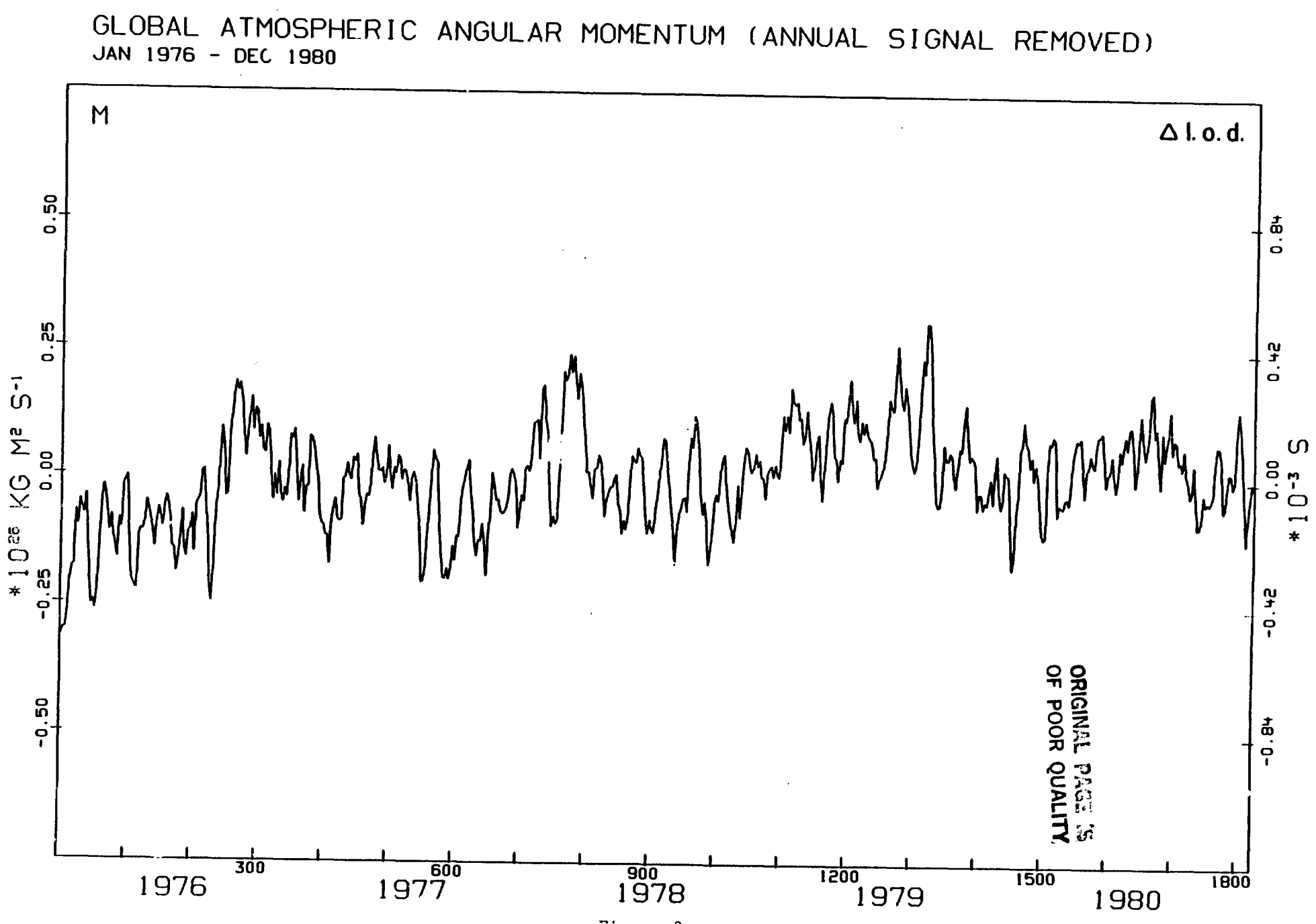
GLOBAL ATMOSPHERIC ANGULAR MOMENTUM (ANNUAL SIGNAL REMOVED)
JAN 1976 - DEC 1980
M
Δ l.o.d.
*10^26 KG M^2 S^-1
*10^-3 S
0.50
0.25
0.00
-0.25
-0.50
0.84
0.42
0.00
-0.42
-0.84
300
600
900
1200
1500
1800
1976
1977
1978
1979
1980
ORIGINAL PAGE IS
OF POOR QUALITY

Figure 2

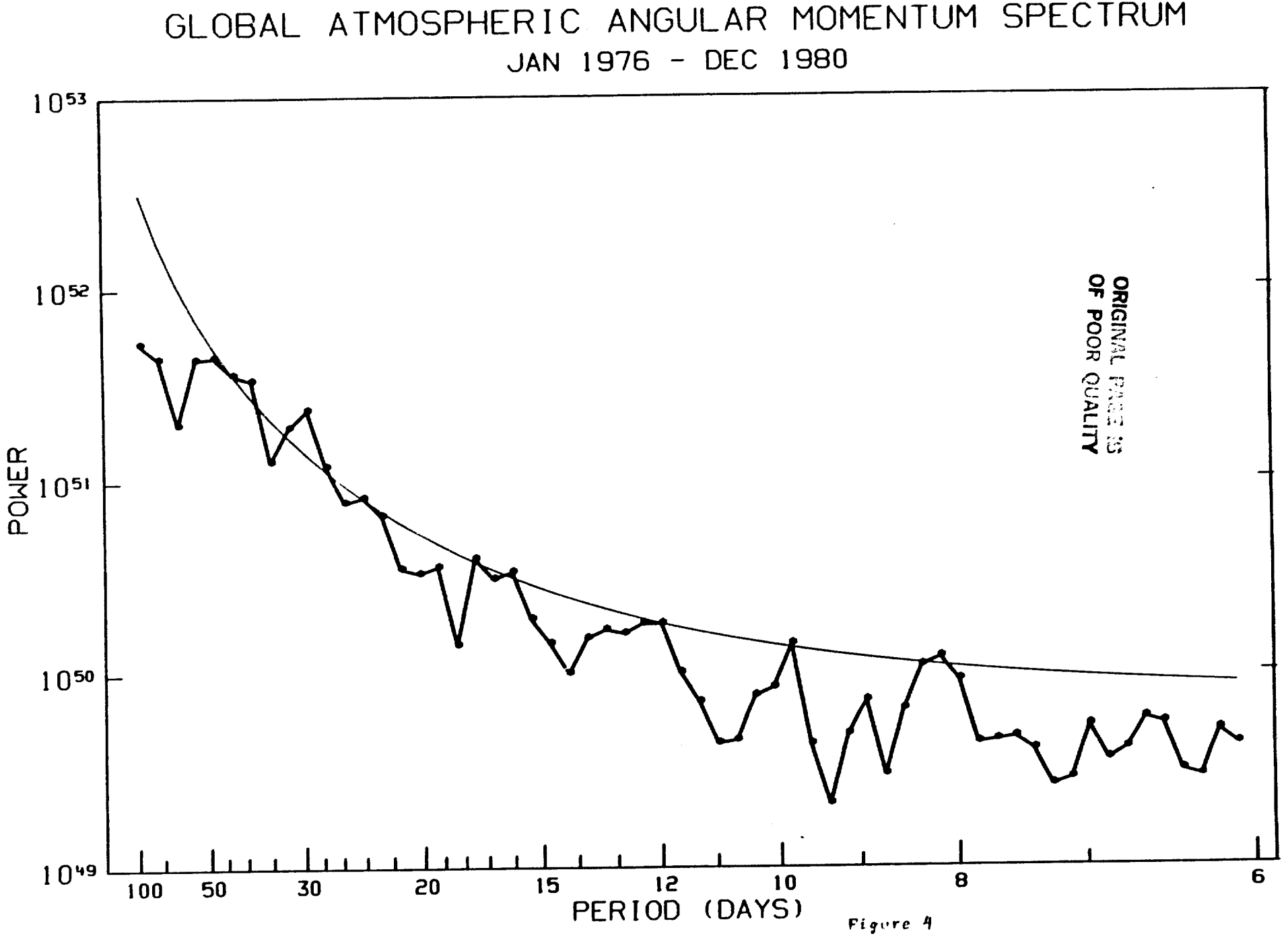
GLOBAL ATMOSPHERIC ANGULAR MOMENTUM SPECTRUM
JAN 1976 - DEC 1980
10^{53}
10^{52}
10^{51}
10^{50}
10^{49}
POWER
100
50
30
20
15
12
10
8
6
PERIOD (DAYS)
ORIGINAL PAGE IS
OF POOR QUALITY

Figure 4

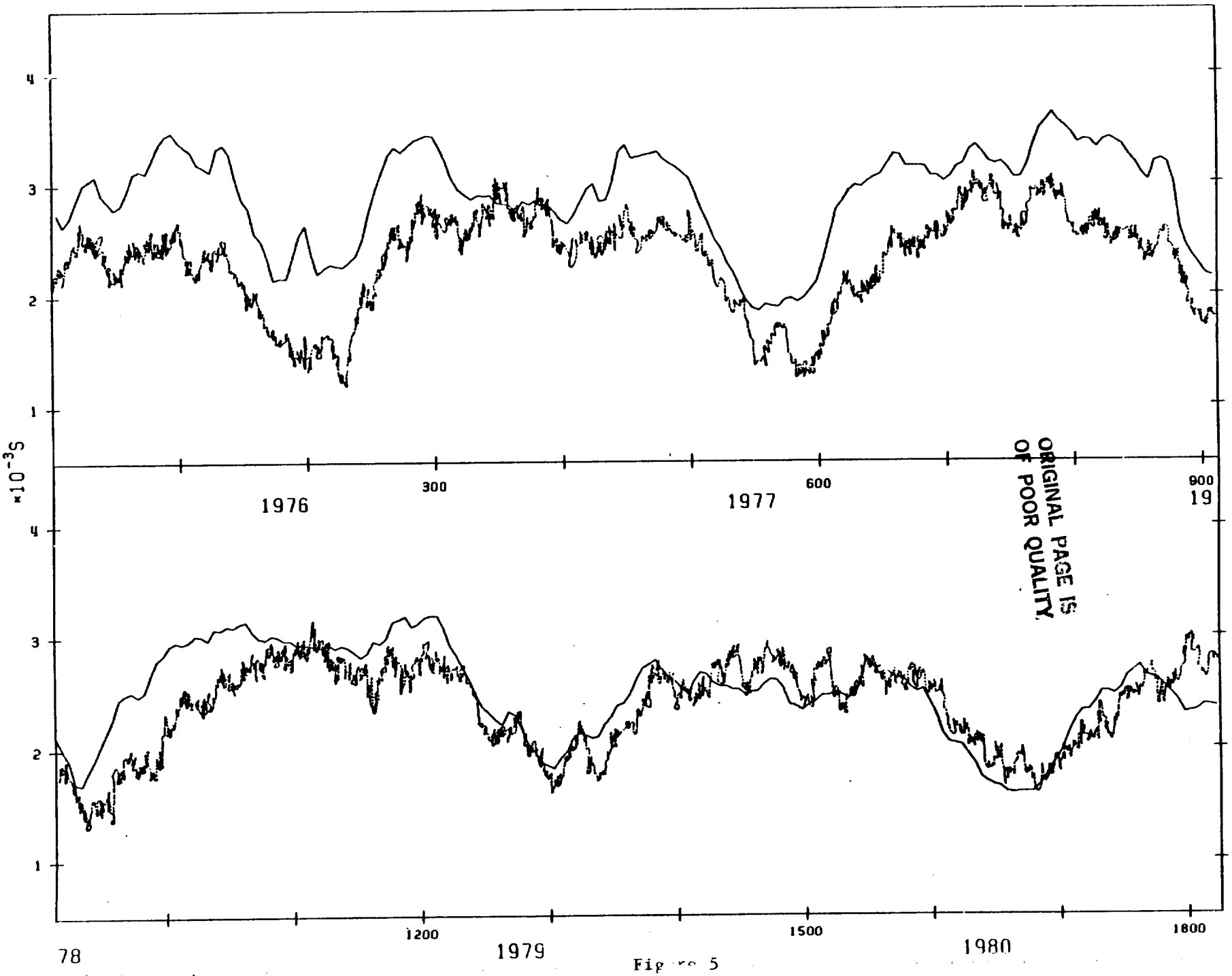

Figure 5

Figure 6

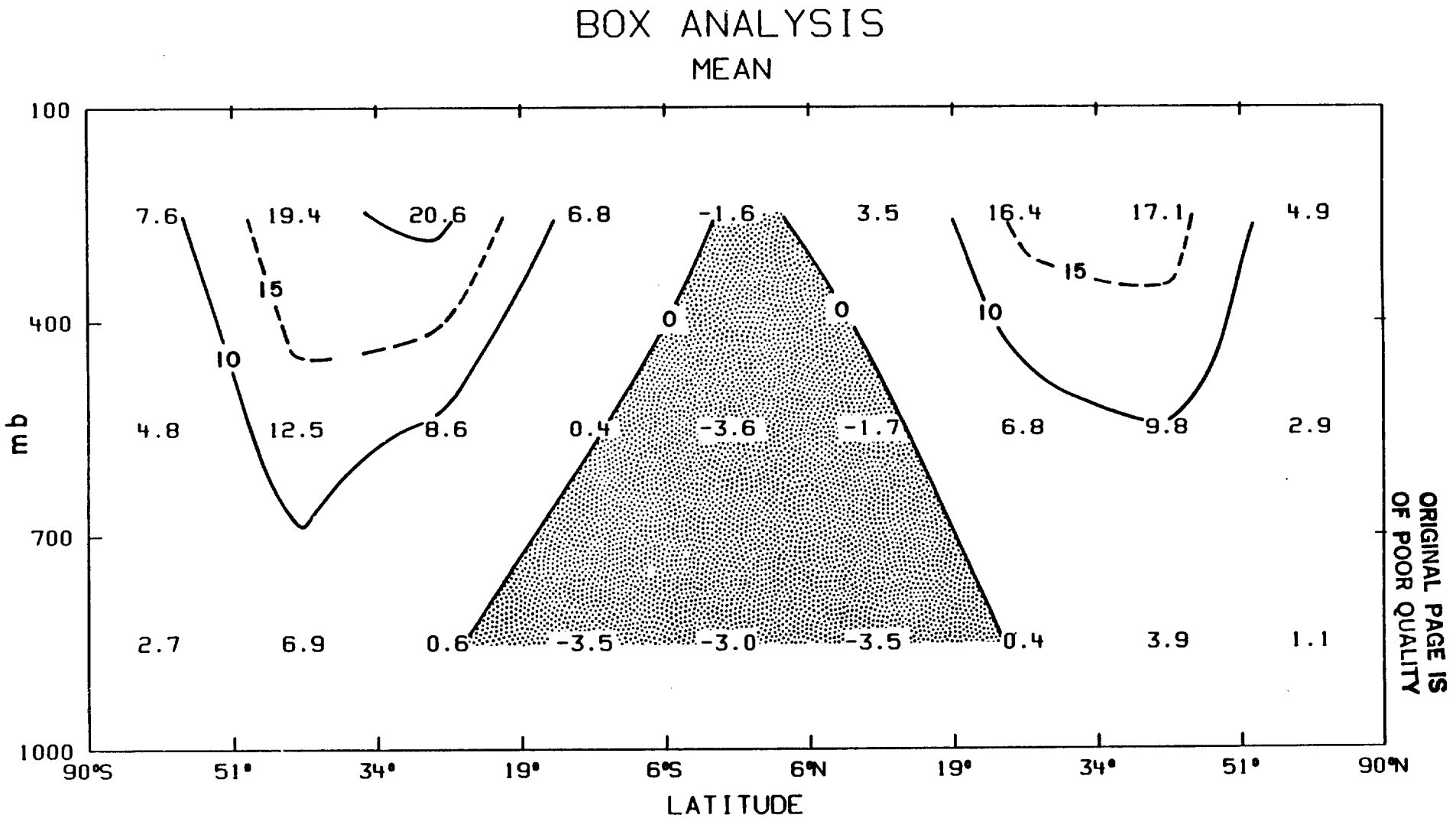
BOX ANALYSIS
MEAN
100
400
700
1000
mb
7.6
19.4
20.6
6.8
-1.6
3.5
16.4
17.1
4.9
15
10
0
0
10
15
4.8
12.5
8.6
0.4
-3.6
-1.7
6.8
9.8
2.9
2.7
6.9
0.6
-3.5
-3.0
-3.5
0.4
3.9
1.1
90°S
51°
34°
19°
6°S
6°N
19°
34°
51°
90°N
LATITUDE
ORIGINAL PAGE IS
OF POOR QUALITY

Figure 7

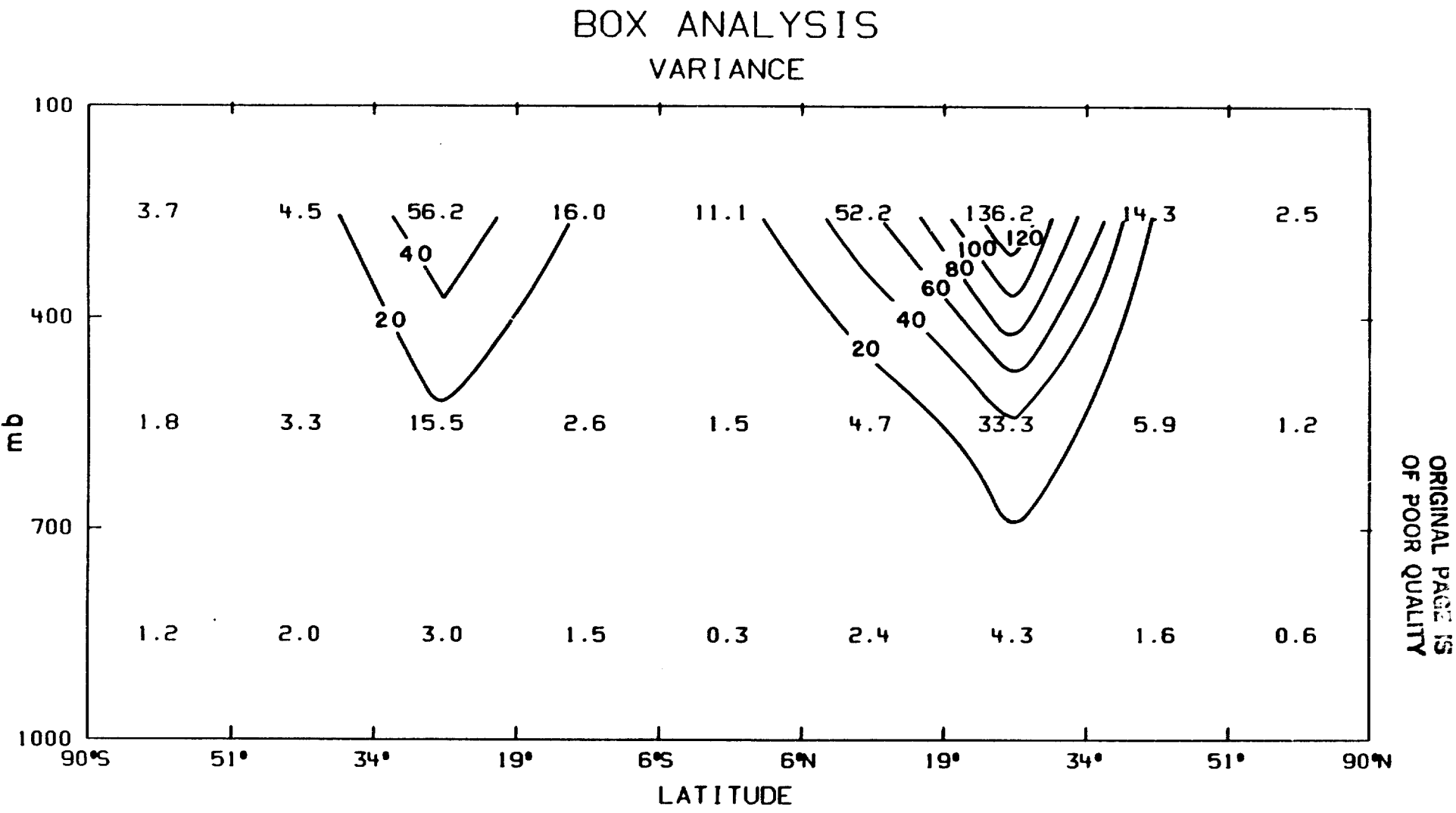

Figure 8

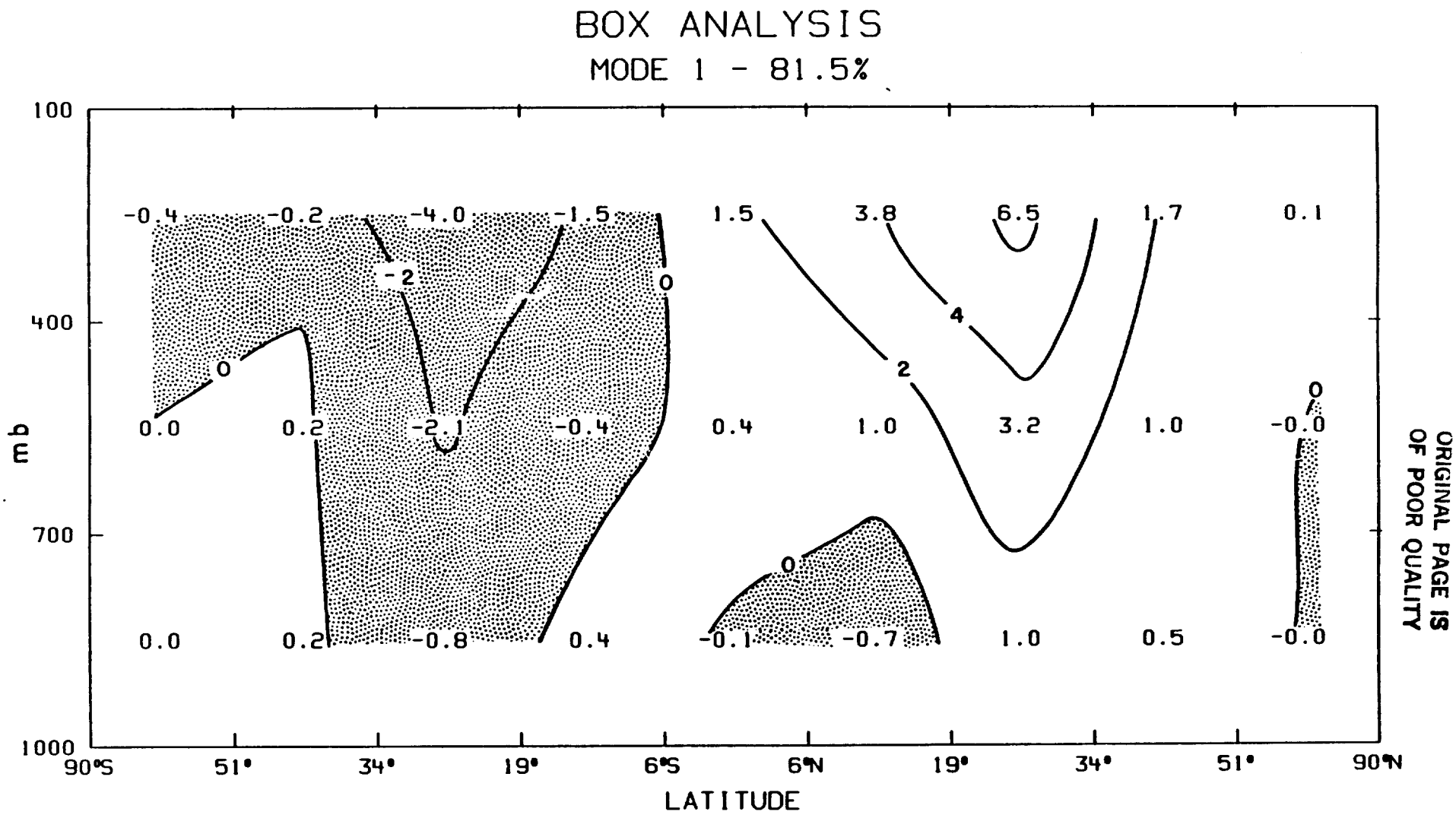
BOX ANALYSIS
MODE 1 - 81.5%
100
400
700
1000
mb
-0.4
-0.2
-4.0
-1.5
-2
0
0
0.0
0.2
-2.1
-0.4
0.0
0.2
-0.8
0.4
1.5
3.8
6.5
1.7
0.1
4
2
0
0.4
1.0
3.2
1.0
-0.0
0
-0.1
-0.7
1.0
0.5
-0.0
90°S
51°
34°
19°
6°S
6°N
19°
34°
51°
90°N
LATITUDE
ORIGINAL PAGE IS
OF POOR QUALITY

Figure 9a

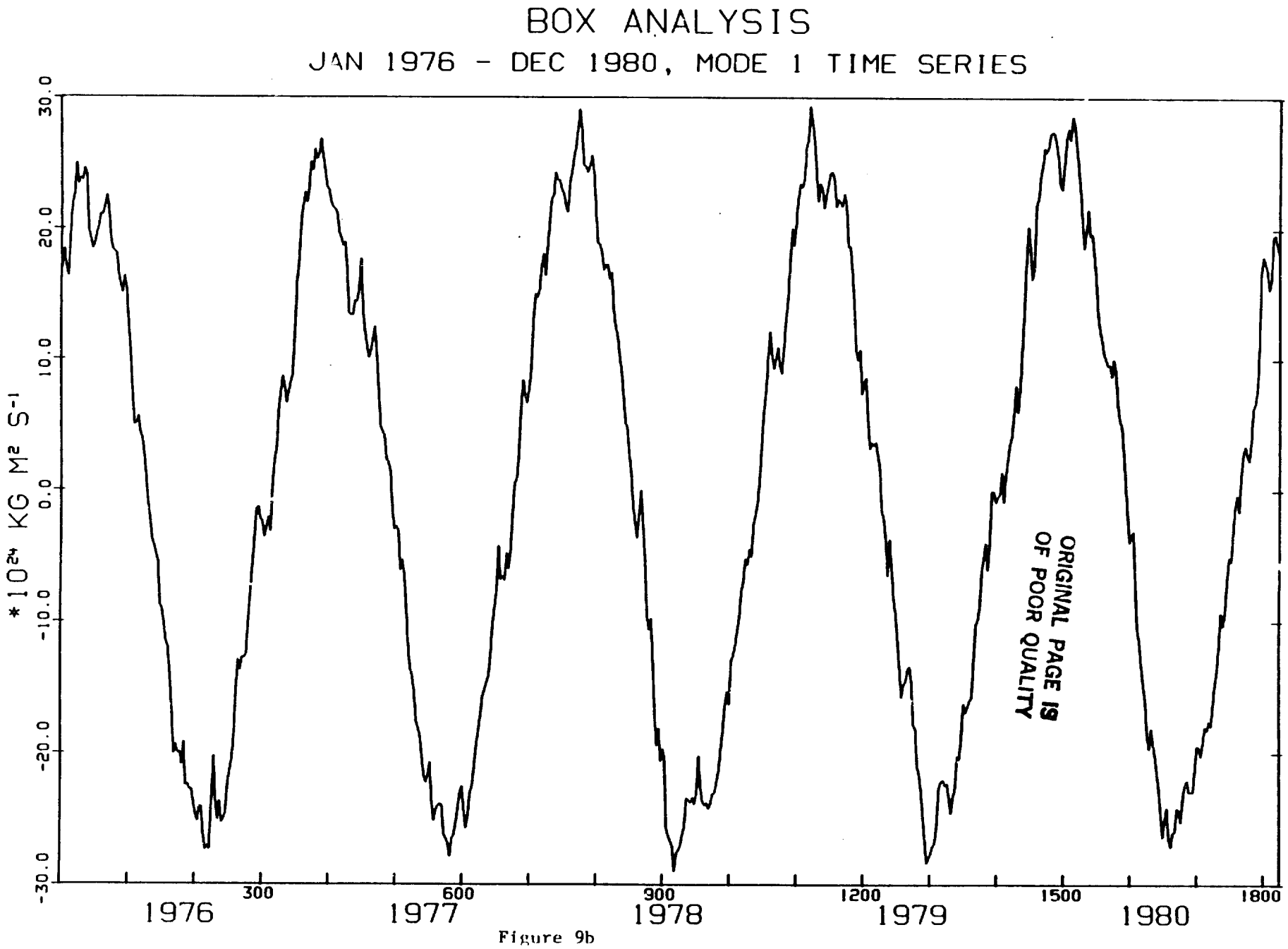
BOX ANALYSIS
JAN 1976 - DEC 1980, MODE 1 TIME SERIES
*10²⁴ KG M² S⁻¹
30.0
20.0
10.0
0.0
-10.0
-20.0
-30.0
300
600
900
1200
1500
1800
1976
1977
1978
1979
1980
ORIGINAL PAGE IS
OF POOR QUALITY

Figure 9b

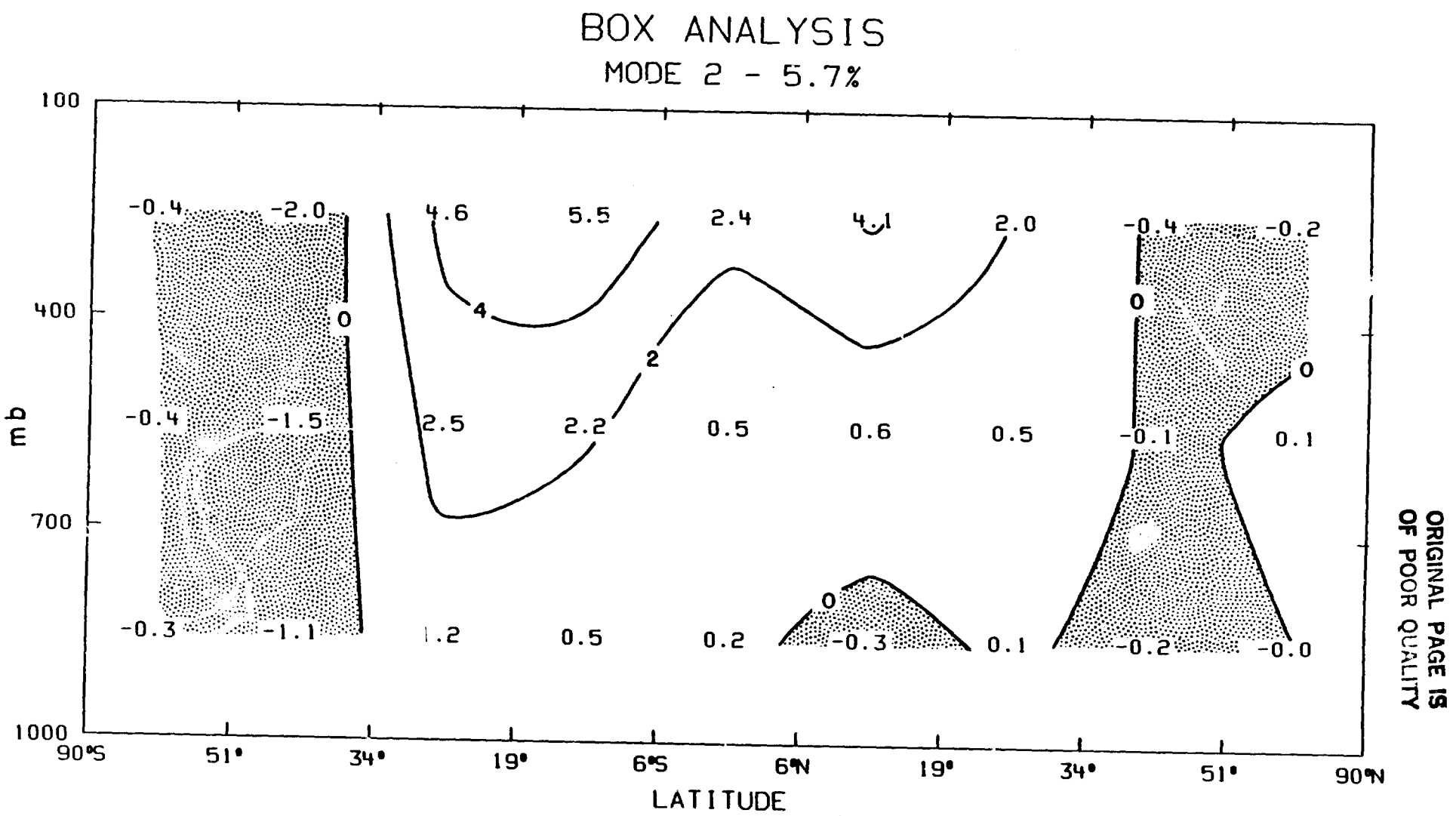

Figure 10a

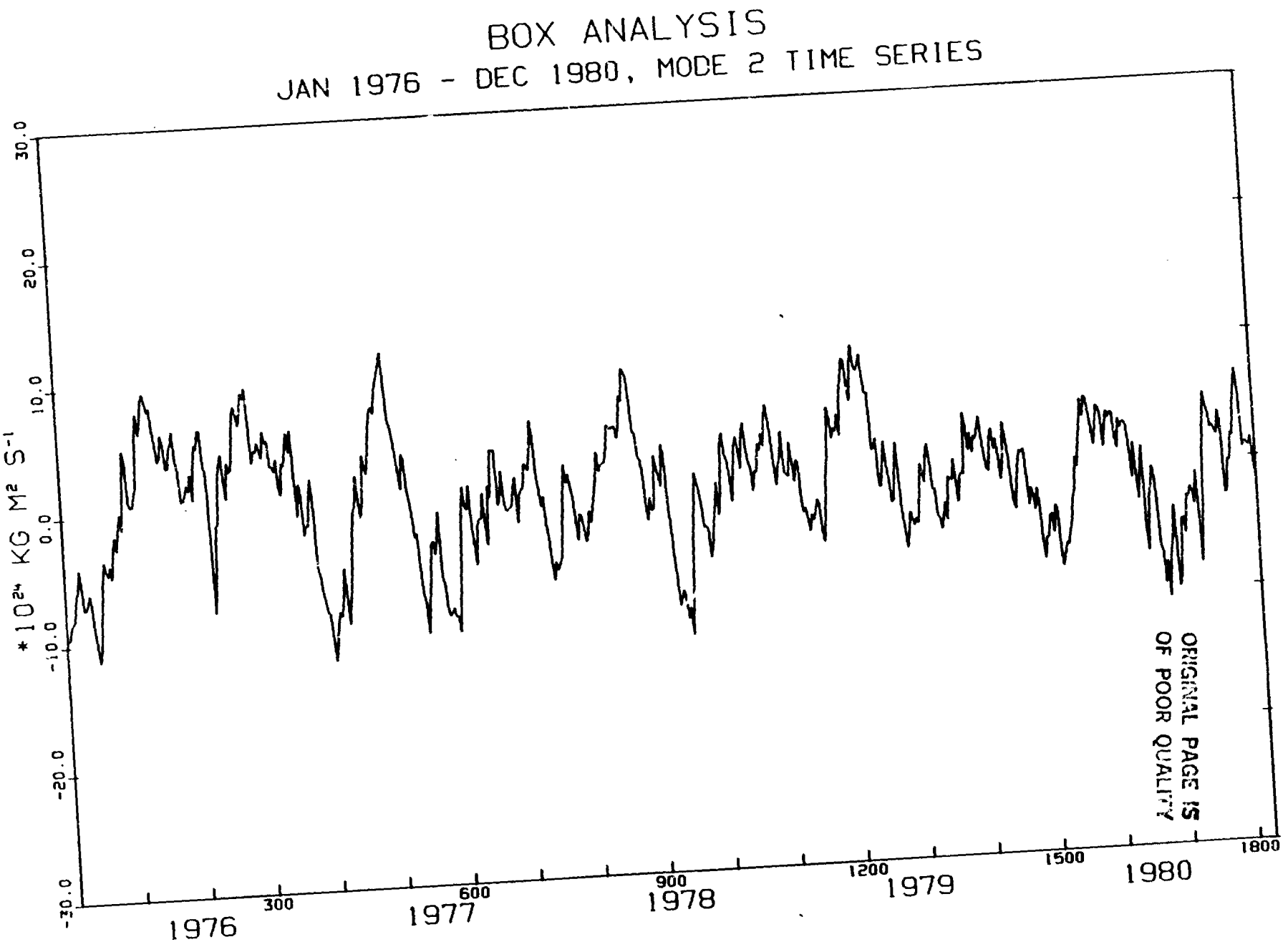
BOX ANALYSIS
JAN 1976 - DEC 1980, MODE 2 TIME SERIES
*10²⁴ KG M² S⁻¹
30.0
20.0
10.0
0.0
-10.0
-20.0
-30.0
300
600
900
1200
1500
1800
1976
1977
1978
1979
1980
ORIGINAL PAGE IS
OF POOR QUALITY

Figure 10b

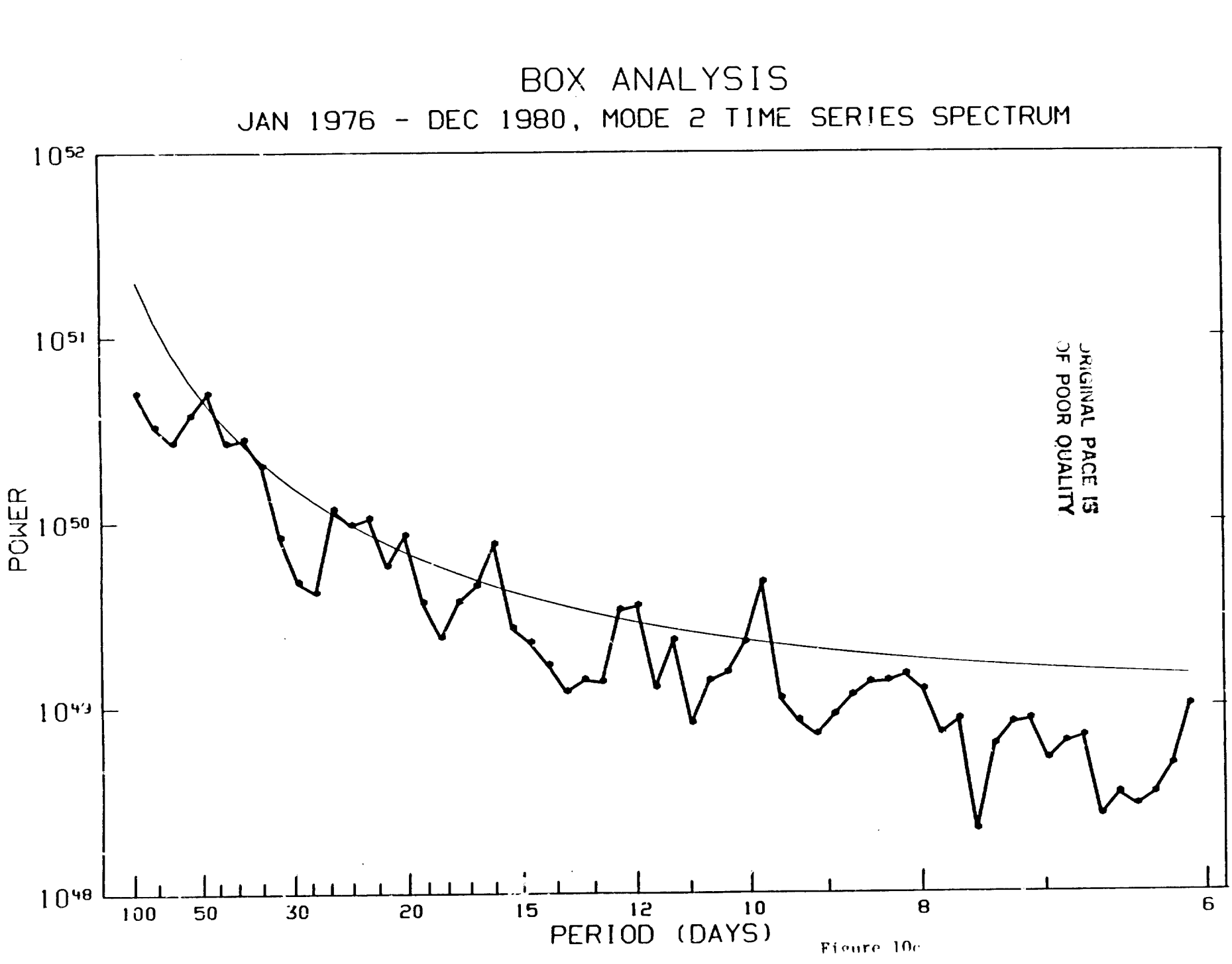

Figure 10c

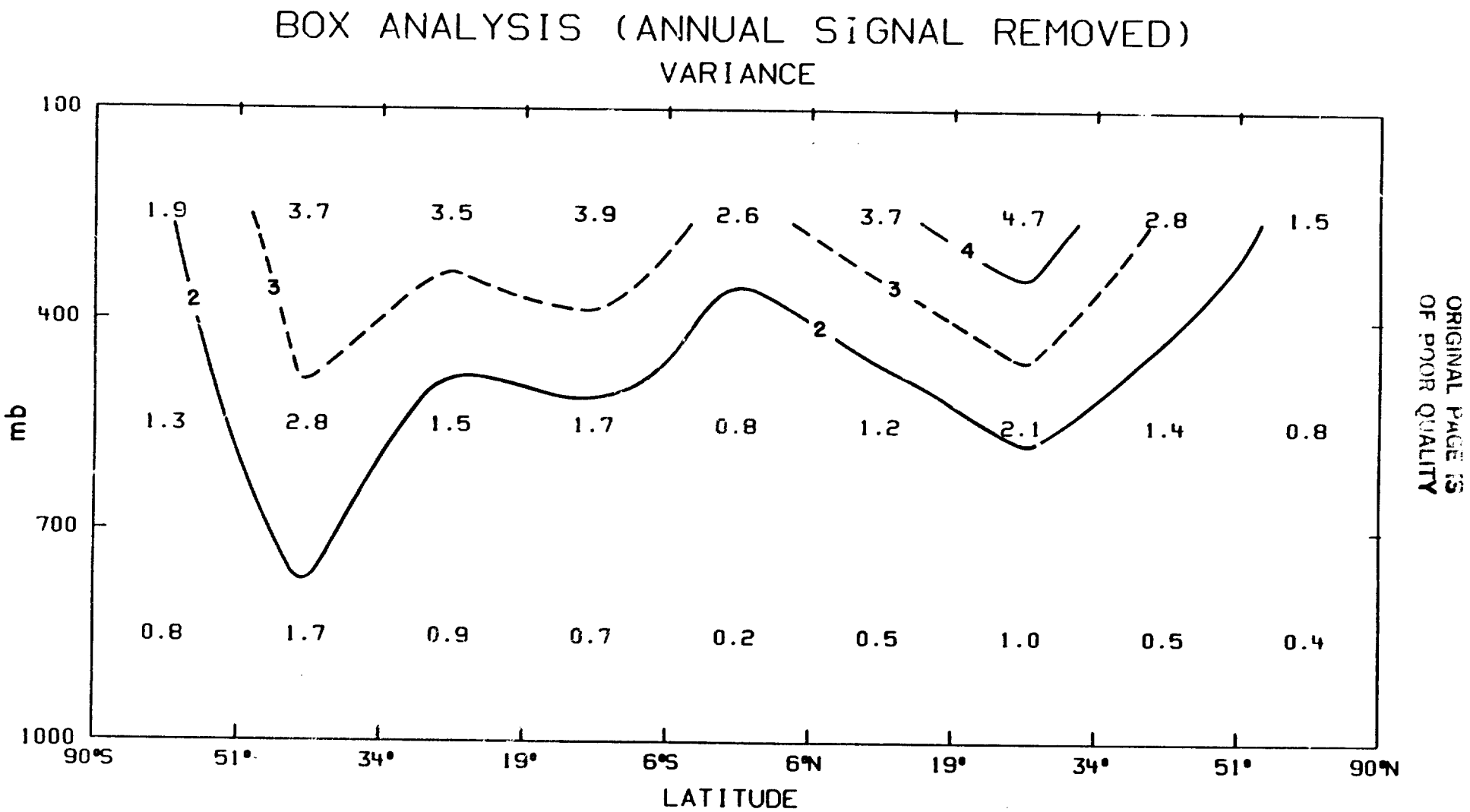

Figure 11

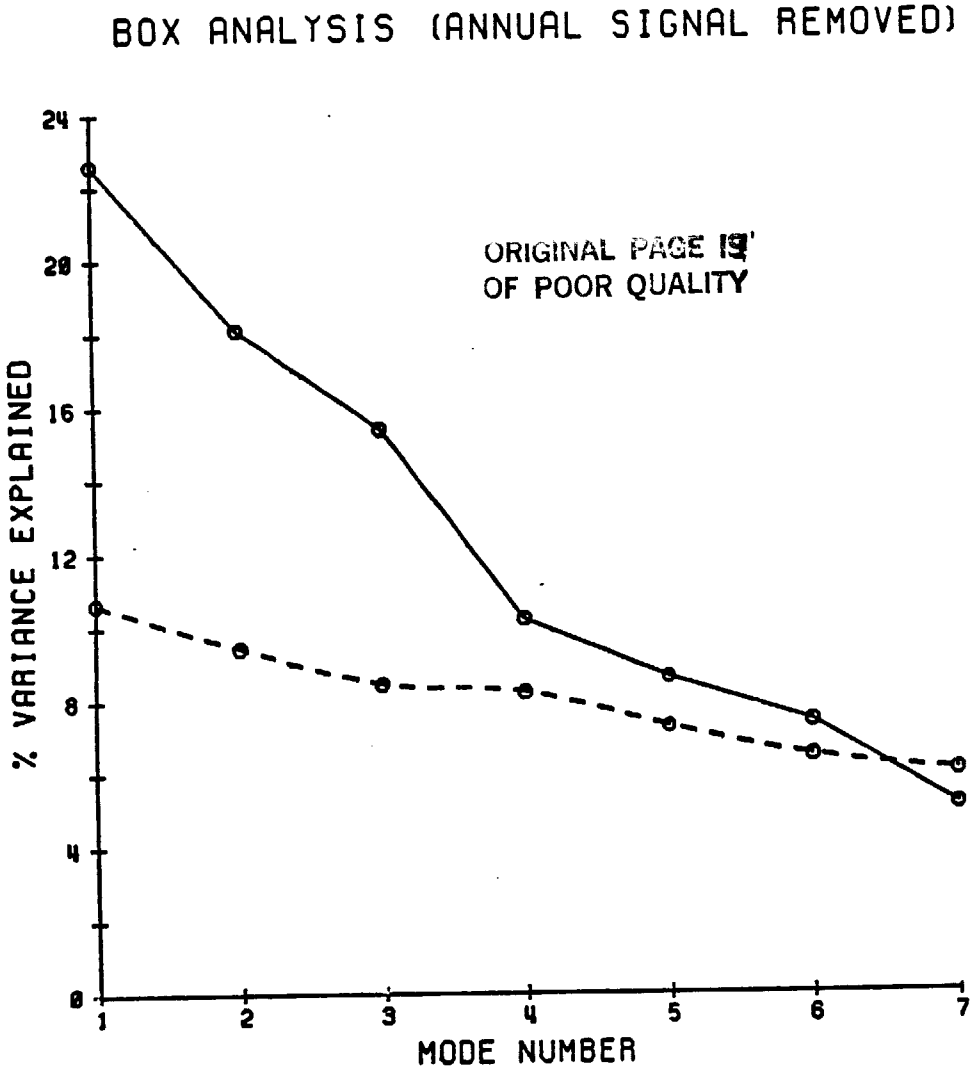
BOX ANALYSIS (ANNUAL SIGNAL REMOVED)
ORIGINAL PAGE IS
OF POOR QUALITY
% VARIANCE EXPLAINED
24
20
16
12
8
4
0
1
2
3
4
5
6
7
MODE NUMBER

Figure 12

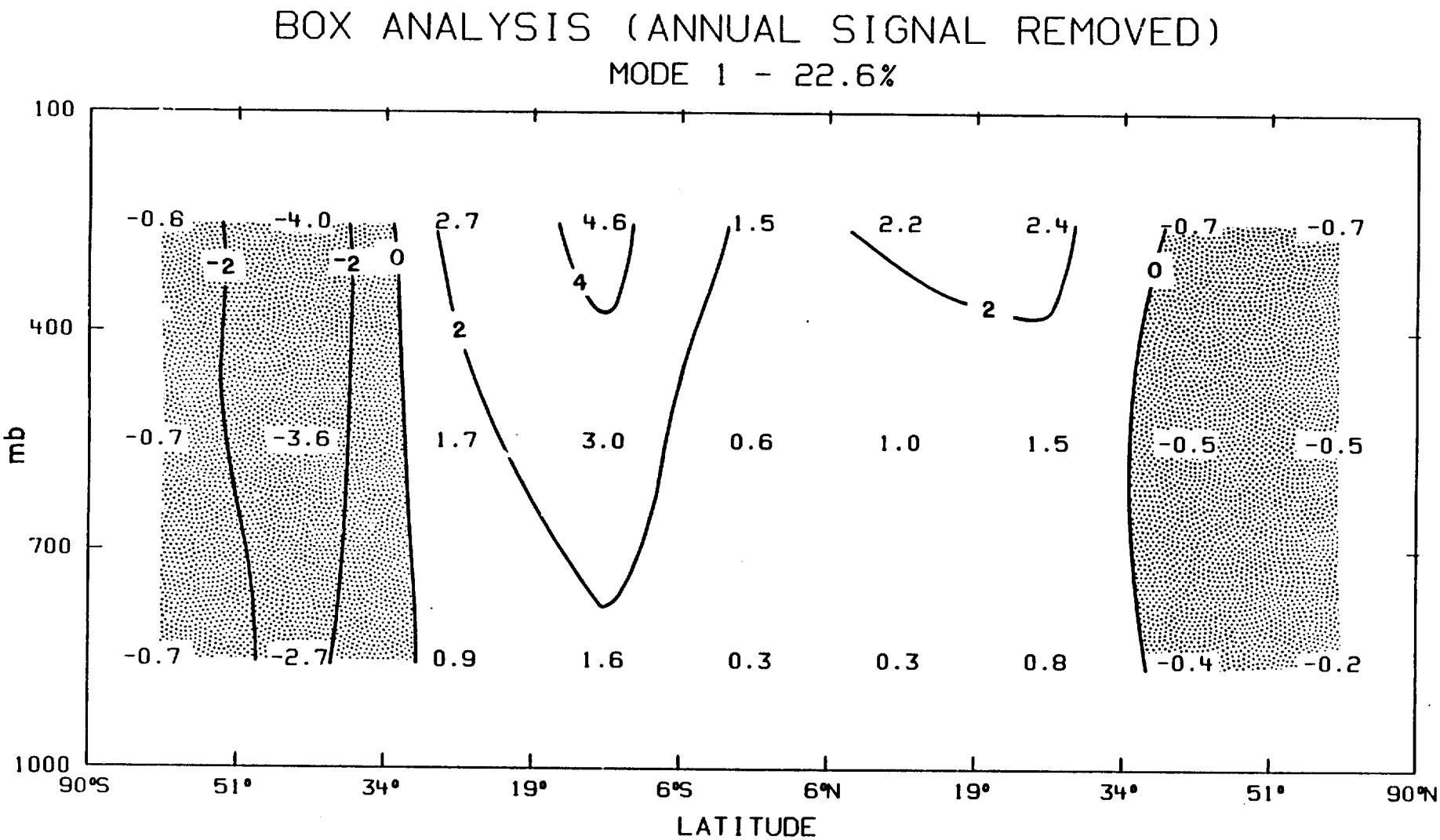

Figure 13a

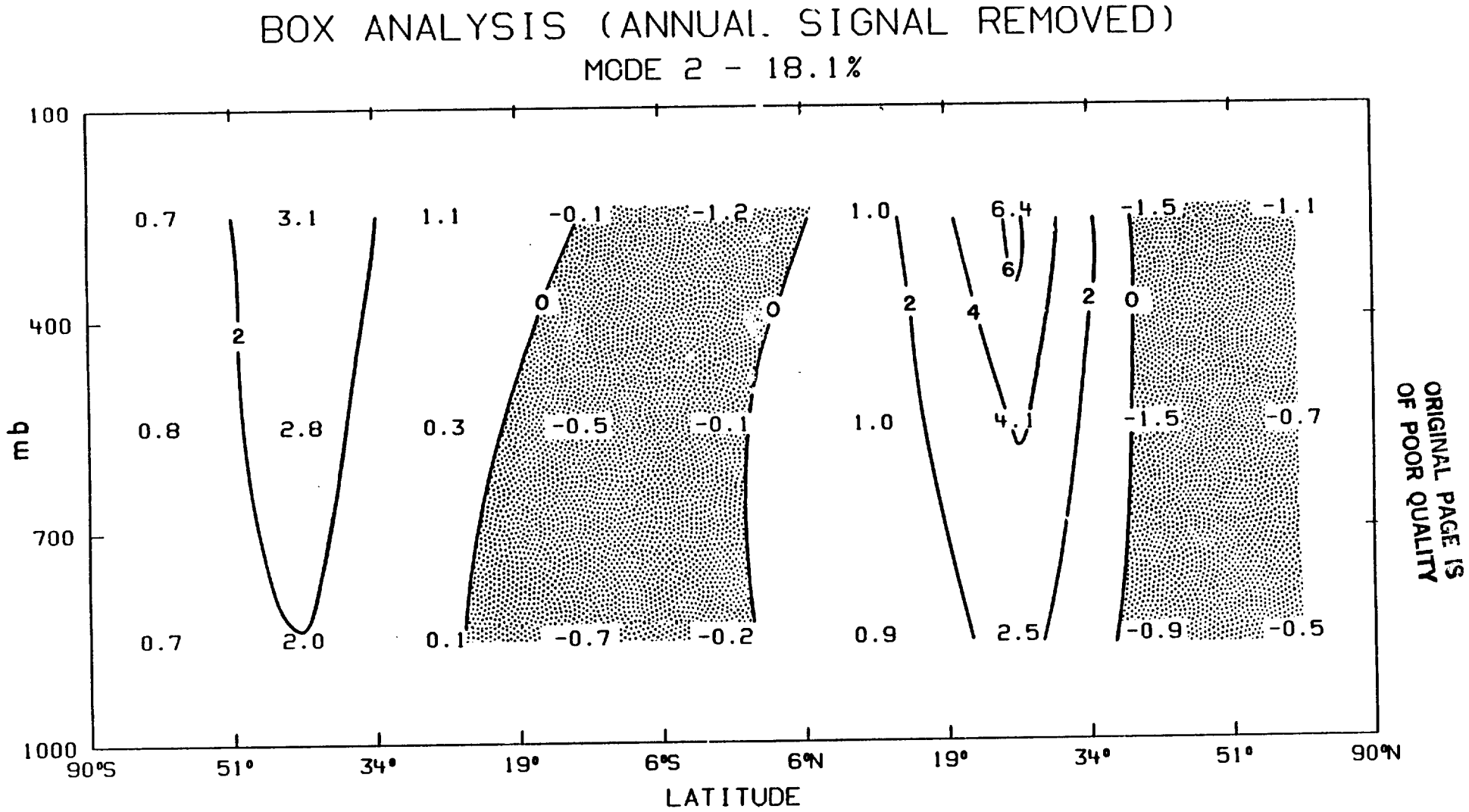
BOX ANALYSIS (ANNUAL SIGNAL REMOVED)
MODE 2 - 18.1%
100
400
700
1000
mb
0.7
3.1
2
0.8
2.8
0.7
2.0
1.1
-0.1
-1.2
0
0
0.3
-0.5
-0.1
0.1
-0.7
-0.2
1.0
6.4
6
2
4
2
1.0
4.1
0.9
2.5
-1.5
-1.1
0
-1.5
-0.7
-0.9
-0.5
90°S
51°
34°
19°
6°S
6°N
19°
34°
51°
90°N
LATITUDE
ORIGINAL PAGE IS
OF POOR QUALITY

Figure 13b

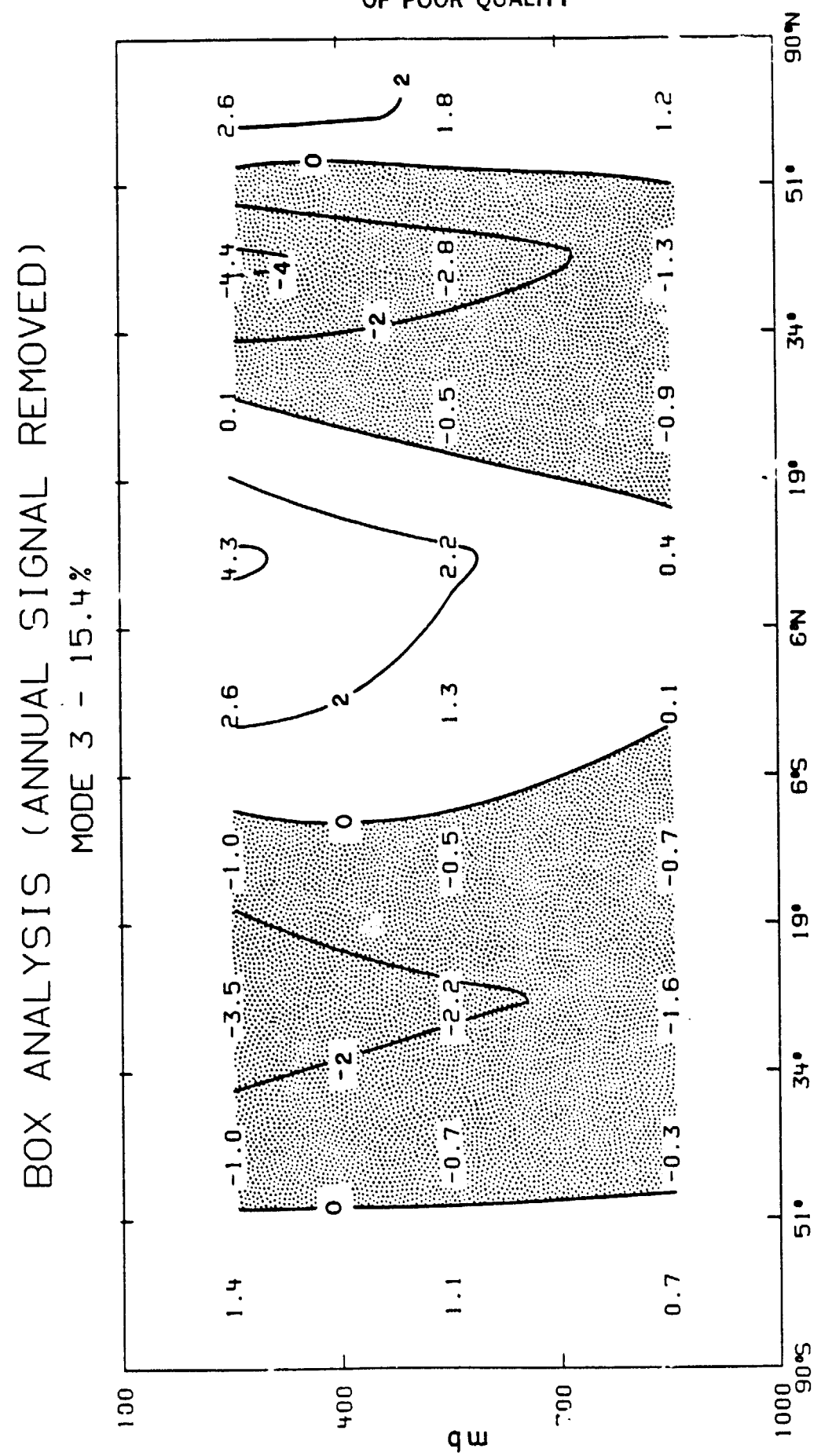

Figure 13c

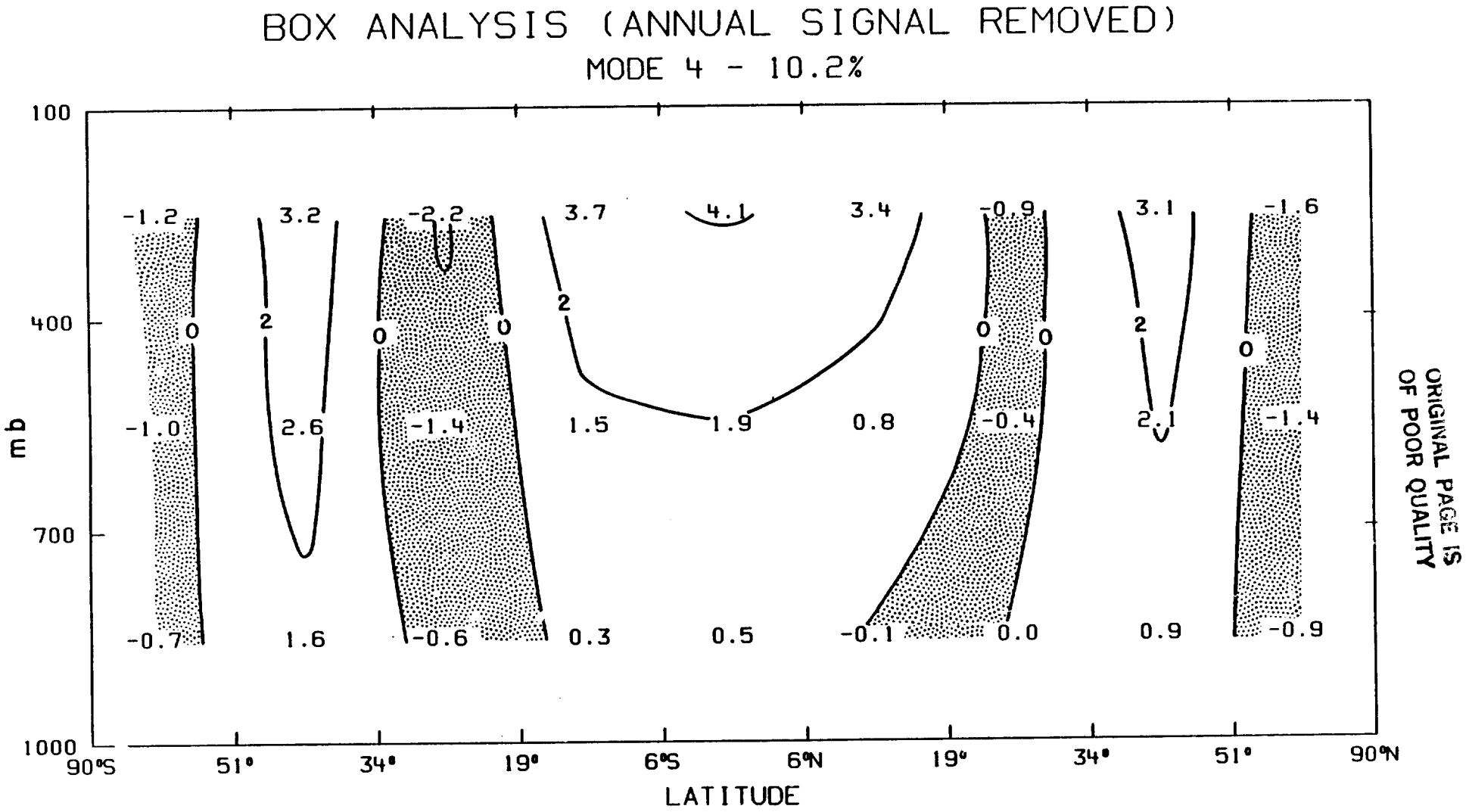
BOX ANALYSIS (ANNUAL SIGNAL REMOVED)
MODE 4 - 10.2%
100
400
700
1000
mb
-1.2
3.2
-2.2
3.7
4.1
3.4
-0.9
3.1
-1.6
0
2
0
0
2
0
0
0
2
0
-1.0
2.6
-1.4
1.5
1.9
0.8
-0.4
2.1
-1.4
-0.7
1.6
-0.6
0.3
0.5
-0.1
0.0
0.9
-0.9
90°S
51°
34°
19°
6°S
6°N
19°
34°
51°
90°N
LATITUDE
ORIGINAL PAGE IS
OF POOR QUALITY

Figure 13d

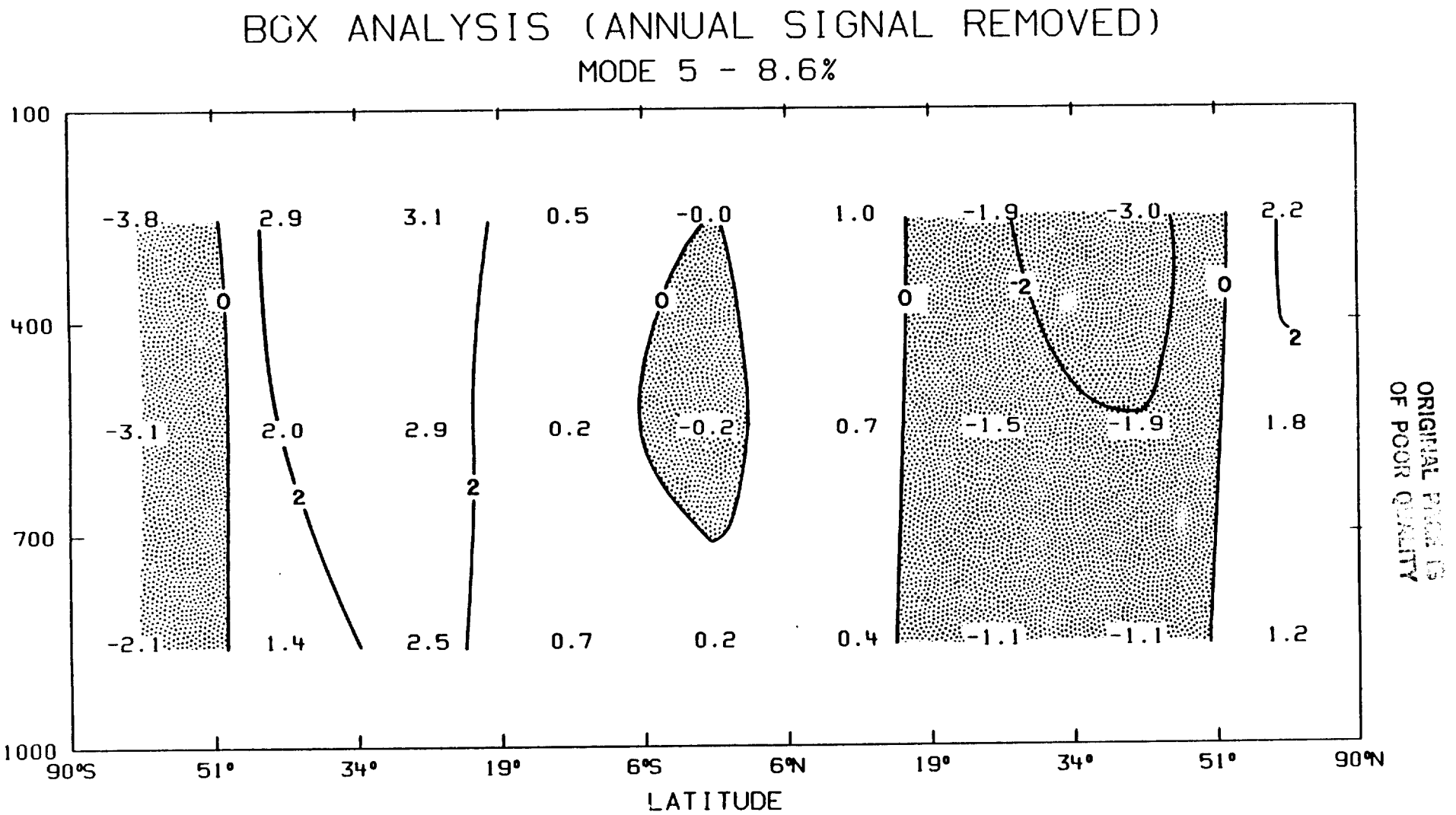
BOX ANALYSIS (ANNUAL SIGNAL REMOVED)
MODE 5 - 8.6%
100
400
700
1000
-3.8
2.9
3.1
0.5
-0.0
1.0
-1.9
-3.0
2.2
0
0
-2
0
2
-3.1
2.0
2.9
0.2
-0.2
0.7
-1.5
-1.9
1.8
2
2
-2.1
1.4
2.5
0.7
0.2
0.4
-1.1
-1.1
1.2
90°S
51°
34°
19°
6°S
6°N
19°
34°
51°
90°N
LATITUDE

Figure 13e

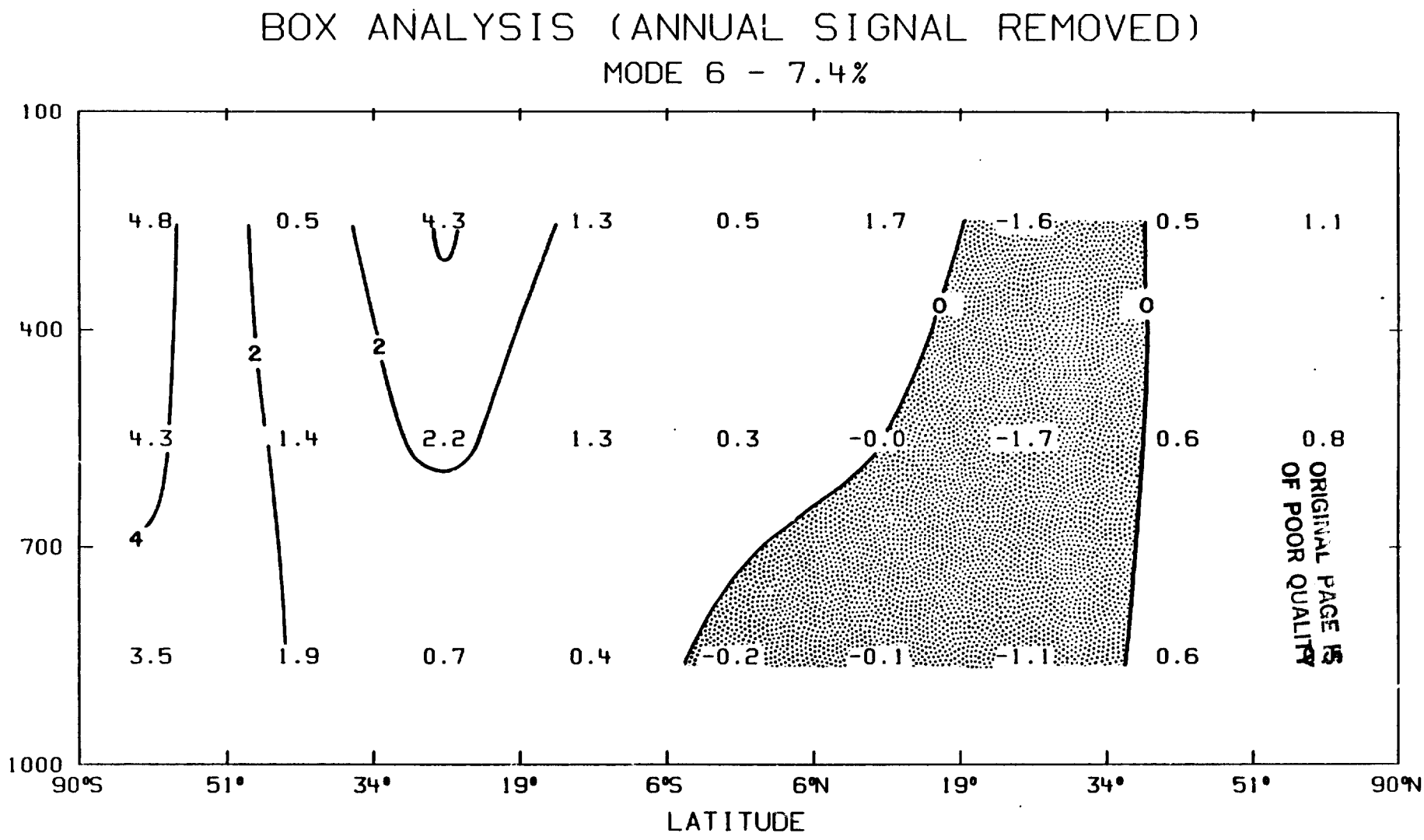
BOX ANALYSIS (ANNUAL SIGNAL REMOVED)
MODE 6 - 7.4%
100
400
700
1000
4.8
0.5
4.3
1.3
0.5
1.7
-1.6
0.5
1.1
0
0
2
2
4.3
1.4
2.2
1.3
0.3
-0.0
-1.7
0.6
0.8
4
3.5
1.9
0.7
0.4
-0.2
-0.1
-1.1
0.6
90°S
51°
34°
19°
6°S
6°N
19°
34°
51°
90°N
LATITUDE
ORIGINAL PAGE IS
OF POOR QUALITY

Figure 13f

BOX ANALYSIS (ANNUAL SIGNAL REMOVED)
JAN 1976 - DEC 1980, MODE TIME SERIES

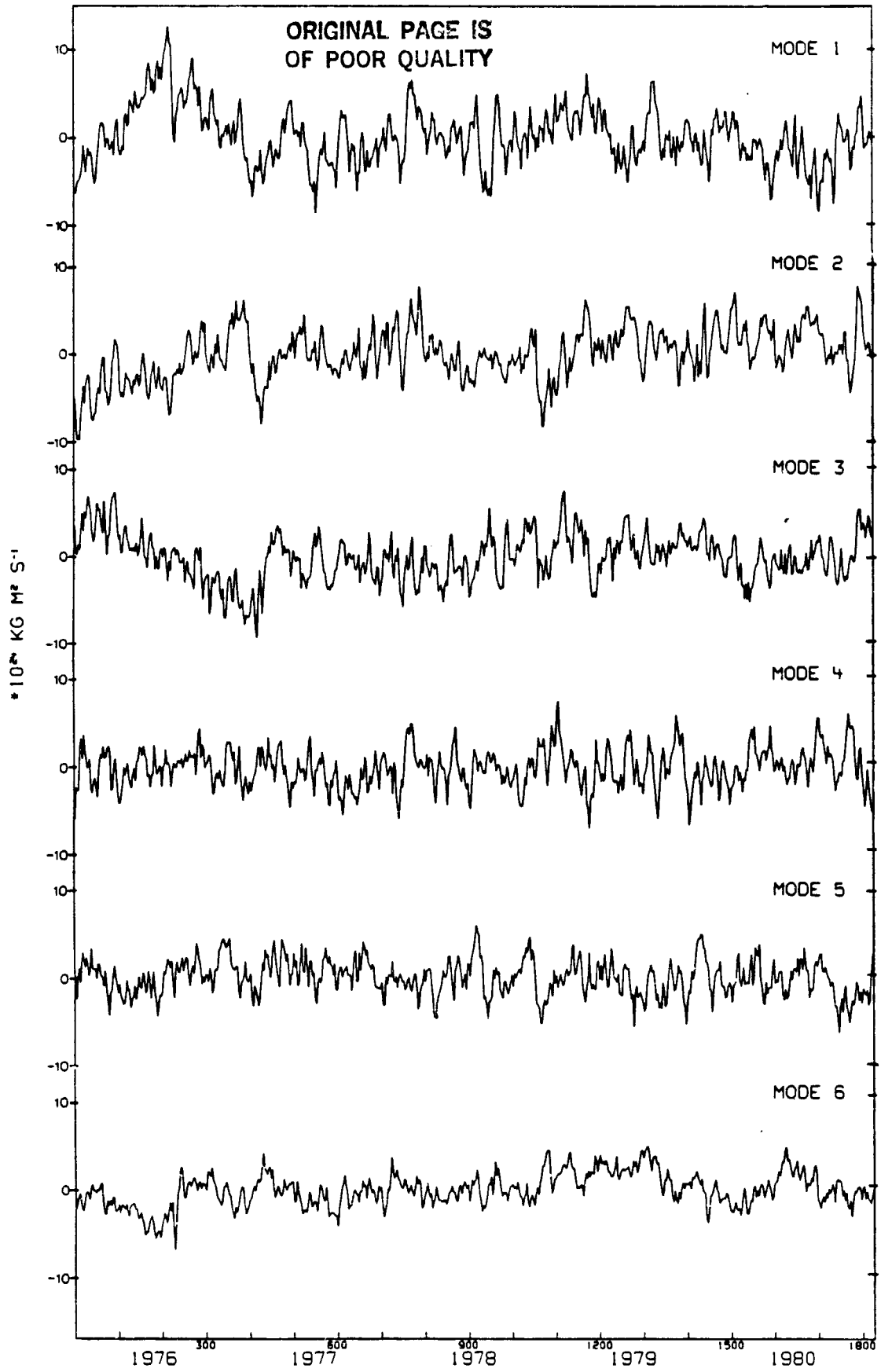

Figure 14

BOX ANALYSIS (ANNUAL SIGNAL REMOVED)
JAN 1976 - DEC 1980, MODE TIME SERIES SPECTRA

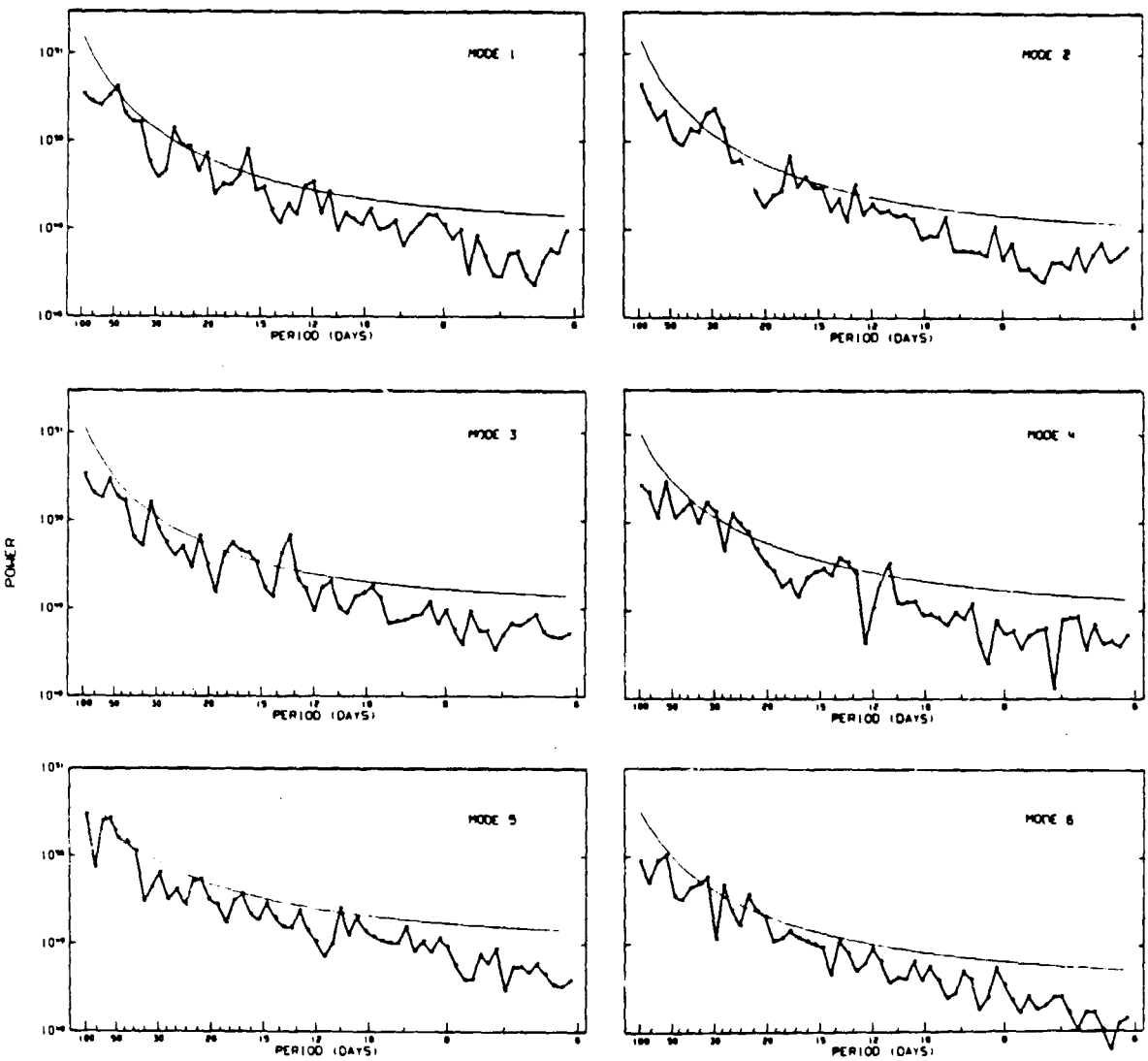

Figure 15

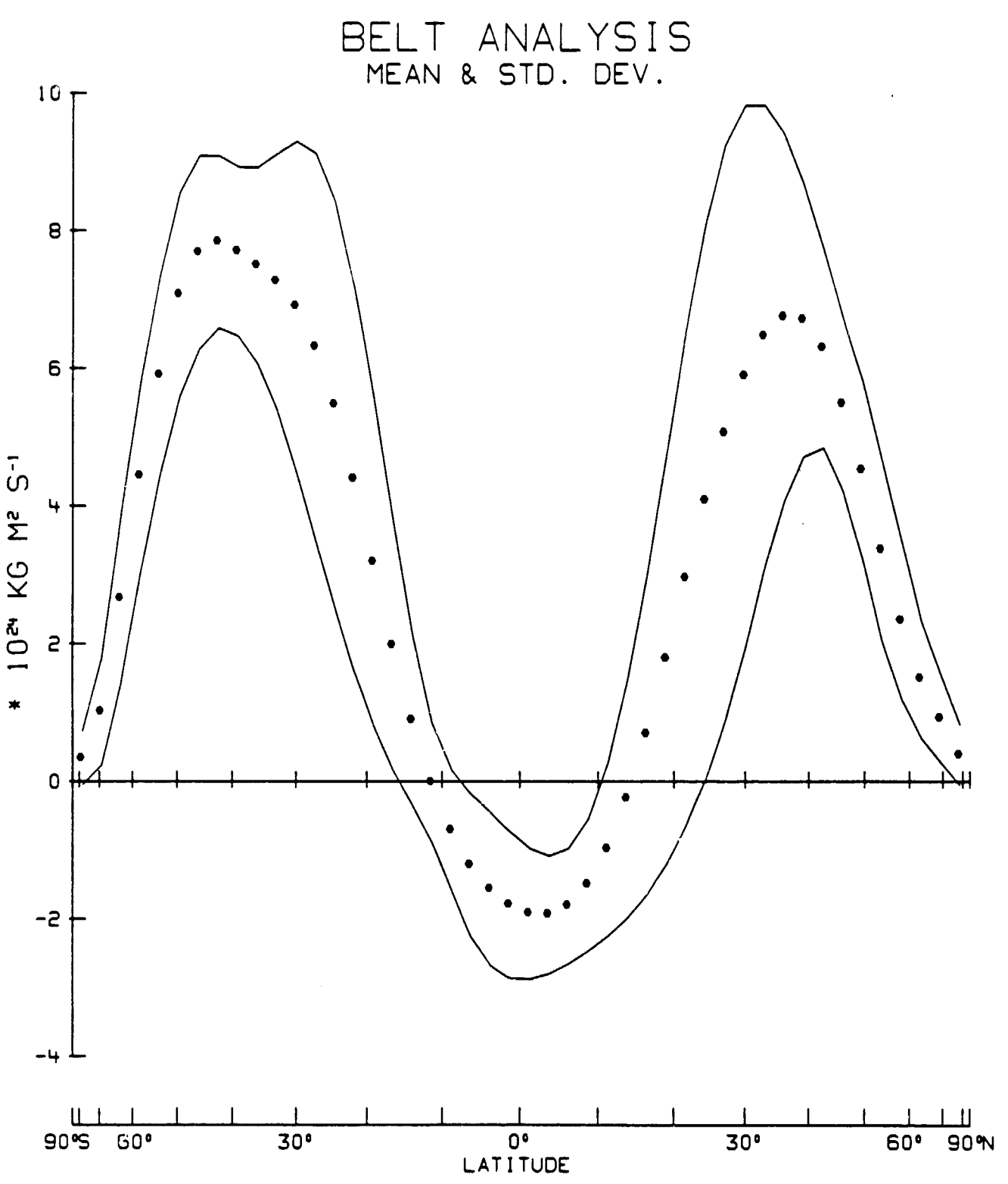

Figure 16

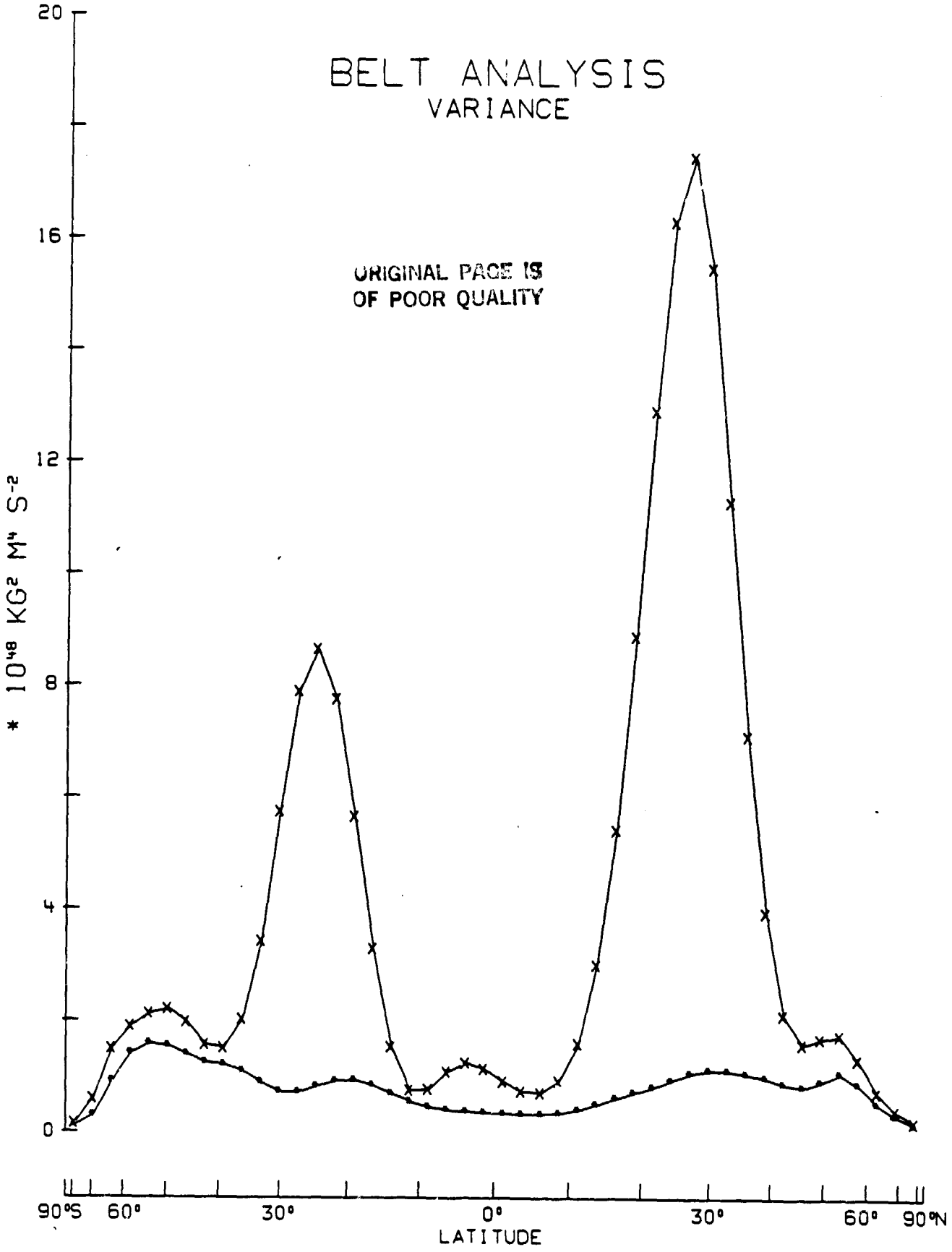
BELT ANALYSIS
VARIANCE
ORIGINAL PAGE IS
OF POOR QUALITY
* 10⁴⁸ KG² M⁴ S⁻²
20
16
12
8
4
0
90°S
60°
30°
0°
30°
60°
90°N
LATITUDE

Figure 17

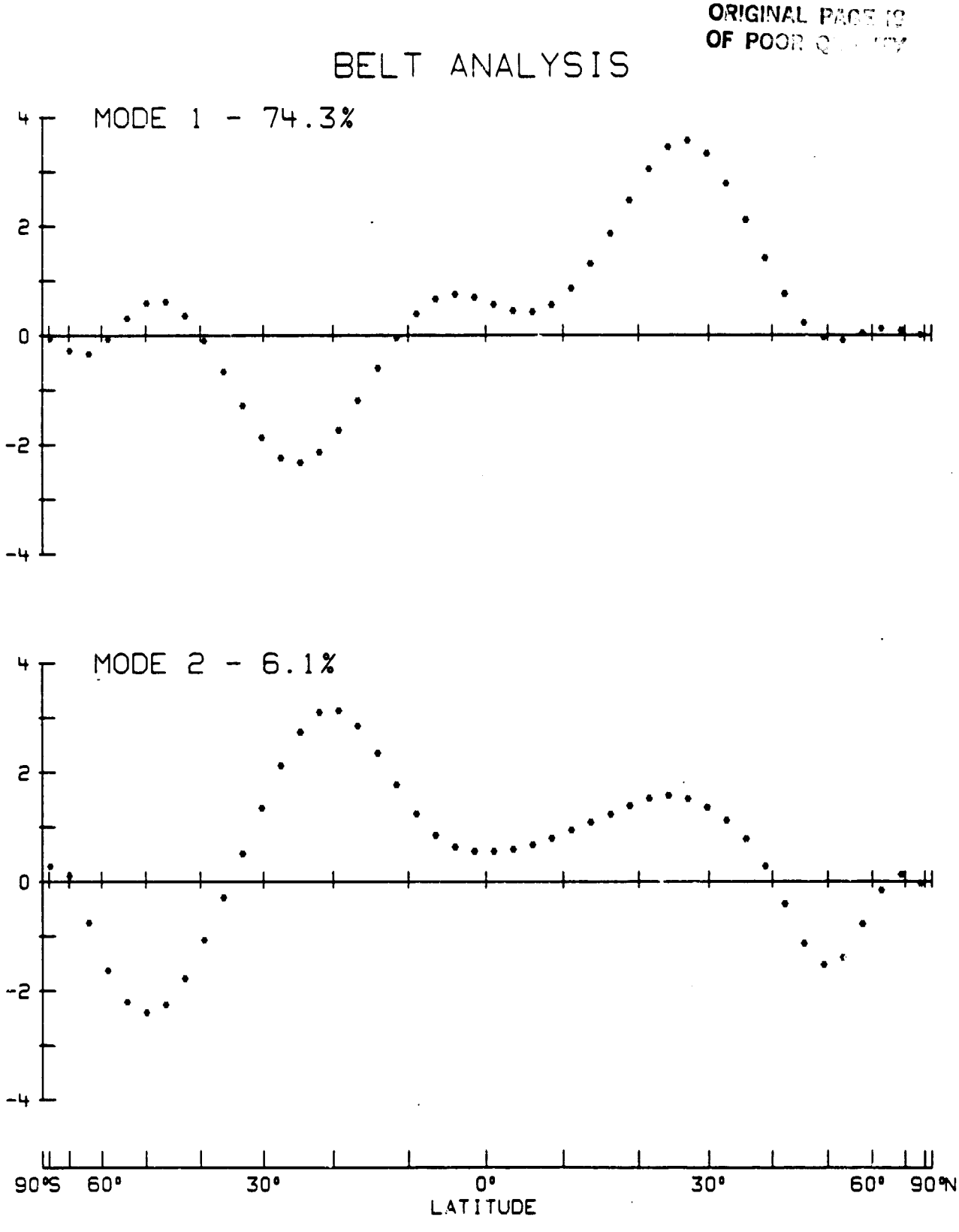

Figure 18a

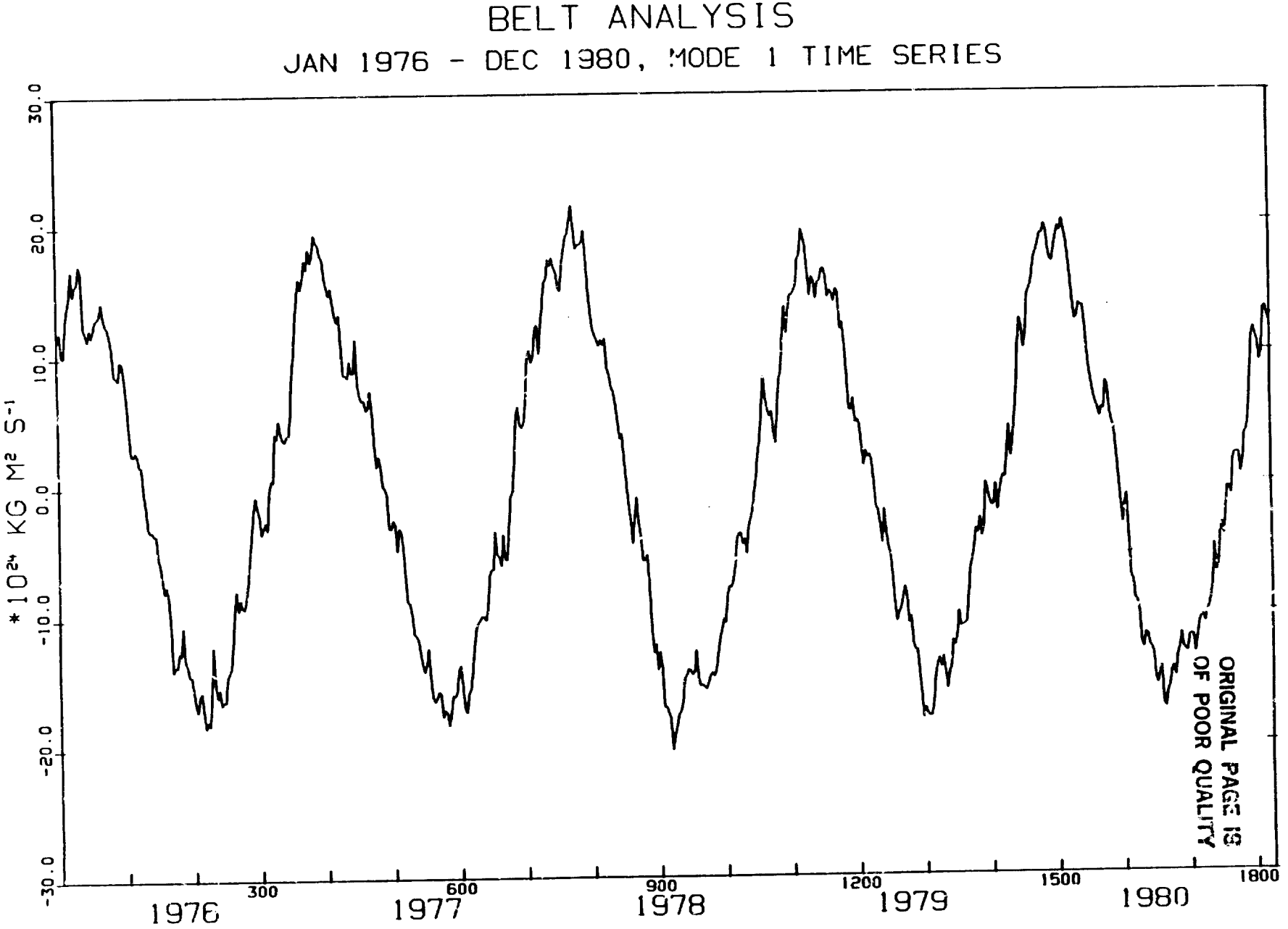
BELT ANALYSIS
JAN 1976 - DEC 1980, MODE 1 TIME SERIES
*10²⁴ KG M² S⁻¹
30.0
20.0
10.0
0.0
-10.0
-20.0
-30.0
300
600
900
1200
1500
1800
1976
1977
1978
1979
1980
ORIGINAL PAGE IS
OF POOR QUALITY

Figure 18b

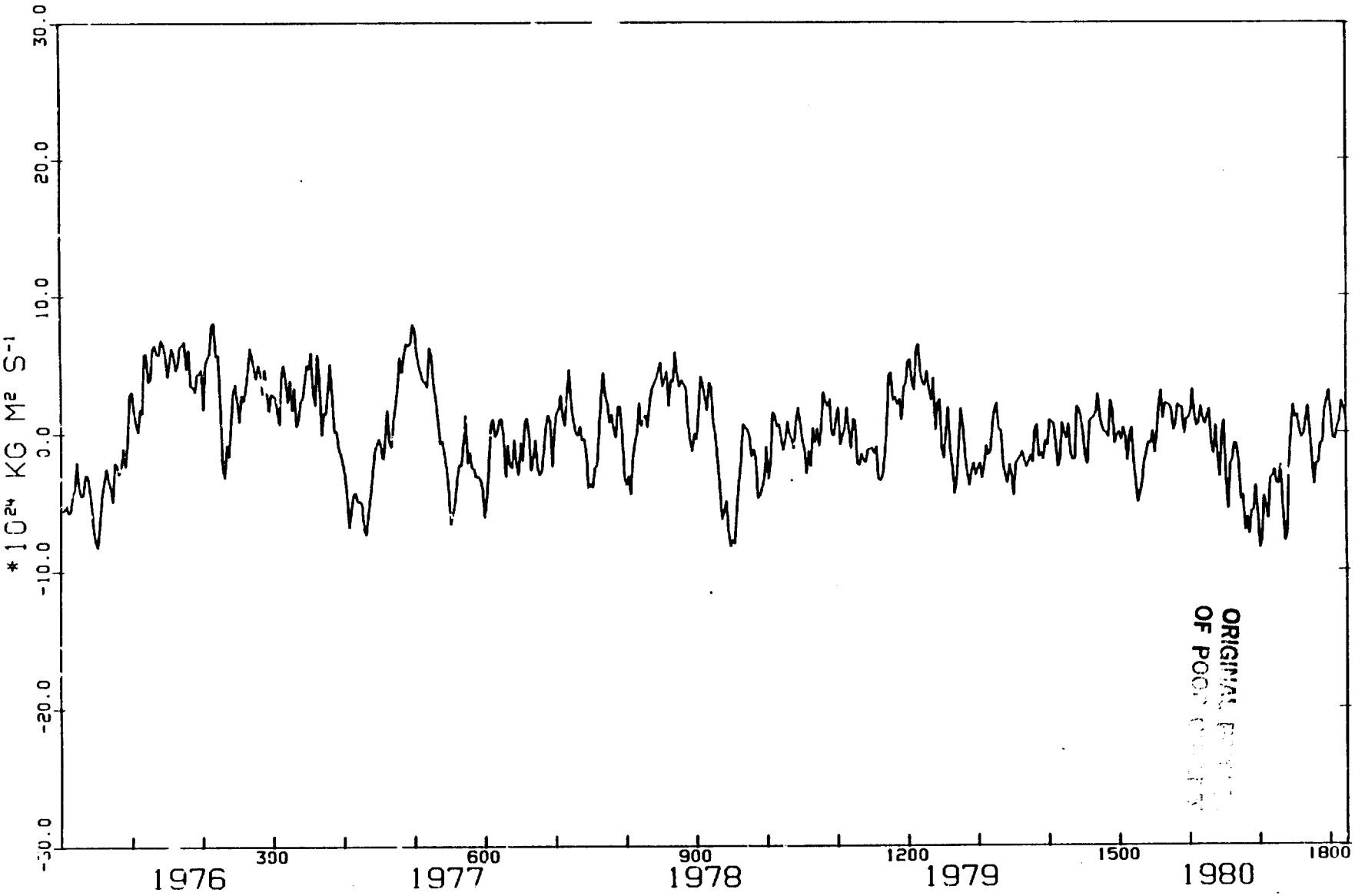
BELT ANALYSIS
JAN 1976 - DEC 1980, MODE 2 TIME SERIES
*10²⁴ KG M² S⁻¹
30.0
20.0
10.0
0.0
-10.0
-20.0
-30.0
300
600
900
1200
1500
1800
1976
1977
1978
1979
1980
ORIGINAL PAGE IS
OF POOR QUALITY

Figure 18c

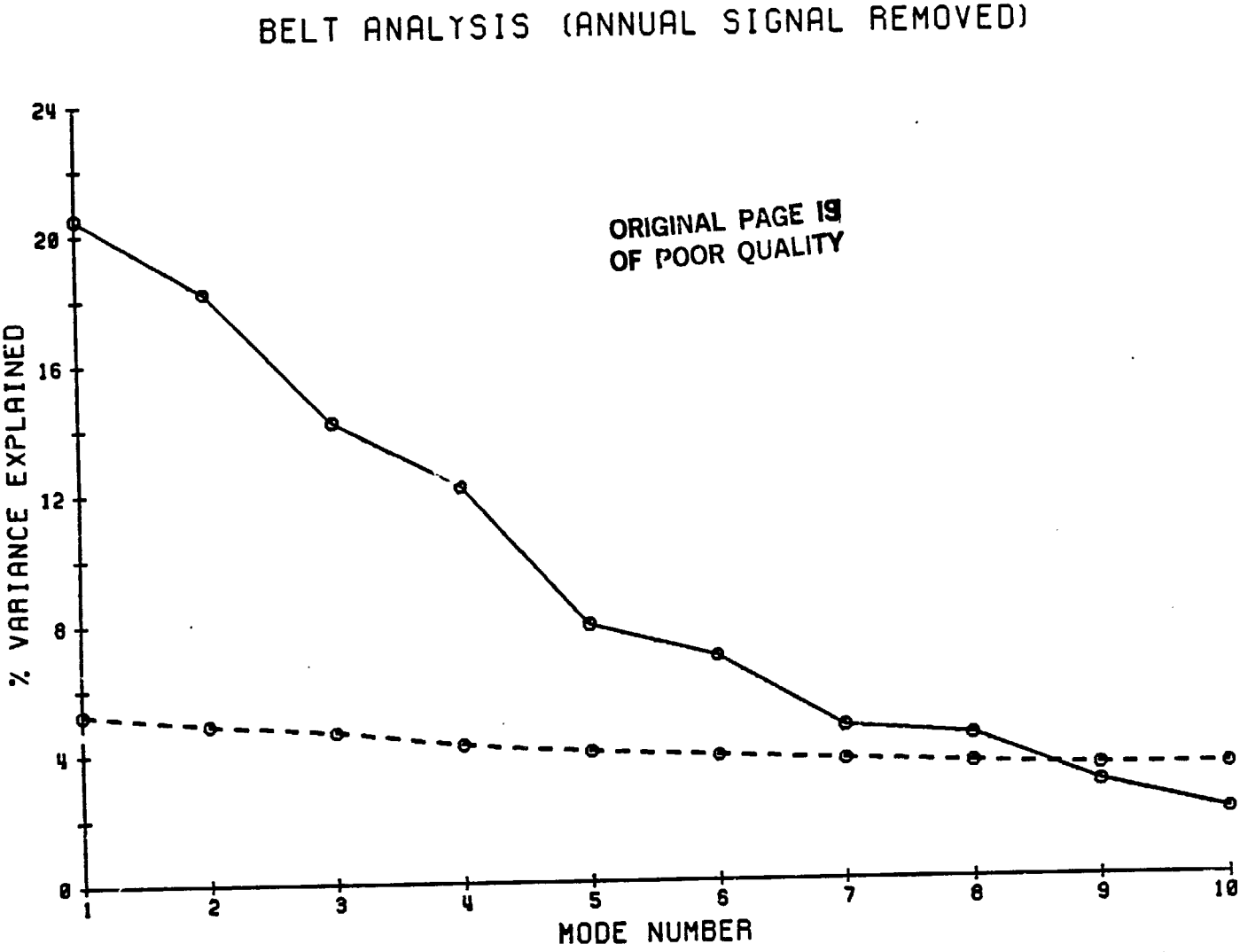
BELT ANALYSIS (ANNUAL SIGNAL REMOVED)
ORIGINAL PAGE IS
OF POOR QUALITY
% VARIANCE EXPLAINED
24
20
16
12
8
4
0
1
2
3
4
5
6
7
8
9
10
MODE NUMBER

Figure 19

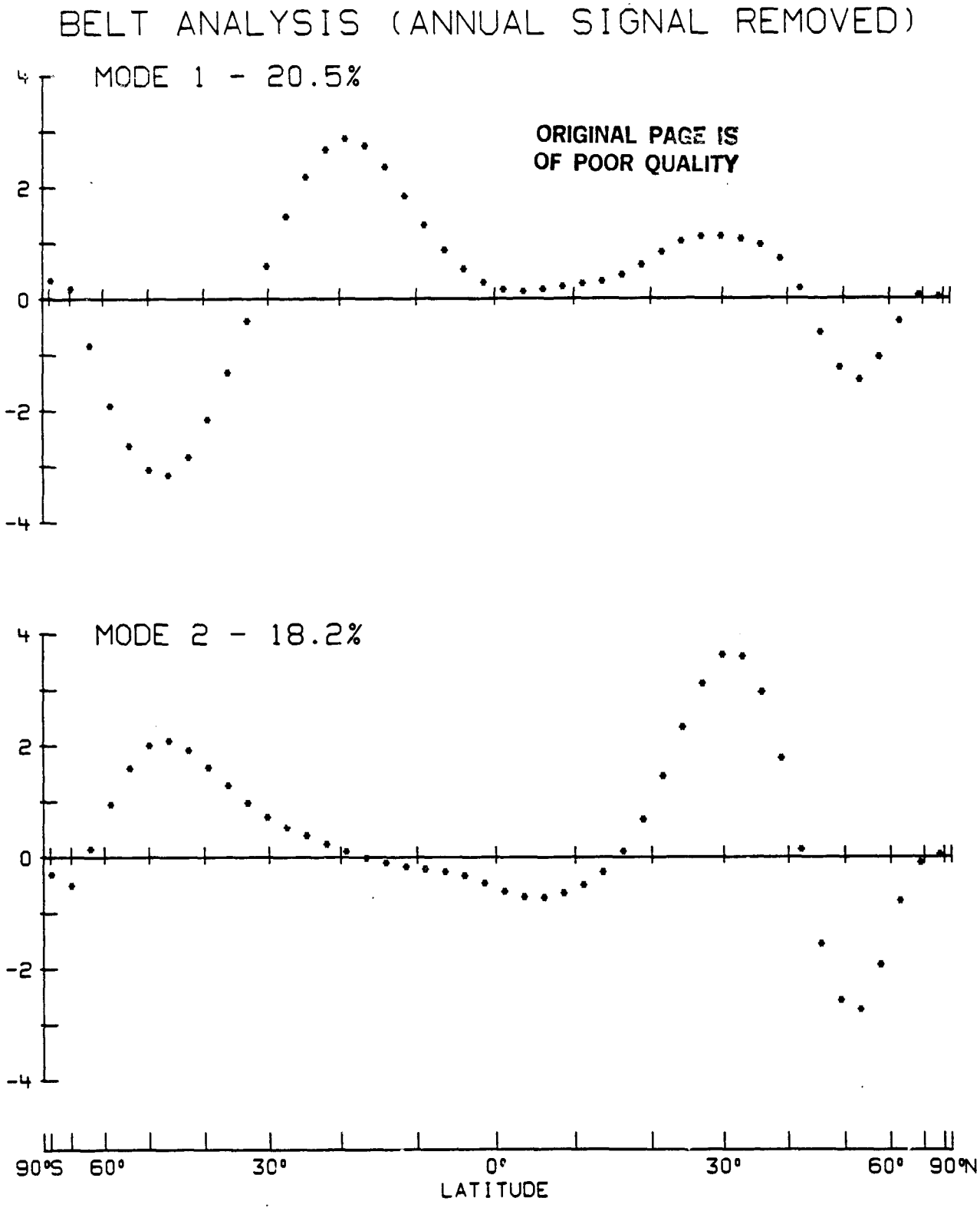
BELT ANALYSIS (ANNUAL SIGNAL REMOVED)
MODE 1 - 20.5%
ORIGINAL PAGE IS
OF POOR QUALITY
MODE 2 - 18.2%
4
2
0
-2
-4
90°S
60°
30°
0°
30°
60°
90°N
LATITUDE

Figure 20

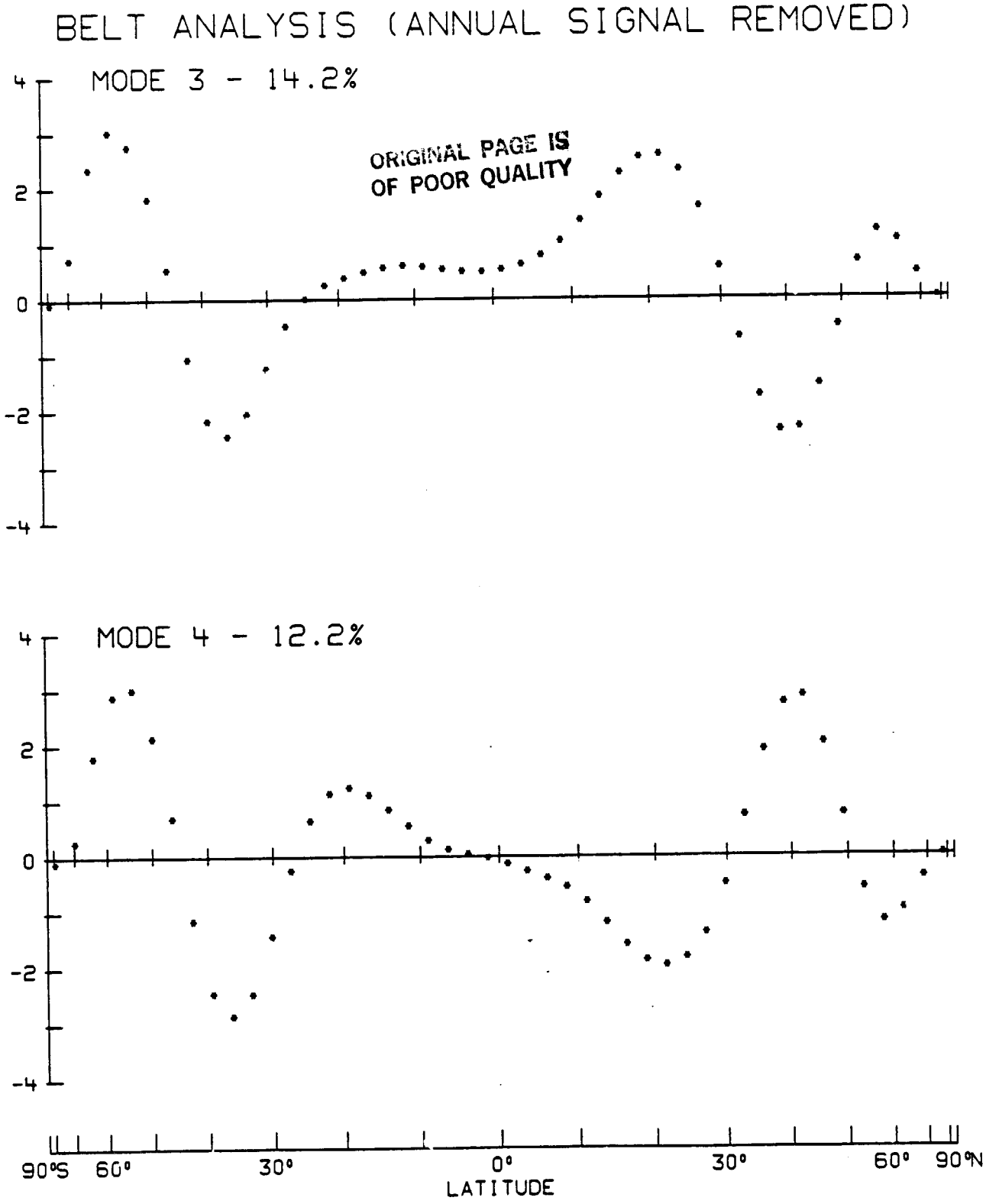

Figure 20 (cont.)

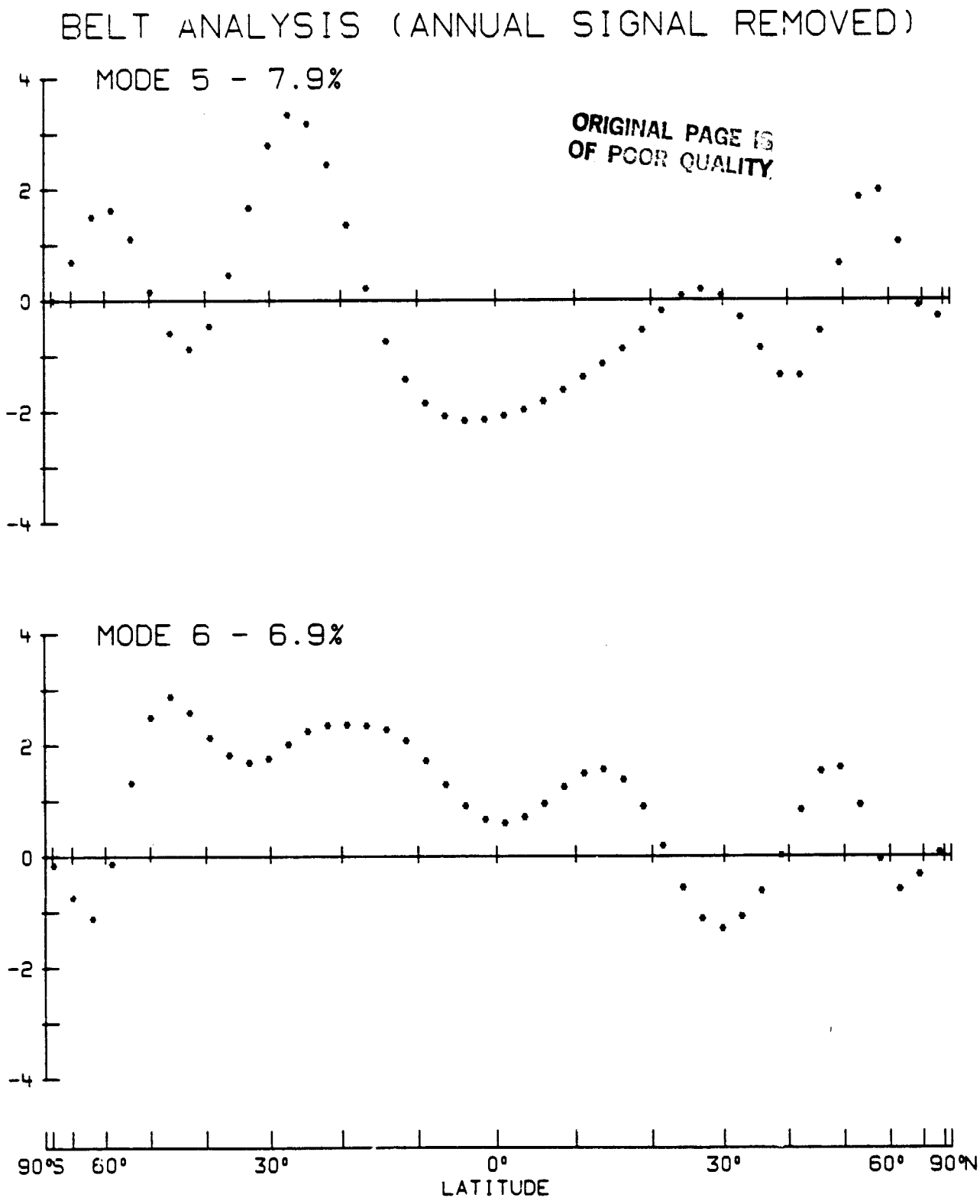

Figure 20 (cont.)

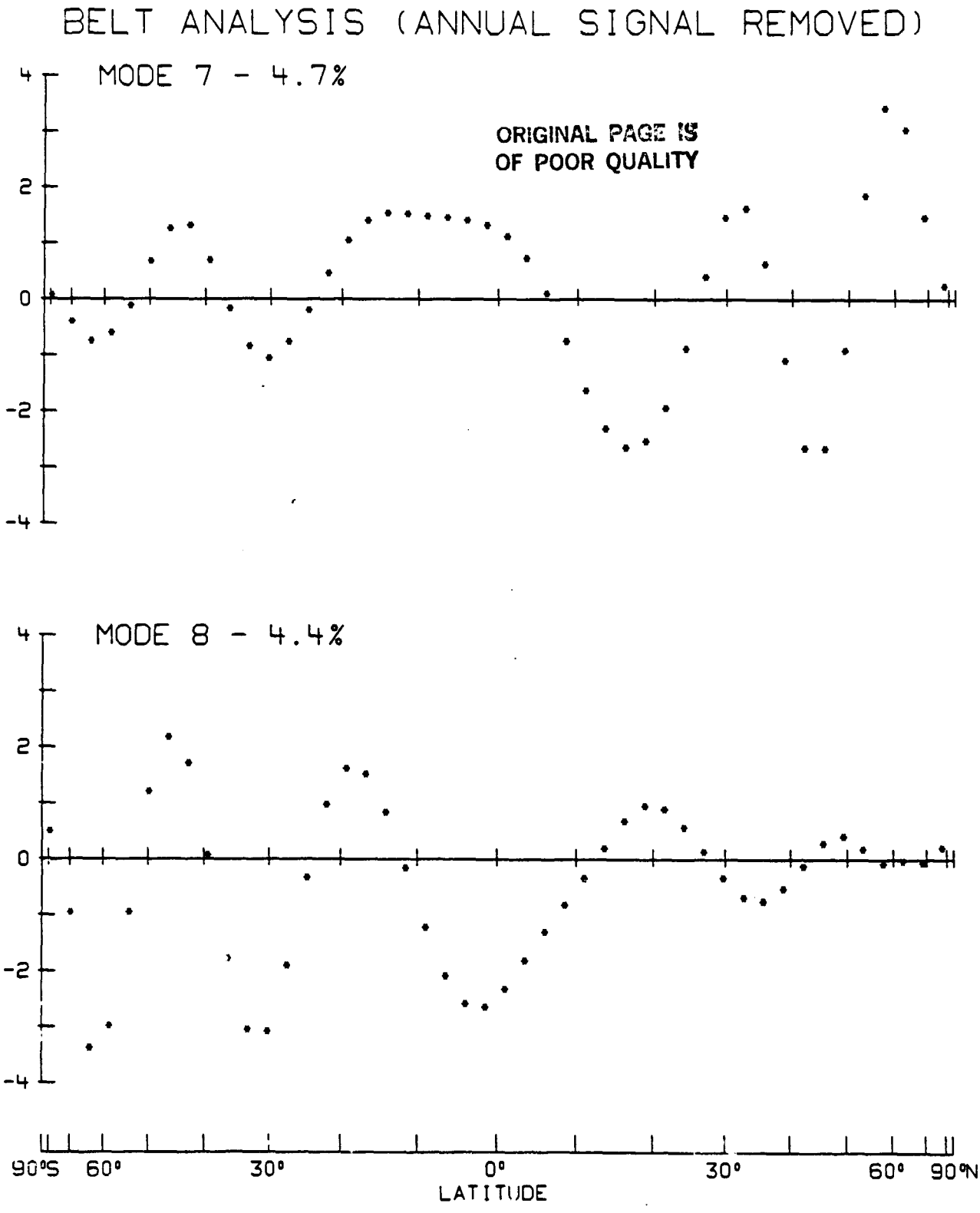

Figure 20 (cont.)

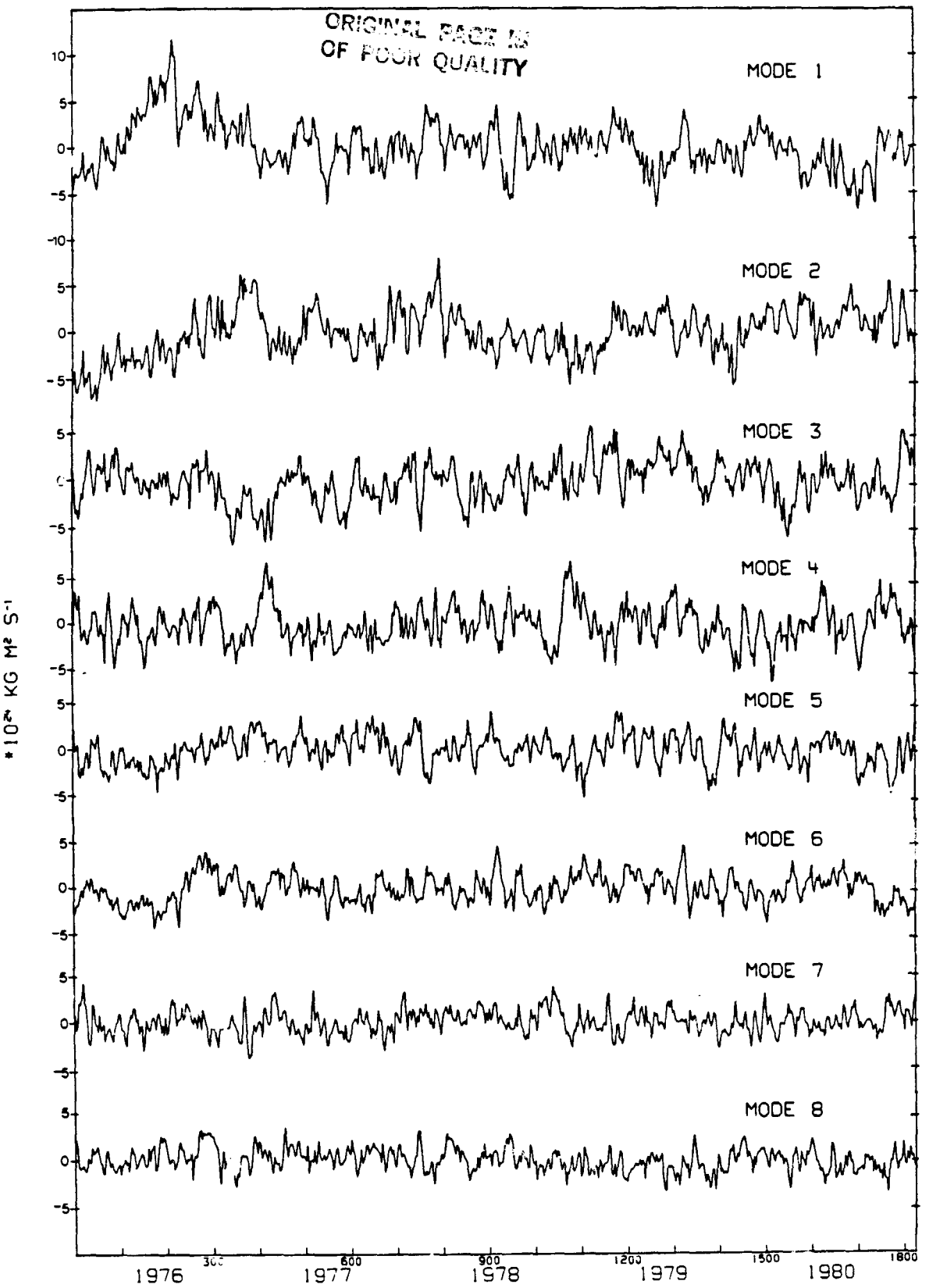
BELT ANALYSIS (ANNUAL SIGNAL REMOVED)
JAN 1976 - DEC 1980, MODE TIME SERIES
ORIGINAL PAGE IS
OF POOR QUALITY
MODE 1
MODE 2
MODE 3
MODE 4
MODE 5
MODE 6
MODE 7
MODE 8
*10²⁴ KG M² S⁻¹
10
5
0
-5
-10
300
600
900
1200
1500
1800
1976
1977
1978
1979
1980

Figure 21

BELT ANALYSIS (ANNUAL SIGNAL REMOVED)
JAN 1976 - DEC 1980, MODE TIME SERIES SPECTRA

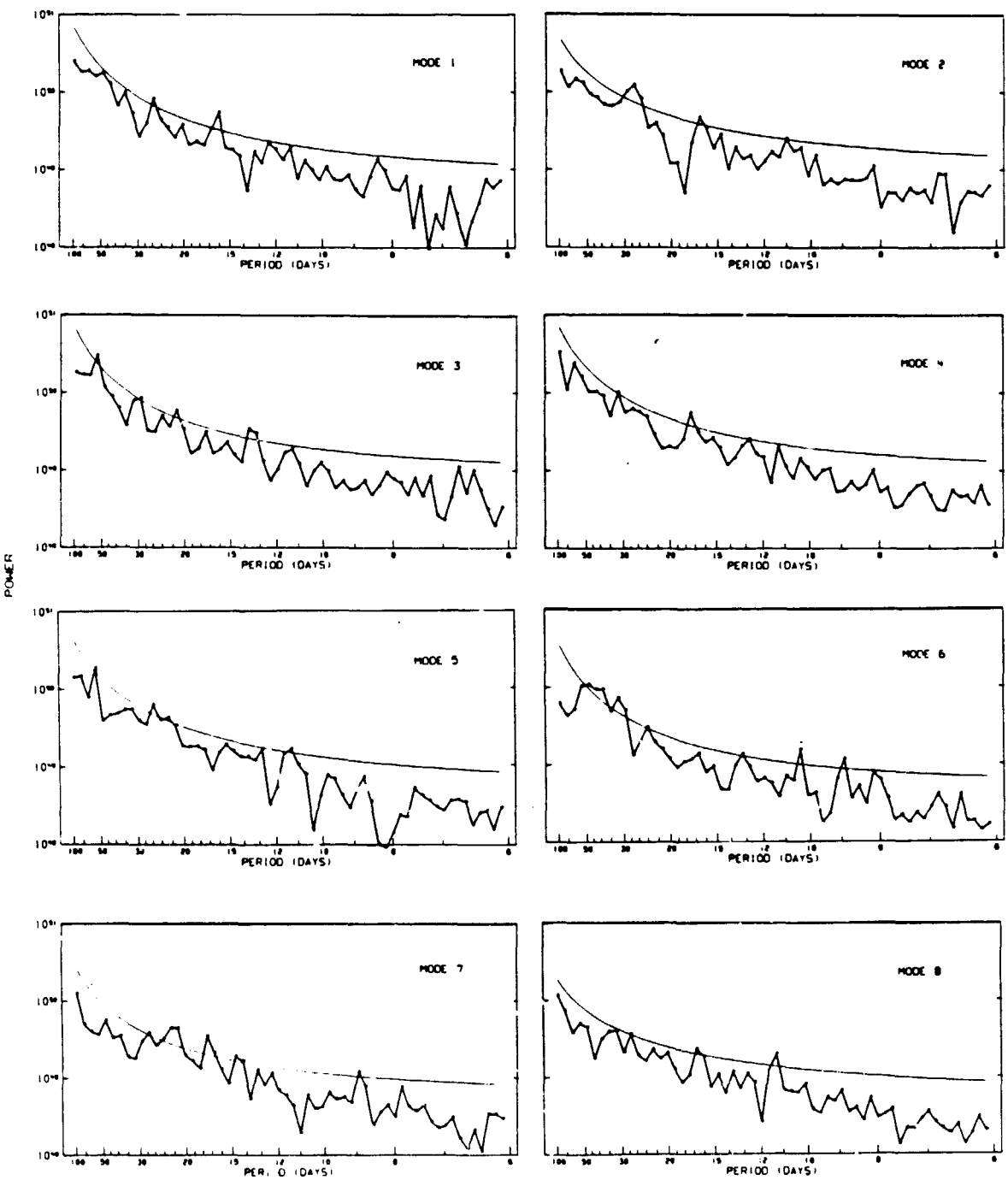

Figure 22

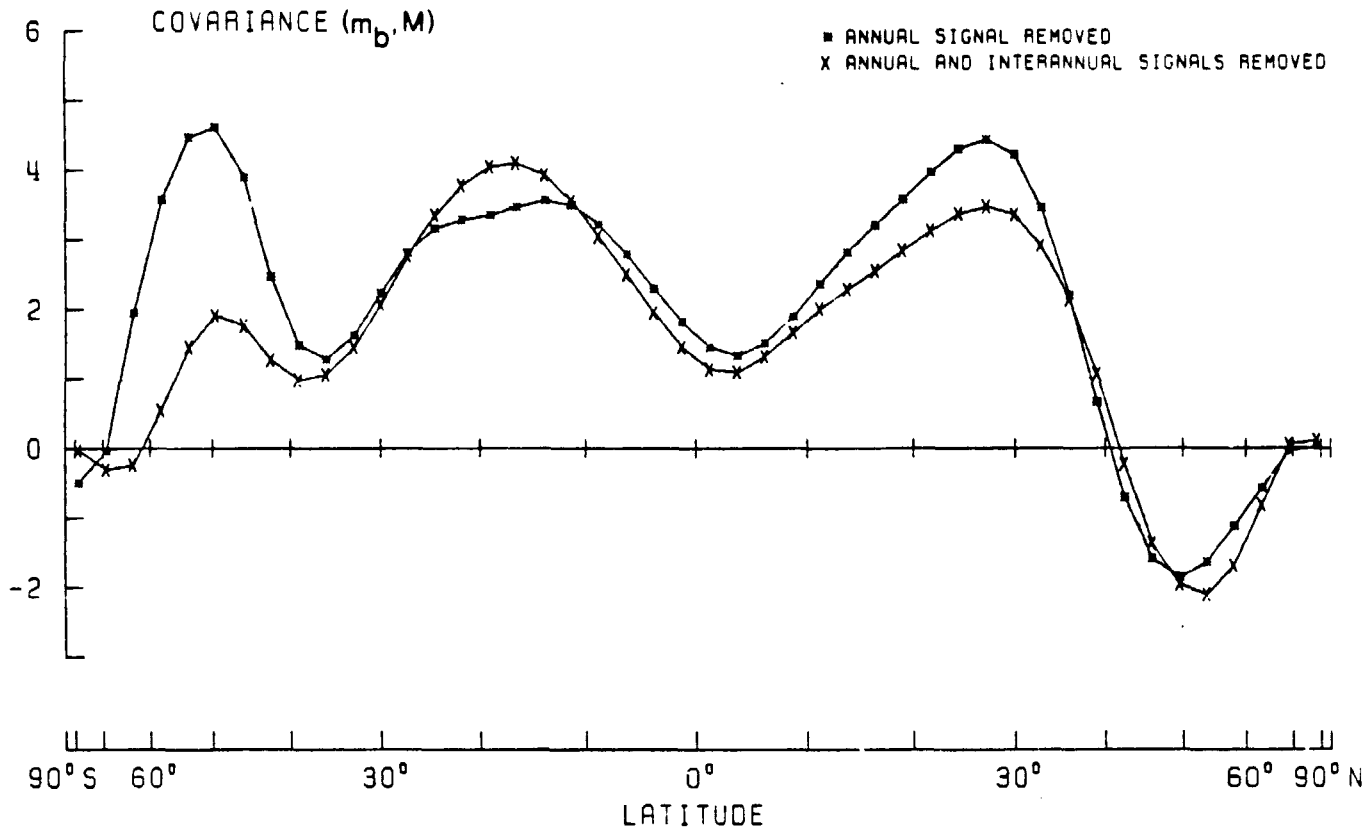

Figure 23